PHOTOSENSITIZERS AND MICROPARTICLES AS TOOLS AGAINST MALIGNANT CELLS

....

Doctoral Thesis presented by
INMACULADA MORA ESPÍ

July 2018

UAB
Universitat Autònoma
de Barcelona

UAB Universitat Autònoma de Barcelona

Departament de Biologia Cel·lular, Fisiologia i Immunologia

PHOTOSENSITIZERS AND MICROPARTICLES

AS TOOLS AGAINST MALIGNANT CELLS

INMACULADA MORA ESPÍ

Report submitted to qualify for the *Doctor Philosophiæ* Degree with International Mention in Cell Biology at the *Universitat Autònoma de Barcelona*

Memòria presentada per optar al Grau de Doctora amb Menció Internacional en Biologia Cel·lular per la Universitat Autònoma de Barcelona

Directors / Directors:

DR. CARME NOGUÉS SANMIQUEL, DR. LLEONARD BARRIOS SANROMÀ AND DR. ELENA IBÁÑEZ DE SANS

Bellaterra, 2018

Unitat de Biologia Cel·lular

La **Dra. Carme Nogués Sanmiquel**, professora titular del Departament de Biologia Cel·lular, Fisiologia i Immunologia de la Universitat Autònoma de Barcelona,

el **Dr. Lleonard Barrios Sanromà**, catedràtic del Departament de Biologia Cel·lular, Fisiologia i Immunologia de la Universitat Autònoma de Barcelona,

i la **Dra. Elena Ibáñez de Sans**, professora agregada del Departament de Biologia Cel·lular, Fisiologia i Immunologia de la Universitat Autònoma de Barcelona,

CERTIFIQUEN:

que **Inmaculada Mora Espí** ha realitzat baix la seua direcció el treball d'investigació que s'exposa a la memòria titulada "Photosensitizers and microparticles as tools against malignant cells" per optar al Grau de Doctora amb Menció Internacional per la UAB.

Que este treball s'ha dut a terme a la Unitat de Biologia Cel·lular del Departament de Biologia Cel·lular, Fisiologia i Immunologia de la Universitat Autònoma de Barcelona.

I per a que conste, firmen el present certificat.

Bellaterra, 5 de Juliol de 2018.

Dra. Carme Nogués Sanmiquel   Dr. Lleonard Barrios Sanromà   Dra. Elena Ibáñez de Sans

Abstract

In the last years, different strategies have been developed to specifically destroy cancer cells minimizing side effects on healthy ones. One of these strategies is photodynamic therapy (PDT), a technique that uses a photosensitizer (PS) in combination with a specific wavelength in the presence of oxygen. When the PS is excited, reactive oxygen species (ROS) are produced, which would kill the surrounding cells. To selectively direct PSs to target cells, they can be attached to drug carries, like nano- and microparticles (NPs and µPs, respectively). In this way, biofunctionalizing NPs or µPs with PSs and molecules able to recognize malignant cells would improve cell targeting, increasing the effectivity of PDT. Another strategy to destroy malignant cells is the use of other therapeutic drugs that interact with intracellular targets to kill the cell. These drugs can also be carried by NPs or µPs to improve cell targeting, but the main limitation of this approach is their entrapment in the endolysosomal compartment after internalization by cells. To overcome this problem, escape enhancing strategies have been developed, like photochemical internalization (PCI), which is based in the same principles as PDT, but in this case the PS must accumulate in the endolysosomal membranes. In this way, disruption of the endolysomal membranes after PS excitation would allow the release of the endocytosed cargo.

The aim of the present thesis is to contribute in the development of the aforementioned strategies for the selective destruction of malignant cells. In the first work, photodynamic treatments with two PSs (Na-H_2TCPP and its zinc derivative Na-ZnTCPP) were found to induce a decrease in cell survival in both tumoral (SKBR3) and non-tumoral (MCF10A) cells, though the latter showed higher resistance at low PSs concentrations. Moreover, different cell death mechanisms were triggered depending on both the PS and the cell line, a result that could be exploited to selectively protect non-malignant cells in photodynamic treatments. In a second work, HER2 was found to be a suitable target to direct anti-HER2 biofunctionalized µPs to a tumorigenic cell line overexpressing this receptor. We also demonstrated that different culture conditions (monoculture or coculture in static or microfluidics systems) influenced µPs internalization, emphasising the importance of performing *in vitro* studies on cells- µPs

interactions in an environment more similar to *in vivo* conditions (cocultures in microfluidic systems). Finally, in our third work, we found that PCI effectively induces endolysosomal membrane disruption, allowing the release of soluble molecules into the cytosol, but not complete membrane disintegration, which would be needed for the release of entrapped µPs.

In conclusion, the present thesis provides new knowledge towards the development of better therapeutic agents and treatments based on the use of PSs and µPs for the selective destruction of malignant cells.

En els últims anys, s'han desenvolupat diverses estratègies per destruir específicament cèl·lules canceroses i minimitzar els efectes secundaris sobre cèl·lules sanes. Una d'estes estratègies és la teràpia fotodinàmica (PDT), una tècnica que utilitza un fotosensibilitzant (PS) juntament amb una longitud d'ona concreta, en presència d'oxigen. En excitar el PS es produïxen espècies reactives de l'oxigen (ROS) que matarien les cèl·lules del voltant. Per dirigir selectivament els PSs cap a les cèl·lules diana, estos es poden vehicular en nano- i micropartícules (NPs i µPs, respectivament). En eixe sentit, biofuncionalitzar NPs o µPs amb PSs y molècules capaces de reconéixer les cèl·lules malignes hauria de permetre fer tractaments més selectius amb PDT. Altra estratègia per destruir cèl·lules malignes és l'ús d'altres fàrmacs terapèutics que interaccionen amb dianes intracel·lulars per induir la mort cel·lular. Estos fàrmacs també poden ser vehiculitzats en NPs o µPs per dirigir-los més eficientment a les cèl·lules diana, però la major limitació d'este enfoc és que després de la internalització poden quedar atrapades junt als seus vehicles al compartiment endolisosomal. Per superar este problema, s'han desenvolupat estratègies com la internalització fotoquímica (PCI), que es basa en els mateixos principis que la PDT però, en este cas, el PS s'acumula en les membranes endolisosomals, que patixen disrupció despuix de l'excitació del PS, permetent l'alliberació del contingut endolisosomal cap al citosol.

L'objectiu de la present tesi és contribuir al desenvolupament de les estratègies mencionades prèviament per eliminar selectivament cèl·lules malignes. En el primer treball, els tractaments fotodinàmics amb dos PSs (Na-H_2TCPP i el seu derivat de zinc Na-ZnTCPP) induïren un descens en la supervivència de cèl·lules tumorals (SKBR3) i no tumorals (MCF10A), encara que este últimes mostraren una major resistència a baixes concentracions dels dos PSs. A més, depenent del PS i la línia cel·lular es van desencadenar diferents mecanismes de mort cel·lular, fet que podria explotar-se per protegir selectivament les cèl·lules no malignes en front dels tractaments fotodinàmics. En el segon treball es va demostrar que HER2, sobreexpressat en cèl·lules d'alguns tipus de càncer, era una diana adequada per dirigir µPs biofuncionalitzades amb anti-HER2. També demostràrem que diferents condicions de cultiu (monocultius o cocultius en

sistemes estàtics o microfluídics) influenciaven la internalització de les µPs, posant en relleu la importància de realitzar estudis sobre les interaccions entre µPs i cèl·lules en condicions més similars a les existents *in vivo*. Finalment, en el nostre tercer treball observàrem que la PCI induïx eficaçment la disrupció de les membranes endolisosomals, permetent l'alliberació de molècules solubles cap al citosol, però no una desintegració completa de la membrana, fet que seria necessari per l'alliberació de les µPs atrapades.

En conclusió, la present tesi proporciona nou coneiximent pel desenvolupament de millors agents terapèutics y tractaments basats en l'ús de PSs i µPs per la destrucció selectiva de cèl·lules malignes.

Resumen

En los últimos años, se han desarrollado diversas estrategias para destruir específicamente células cancerosas y minimizar los efectos secundarios en células sanas. Una de estas estrategias es la terapia fotodinámica (PDT), una técnica que utiliza un fotosensibilizante (PS) y luz de una longitud de onda concreta, en presencia de oxígeno. Cuando el PS es excitado por la luz, produce especies reactivas del oxígeno (ROS) que inducen la muerte de las células circundantes. Para dirigir selectivamente los PSs hacia las células diana, éstos pueden vehiculizarse en nano- y micropartículas (NPs y μPs, respectivamente). En este sentido, biofuncionalizar NPs o μPs con PSs y con moléculas capaces de reconocer las células malignas debería permitir hacer tratamientos más selectivos con PDT. Otra estrategia para destruir células malignas es el uso de otros fármacos terapéuticos que interaccionen con dianas intracelulares para matar la célula. Estos fármacos también pueden ser vehiculizados en NPs o μPs para dirigirlos con más eficiencia a las células diana, pero la mayor limitación de este enfoque es que tras la internalización pueden quedar atrapados junto a sus vehículos en el compartimento endolisosomal. Para superar este problema, se han desarrollado estrategias como la internalización fotoquímica (PCI), que se basa en los mismos principios que la PDT pero, en este caso, el PS se acumula en las membranas endolisosomales, que sufren una disrupción tras la excitación del PS, permitiendo la liberación del contenido endolisosomal hacia el citosol.

El objetivo de la presente tesis es contribuir al desarrollo de las estrategias mencionadas previamente, para eliminar selectivamente células malignas. En el primer trabajo, los tratamientos fotodinámicos con dos PSs (Na-H$_2$TCPP y su derivado de zinc Na-ZnTCPP) indujeron un descenso en la supervivencia de células tumorales (SKBR3) y no tumorales (MCF10A), aunque éstas últimas mostraron mayor resistencia a bajas concentraciones de ambos PSs. Además, según el PS y la línea celular se desencadenaron diferentes mecanismos de muerte celular, hecho que podría explotarse para proteger selectivamente las células no malignas durante los tratamientos fotodinámicos. En el segundo trabajo, se demostró que HER2, sobreexpresado en células de algunos tipos de cáncer, era una diana adecuada para dirigir μPs biofuncionalizadas con anti-HER2.

También demostramos que diferentes condiciones de cultivo (mono o cocultivos en sistemas estáticos o microfluídicos), influenciaban la internalización de las µPs, lo que puso de relieve la importancia de realizar estudios sobre las interacciones entre µPs y células en condiciones más similares a las existentes *in vivo*. Finalmente, en nuestro tercer trabajo observamos que la PCI induce eficazmente la disrupción de las membranas endolisosomales, permitiendo la liberación de moléculas solubles hacia el citosol, pero no una desintegración completa de la membrana, lo que sería necesario para la liberación de las µPs atrapadas.

En conclusión, la presente tesis proporciona nuevo conocimiento para el desarrollo de mejores agentes terapéuticos y tratamientos basados en el uso de PSs y µPs para la destrucción selectiva de células malignas.

Table of contents

Abbreviations

µP	Microparticle
µP-antiH	µP biofunctionalized with antiH
µP-secAb	µP biofunctionalized with secAb
3-AB	3-aminobenzamide
5-ALA	5-aminolevulinic acid
ACD	Accidental cell death
AlPc	Al (III) Phthalocyanine chloride disulfonic acid
AlTSPc	Aluminium tetra sulfo-phthalocyanine
antiH	mouse Anti-c-ERBB2/c-Neu (Ab-5) clone TA-1
ANV	Annexin-V-FLUOS
APAF1	Apoptotic peptidase-activating factor 1
BAK1	BCL2-antagonist/killer 1
BAX	BCL2-associated X protein
BCL2	B-cell CLL/lymphoma 2
BCL-X$_L$	BCL2-like 1
BH3	BCL2 homology domain 3
BID	BH3-interacting death domain agonist
BPD-MA	Benzoporphyrin derivative monocarboxylic acid
CLSM	Confocal laser scanning microscopy
CNT	Carbon nanotube
CPPs	Cell-penetrating peptides
D492	Human breast epithelial cell line
D492HER2	D492 human breast cell line overexpressing HER2
DAMPs	Damage-associated molecular patterns
DIABLO	IAP-binding mitochondrial protein
DMSO	Dimethylsulfoxide
DT	Dark toxicity
EDX	Energy dispersive x-ray
EEA1	Early endosome antigen 1

EGF	Epidermal growth factor
EGFR	EGF receptor
EPR	Enhanced permeability and retention
ER	Endoplasmic reticulum
FADD	FAS-associated death domain
FAS	Fas cell surface death receptor
GNPs	Gold NPs
HAADF	High angle annular dark field
HER2	Human epidermal growth factor receptor 2
Hp	Hematoporphyrin
HPD	Hematoporphyrin derivative
IAP	inhibitor of apoptosis
LAMP1	Lysosome-Associated Membrane Protein 1
LC3	Microtubule-associated protein 1 light chain 3
LDL	Low density lipoproteins
MAL	Methylated ester of 5-ALA
MAP1LC3	Microtubule-associated protein 1 light chain 3
MCF10A	Human breast epithelial cell line
MLKL	Mixed lineage kinase domain-like
MMICCs	Multi-material polysilicon-Cr-Au intracellular chips
MMNPs	Multifunctional or multimodal NPs
MOMP	Mitochondrial outer membrane permeabilization
MRI	Magnetic resonance imaging
m-THPC	m-tetrahydroxyphenylchlorin
Na-H$_2$TCPP	meso-tetrakis (4-carboxyphenyl) porphyrin sodium salt
Na-ZnTCPP	Na-H$_2$TCPP zinc derivative
NCCD	Nomenclature Committee on Cell Death
NP	Nanoparticle
PARP-1	Poly-(ADP-ribose)-polymerase-1
PCD	Programmed cell death
PCI	Photochemical Internalization

PDT	Photodynamic therapy
PdTPPo	Palladium (II)-tetra phenyl-porphycene
PEI	Polyethyleneimine
PI	Propidium iodide
PLGA	Poly (lactic-co-glycolic acid)
PS	Photosensitizer
QD	Quantum dot
RCD	Regulated cell death
RIPK1	Receptor-interacting protein kinase 1
RIPK3	Receptor-interacting protein kinase 3
ROS	Reactive oxygen species
secAb	Goat anti-Mouse IgG2a Secondary Antibody Alexa Fluor® 647 conjugate
SKBR3	Human breast epithelial adenocarcinoma cell line
SMAC	IAP-binding mitochondrial protein
SQSTM1	sequestosome 1
STEM	Scanning TEM
TEM	Transmission electron microscopy
Tf	Transferrin
Tf-A488	Transferrin from human serum-Alexa Fluor® 488 conjugate
TfR	Transferrin receptor
TMPP	Meso-tetrakis (p-methoxyphenyl) porphyrin
TNFR	Tumor necrosis factor receptor
TNFR1	Tumor necrosis factor receptor 1
TNFα	Tumor necrosis factor alpha
TUNEL	Terminal deoxynucleotidyl transferase dUTP nick end labeling
XIAP	X-linked inhibitor of apoptosis protein
ZnTSPc	Zinc tetra sulfo-phthalocyanine

I

Introduction

In the last years, several strategies have been developed to selectively destroy malignant cells. One of these strategies is photodynamic therapy (PDT), a clinically approved therapeutic procedure for some types of cancer and other pathologies. PDT uses (photosensitizers (PSs) and a specific wavelength (light) in the presence of oxygen to destroy the target cells through the generation of reactive oxygen species (ROS) that occurs upon PSs activation. Research on the development of new PSs and the characterization of the types of cell death that they induce is currently a hot topic in the PDT field.

To selectively deliver PSs to the malignant cells, PDT can be combined with the use of nano- and microsystems, another promising strategy in cancer therapies. Different nano- and microsystems have been developed, each of them showing some advantages and disadvantages over the others. In general, however, these systems are characterized by having a chemically modifiable surface to which several types of ligands can be attached. Thus, biofunctionalization of nano- and microsystems allows them to act both as targeting and PSs delivery vehicles, among other potential functions.

Nano- and microsystems can also be used as vehicles to target and deliver other types of therapeutic drugs, often designed to interact with intracellular targets to destroy malignant cells. The main limitation of these systems, however, is that they can become entrapped inside the endolysosomal compartment once they enter the targeted cells, which prevents the carried drugs from reaching their intracellular targets and exert their effects. To avoid this, escape enhancing strategies, such as photochemical internalization (PCI), can be applied. PCI technology is based on the same principles as PDT, but the PSs used in PCI need to accumulate in the endolysosomal membrane of the targeted cells. In this way, after activation with light, they will induce the disruption of the endolysosomal membranes and potentially allow the release of the endocytosed drugs into the cytosol. The therapeutic drugs would then be free to reach their intracellular site of action.

In the next pages, the basic principles, advances and limitations of PDT, PCI and the use of nano- and microsystems as targeting vehicles and drug carriers in cancer research will be reviewed.

I   1. Photodynamic therapy

PDT is a clinical treatment by which malignant cells are killed due to the activation of a PS when it is exposed to a specific wavelength, usually in the range of visible or near infrared spectrum. PS excitation induces reactive ROS generation that, ultimately, will produce cell damage and death (YOON, LI AND SHIM, 2013; ONISZCZUK ET AL., 2016). As ROS have a short half-life, the damage is limited to a local effect, avoiding the diffusion that could affect neighboring healthy cells (FONDA-PASCUAL ET AL., 2016).

PDT can be used for the treatment of head and neck, gastrointestinal tract, gynecological, lung or urologic cancers (FAYTER ET AL., 2010; AGOSTINIS ET AL., 2011). PDT is also used for the treatment of other pathologies, such as macular degeneration, choroidal neovascularization, psoriasis, acne or epithelial tumors (JUARRANZ ET AL., 2008). The use of PDT is also expanding towards anti-microbiological (bacterial, viral, fungal or parasitic) action (CASSIDY ET AL., 2009; ST. DENIS ET AL., 2011). As many PSs used in PDT emit fluorescence when excited, they can also be applied as imaging molecules for tumor diagnosis (OTTO ET AL., 2011; SEITZ ET AL., 2012).

When PDT is used, different cell death mechanisms can be induced depending on several factors, such as the cell type, the PS or the exposure time. Traditionally, the desired end for malignant cells has been apoptosis, since it does not induce a systemic response as aggressive as the one induced by necrosis, which has been considered harmful especially due to the inflammatory effect (GARG ET AL., 2010). Nowadays, knowledge on cell death is increasing and new mechanisms are being discovered (GALLUZZI, KEPP, ET AL., 2012; GALLUZZI ET AL., 2018). This opens the door to activate other cell death mechanisms to induce malignant cells death.

Several mechanisms of cell death have been described in unicellular and pluricellular organisms. Nevertheless, classification and characterization of cell death mechanisms is challenging due to the intricate biochemistry involving normal cell function. As a result, characteristic features of a particular cell death mechanism may not be exclusive. For example, mitochondrial outer membrane permeabilization (MOMP), a characteristic process of intrinsic apoptosis, also occurs during extrinsic apoptosis and during normal differentiation of megakaryocytes and granulocytes (GALLUZZI ET AL., 2008). Another example is the implication of Fas cell surface death receptor (FAS) and tumor necrosis factor receptor 1 (TNFR1) both in extrinsic apoptosis and necroptosis (GALLUZZI ET AL., 2018).

The Nomenclature Committee on Cell Death (NCCD) recommended in 2012 a classification of cell death in three types: apoptosis, necrosis and autophagy. They also considered mitotic catastrophe, despite not being a "true" cell death type (GALLUZZI, VITALE, ET AL., 2012). In spite of the advances at molecular level, this morphological classification of cell death mechanisms is still extensively used, albeit it has some limitations to fit the current knowledge in this field (GALLUZZI ET AL., 2018). It is known that apoptotic cells maintain their plasma membrane integrity and metabolic activity until the end of the process, when a fast clearance by macrophages (and other phagocytic cells) occurs. Apoptosis has been traditionally defined as a highly regulated process involved in both physiological and pathological situations (RAFF, 1992; STELLER, 1995; WHITE, 1996). Deregulation of apoptosis has been related to carcinogenesis, tumor progression and radio- and chemotherapy resistance (LU ET AL., 2005; RAMP ET AL., 2005).

On the other hand, necrosis was traditionally considered for many years an unregulated, and just accidental, cell death that courses with a strong inflammatory response due to a plasma membrane disruption resulting in the liberation of some intracellular molecules known as damage-associated molecular patterns (DAMPs) or alarmins (GREEN ET AL., 2009; POON, HULETT AND PARISH, 2010). Nowadays, it is accepted that necrosis can also occur in a regulated manner and that it plays a role in multiple physiological and pathological situations, and multiple terms have been coined to identify the more

recently described cell death mechanisms (GALLUZZI, VITALE, ET AL., 2012; GALLUZZI ET AL., 2018).

More recently, the NCCD modified and updated the previous recommended classification, which was based on morphological criteria, to include more detailed molecular definitions that remark the differences between essential and accessory aspects of cell death and the interconnectivity of the different cell death types from a therapeutic perspective (GALLUZZI ET AL., 2015, 2018). Thus, cell death classification has changed from the original three morphologically-based types to a new one with only two types: accidental cell death (ACD), which involves instantaneous and catastrophic death after large injuries, and regulated cell death (RCD), normally related to homeostasis maintenance. There is also a particular form of RCD known as programmed cell death (PCD) that occurs in physiological conditions and is not related to homeostasis disruption and adaptation failure to stress (GALLUZZI ET AL., 2018). The current classification of RCD mechanisms is summarized in Figure 1.

Some of the best known mechanisms of RCD are explained below:

- **Intrinsic apoptosis:** It starts with intracellular stress conditions, like DNA damage, oxidative stress or excessive Ca^{2+} concentration in the cytosol, among others (GALLUZZI, VITALE, ET AL., 2012). Although there are a wide variety of triggering cascades for intrinsic apoptosis, they are all connected to a central mitochondrial mechanism of control (KROEMER, GALLUZZI AND BRENNER, 2007). Caspases play an important role in intrinsic apoptosis. They are a family of cysteine-aspartate-proteases consisting of more than a dozen proteins of which only eight are involved in apoptotic processes (ULUKAYA ET AL., 2011). Intrinsic apoptosis has MOMP as the critical step, a process controlled by B-cell lymphoma 2 (BCL2) family members, which include pro-apoptotic (killers and regulators) and anti-apoptotic (protectors) proteins (Figure 2). MOMP necessarily requires BCL2-associated X (BAX) protein and BCL2-antagonist/killer 1 (BAK1) protein, although their activities can be inhibited by the protector members of the BCL2 family, such as BCL2 or BCL2-like 1 (BCL-X$_L$). The regulator BCL2 proteins (which contain a BCL2 homology 3 (BH3) domain) are activated

A modality of RCD triggered by perturbations of extracellular or intracellular homeostasis that critically depends on MLKL, RIPK3, and (at least in some settings) on the kinase activity of RIPK1.

A form of RCD initiated by oxidative perturbations of the intracellular microenvironment that is under constitutive control by GPX4 and can be inhibited by iron chelators and lipophilic antioxidants.

A type of RCD that critically depends on the formation of plasma membrane pores by members of the gasdermin protein family, often (but not always) as a consequence of inflammatory caspase activation.

A modality of RCD initiated by PARP1 hyperactivation and precipitated by the consequent bioenergetic catastrophe coupled to AIF-dependent and MIF-dependent DNA degradation.

A type of RCD that originates from actomyosin-dependent cell-in-cell internalization (entosis) and is executed by lysosomes.

A ROS-dependent modality of RCD restricted to cells of hematopoietic derivation and associated with NET extrusion.

Specific form of RCD triggered by perturbations of the intracellular microenvironment and relying on CYPD.

Specific variant of RCD initiated by perturbations of the extracellular microenvironment detected by plasma membrane receptors, propagated by CASP8 and precipitated by executioner caspases, mainly CASP3.

Type of RCD initiated by perturbations of the extracellular or intracellular microenvironment, demarcated by MOMP, and precipitated by executioner caspases, mainly CASP3.

A form of RCD that is sufficient to activate an adaptive immune response in immunocompetent hosts.

A form of RCD that mechanistically depends on the autophagic machinery (or components thereof).

A type of RCD demarcated by primary LMP and precipitated by cathepsins, with optional involvement of MOMP and caspases.
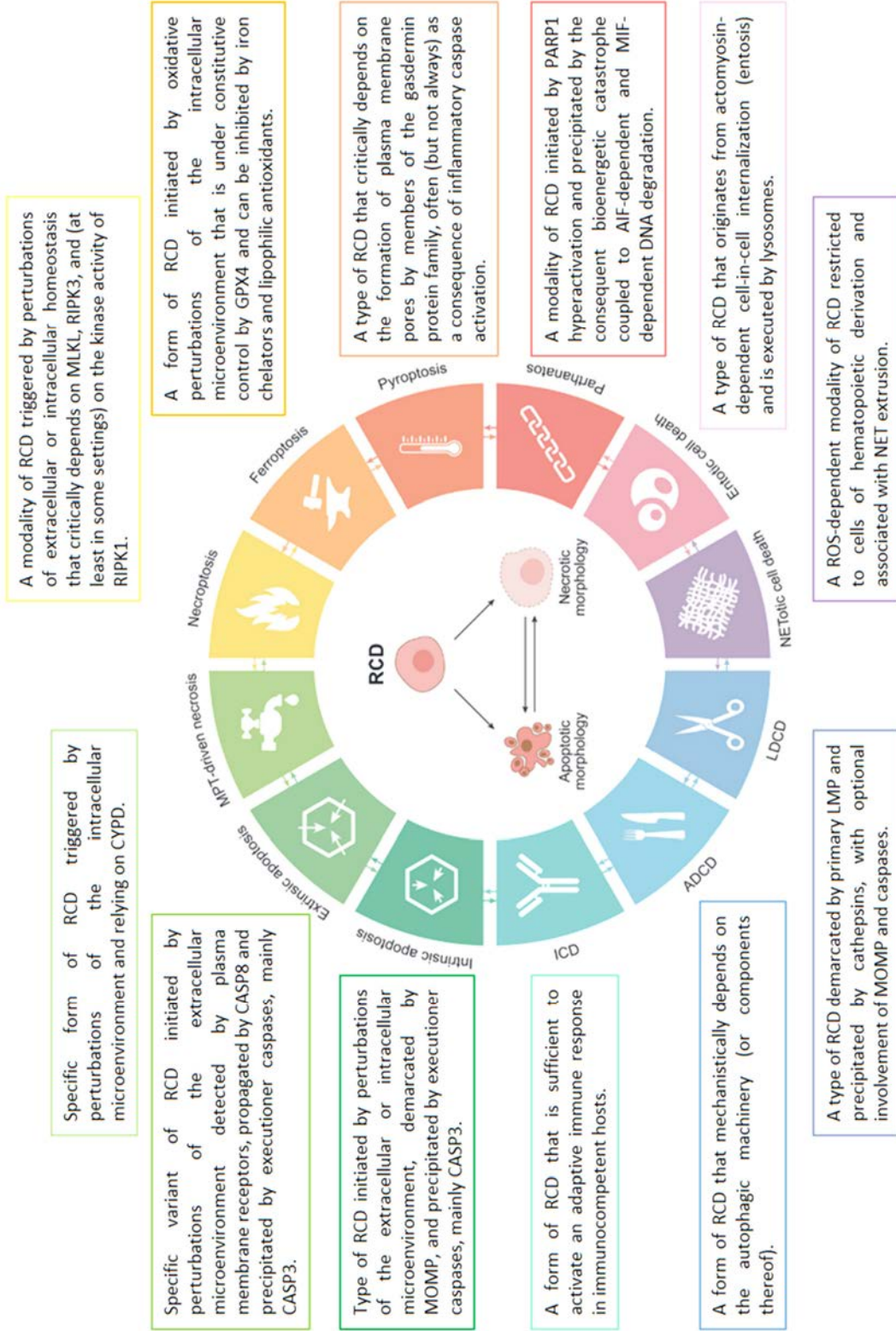
Figure 1. Principal regulated cell death (RCD) mechanisms (adapted from GALLUZZI ET AL., 2018).

transcriptionally or post-transcriptionally, depending on the disturbances suffered in the homeostasis of specific organelles or cell compartments, leading to BAX and BAK activation, which triggers MOMP. Then, mitochondrial intermembrane space proteins, like inhibitor of apoptosis (IAP)-binding mitochondrial protein (known as DIABLO or SMAC) and cytochrome *c*, are released into the cytosol. Cytochrome *c* interacts with deoxy-ATP and apoptotic peptidase-activating factor 1 (APAF1) to assemble the apoptosome, which activates caspase-9 (Ichim and Tait, 2016). The activation of caspase-9 leads to caspase-3 activation, inducing the apoptotic death of the cell (Galluzzi et al., 2015, 2018). SMAC can block the X-linked inhibitor of apoptosis protein (XIAP), facilitating apoptosis to occur (Ichim and Tait, 2016).
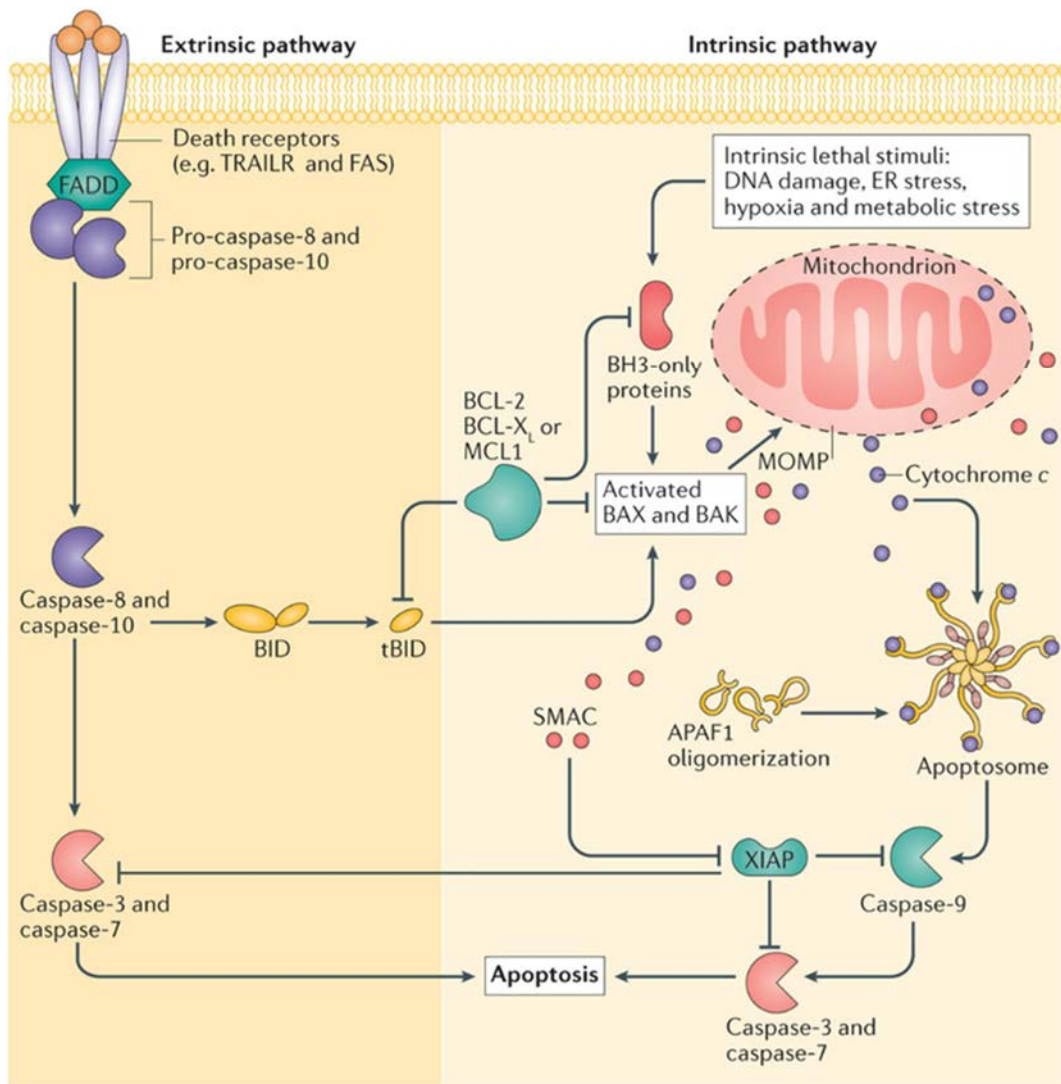

Figure 2. Extrinsic and intrinsic apoptotic pathways (Ichim and Tait, 2016).

- **Extrinsic apoptosis:** This mechanism is triggered by extracellular stress signals sensed and propagated by specific death receptors, including FAS and tumor necrosis factor receptor (TNFR) family members (Figure 2) (GALLUZZI ET AL., 2018). In 2012, the NCCD proposed a definition of extrinsic apoptosis as a caspase-dependent cell death subroutine, so that it can be suppressed by caspase inhibitors (GALLUZZI, VITALE, ET AL., 2012). The initiator caspases (caspase-8 and caspase-10) are activated through proteolytic cleavage and posterior dimerization mediated by adaptor proteins, like FAS-associated death domain (FADD) protein. These active caspases induce the activation of effector caspase-3 and caspase-7, which lead to apoptosis (ICHIM AND TAIT, 2016). The activation of a caspase-8/caspase-3 signal transduction axis that, in some cases, also involves MOMP through the activation of BH3-interacting death domain agonist (BID), enables a crosstalk between intrinsic and extrinsic apoptosis. The extracellular signal will or will not lead to MOMP depending on the expression of XIAP, whose high levels actually prevent the direct activation of caspase-3 by caspase-8. This blocking can be avoided by the release of SMAC and other XIAP inhibitors (GALLUZZI ET AL., 2015; ICHIM AND TAIT, 2016).

- **Necroptosis:** Although it was first considered a type of intrinsic apoptosis, nowadays it is known and accepted that necroptosis can be triggered by perturbations that affect extracellular or intracellular homeostasis. Necroptosis critically depends on the activation of mixed lineage kinase domain-like (MLKL) and receptor-interacting protein kinase 3 (RIPK3), and also on RIPK1 kinase activity in some cases. Necroptosis mediates adaptative responses to stress, but it is also involved in developmental safeguard programs and in the maintenance of T-cell homeostasis in adults (GALLUZZI ET AL., 2018).

- **Parthanatos:** It occurs as a response to DNA damages produced by alkylating agents (ZONG ET AL., 2004; WANG, DAWSON AND DAWSON, 2009) but not only, since oxidative stress, hypoxia, hypoglycemia or inflammatory cues can also induce this death mechanism, which is characterized by DNA fragmentation independent of apoptotic caspases (GALLUZZI ET AL., 2018). In parthanatos, poly-

(ADP-ribose)-polymerase-1 (PARP-1), an enzyme involved in DNA repair, is overactivated consuming a lot of energy and producing, as a consequence, cell death through energy depletion (MOUBARAK ET AL., 2007; BARITAUD ET AL., 2010). Specific pharmacological inhibitors of PARP1 can delay the parthanatos response in several cell types, both *in vivo* and *in vitro* (GALLUZZI ET AL., 2018).

- **Autophagy-dependent cell death:** Autophagy is a normal process in all cell types, that occurs in a lysosome-dependent manner. It is also named "self-eating" because it is used to remove the cell's own organelles and molecules. Autophagy is important to maintain homeostasis in adaptive responses to stress (like starvation or infection), but also in normal cell differentiation. When autophagy fails to maintain homeostasis, an autophagy-dependent cell death can occur (ALBERTS ET AL., 2014). During autophagy, cytoplasmic material is entrapped into vesicles known as autophagosomes, which contain cytosolic portions and intact organelles, such as mitochondria. These autophagosomes fuse with lysosomes generating autolysosomes where their contents are digested (KROEMER AND LEVINE, 2008). Autophagic cell death refers to a cell death mechanism accompanied by a massive vacuolization of the cytoplasm, which is activated under cell stress states (GALLUZZI ET AL., 2007; KROEMER ET AL., 2009). Autophagic responses are not related to caspases, as many other RCD variants, but they are biochemically associated with the microtubule-associated protein 1 light chain 3 (MAP1LC3 or LC3) lipidation and the sequestosome 1 (SQSTM1) degradation, among others (GALLUZZI ET AL., 2015).

I   1.2. Mechanism of action of PDT

PDT is based on the combination of three elements that have no effect by themselves, but that can produce a toxic effect when combined. These elements are: i) a photosensitizer that accumulates in target cells or tissues, ii) a light source of a specific wavelength to excite the PS (usually red light due to its higher tissue penetration capacity), and iii) oxygen, the raw material for ROS production (DOLMANS, FUKUMURA AND JAIN, 2003; JUARRANZ ET AL., 2008; AGOSTINIS ET AL., 2011; YOON, LI AND SHIM, 2013).

When a PS is excited by a specific wavelength, it changes from its basal state (S_0) to an excited singlet state (S_1), which may undergo intersystem crossing to a triplet state (T_1). At this point, the T_1 PS can transfer its energy to triplet state molecular oxygen ($^3O_2$), forming singlet oxygen ($^1O_2$), while the PS returns to its basal state (type II reaction. Figure 3). Singlet oxygen is highly reactive and can interact with many biomolecules, such as lipids, proteins or nucleic acids, producing cell death. Alternatively, the T_1 PS can interact with an organic molecule, becoming reduced (type I reaction). The subsequent reactions of the reduced PS produce several types of ROS. For instance, its autooxidation promotes the formation of superoxide anion (O^{2-}), whose dismutation or one-electron reduction produces hydrogen peroxide (H_2O_2). This H_2O_2 can produce hydroxyl radical ($OH\cdot$) if it suffers one-electron reduction. All the mentioned ROS are highly reactive and can damage cells and even cause cell death (AGOSTINIS ET AL., 2011). Type II reaction predominates in environments that are rich in oxygen, whereas type I reaction occurs mainly in hypoxic conditions (JUARRANZ ET AL., 2008; JEONG ET AL., 2011) (Figure 3).
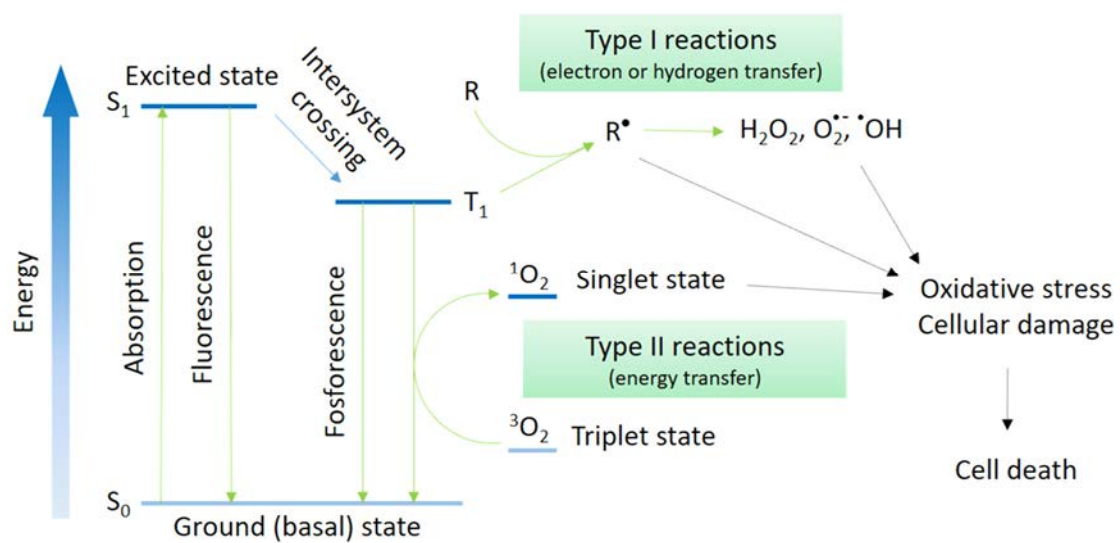

Figure 3. Jablonski diagram adapted to photophysical processes that occur to a photosensitizer (PS) during photodynamic therapy.

In vivo, PDT can act at different levels to destroy tumors (AGOSTINIS ET AL., 2011; ALLISON AND MOGHISSI, 2013):

- **Direct damage on cancer cells.** It occurs when the PS accumulates in cancer cells, producing ROS that directly kill the tumoral cells (BUYTAERT, DEWAELE AND AGOSTINIS, 2007).

- **Damage on tumor vasculature.** Many tumors induce angiogenesis to achieve more irrigation for a faster growth. When PDT damages these new vessels, causing thrombosis and hemorrhages, the consequent lack of oxygen will slow down tumor growth or even destroy it (BHUVANESWARI ET AL., 2009).

- **Immune system activation.** Due to the blood-vessel damage in tumors, a local inflammation occurs and cytokines and stress-response proteins are released. All these attract leukocytes and stimulate the immune system, finally leading to the recognition and destruction of tumoral cells (BRACKETT AND GOLLNICK, 2011). This is an advantage over other therapies, such as radio- or chemotherapy, whose effects are the opposite, leaving an immunosuppressed patient more sensitive to other diseases (NOWIS ET AL., 2005; BRACKETT AND GOLLNICK, 2011).

Several factors modulate the importance of these mechanisms, such as the type of PS, the treatment dose, the time between PS administration and irradiation, and the oxygen concentration present in the target tissue (AGOSTINIS ET AL., 2011).

I   1.3. Photosensitizers

The first PS used in PDT was hematoporphyrin (Hp), which was characterized by Meyer-Benz at the beginning of the 20th century. Later, the hematoporphyrin derivative (HPD) was synthesized by Lipson and Baldes (LIPSON AND BALDES, 1960), being this considered the start of modern PDT. Lipson and Baldes observed that HPD accumulated preferentially in tumoral cells and emitted red fluorescence when irradiated with UV light (LIPSON, BALDES AND OLSEN, 1961). Afterwards, Dougherty's group discovered that irradiation of HPD produced the regression of breast tumors in mice (DOUGHERTY ET AL., 1975), and they later synthetized new porphyrins modifying their structure by acetilation (DOUGHERTY, 1983) and characterized the HPD active principle (DOUGHERTY, POTTER AND WEISHAUPT, 1984). The first approved PS for clinical use was Photofrin® (ALLISON AND SIBATA, 2010), a HPD preparation more purified than its predecessors, but

still a mixture of more than 60 compounds. Photofrin® has not enough tumoral specificity, requires high doses, and can produce skin hypersensitivity after each session. These non-ideal features and disadvantages lead the scientific community to look for more efficient PSs with better physicochemical characteristics and biological responses.

Based on the history and evolution of PSs, they can be classified in three groups:

- **First generation PSs**. The first molecules used as PSs were the porphyrins, like Photofrin®. They showed some limitations, such as low selectivity and high cutaneous photosensitivity (Kossodo and LaMuraglia, 2001; Allison and Moghissi, 2013).

- **Second generation PSs**. These are more tumor-selective agents with reduced side effects. Most of them are cyclic tetrapyrroles, comprising substituted derivatives of porphyrin, chlorin and bacteriochlorin. This group includes several PSs currently used in the clinic, such as benzoporphyrin derivative monocarboxylic acid (BPD-MA), m-tetrahydroxyphenylchlorin (m-THPC, Foscan®) or some phthalocyanines (Yoon, Li and Shim, 2013).

- **Third generation PSs**. Finally, in order to achieve better target specificity, the third generation PSs combine the PS with a vehicle, such as monosaccharides (Zheng and Pandey, 2008), peptides (Shadidi and Sioud, 2003), low density lipoproteins (LDL) (Polo et al., 2002), antibodies (Vrouenraets et al., 2000), polymers (Greco, 2008) or nanoparticles (María E Alea-Reyes et al., 2017).

Nowadays, several PSs can be used in the clinic, such as the 5-aminolevulinic acid (5-ALA) and its methylated ester (MAL), or the benzoporphyrin derivative (verteporfin, Visudyne®), as second or third generation PSs (Juarranz et al., 2008; Agostinis et al., 2011; Allison and Moghissi, 2013). Nevertheless, none of these PSs possess all the ideal features, being the development and characterization of new PSs one of the current goals of PDT.

The cellular response to photodynamic treatments depends on multiple factors, like the PS concentration, irradiation dose, the cell type, the PS subcellular location or the PS vehicle (PENG, MOAN AND NESLAND, 1996; CAÑETE, STOCKERT AND VILLANUEVA, 2009; KRAMMER AND VERWANGER, 2012). Studying the influence of these parameters in cell cultures is the first step towards the clinical use of PDT. Depending on the tumor, different outcomes would be desired. For instance, a necrotic response that generates a local inflammation and immune system activation is sought in some tumors, but in cerebral tumors these mechanisms should be avoided in favor of an apoptotic response that excludes inflammation (GARG ET AL., 2010).

I   1.4.1. Treatment conditions

Treatment depends mainly on three parameters: PS concentration, time after PS administration and irradiation dose. By regulating these parameters, different responses can be induced in target cells.

- **PS concentration:** Depending on the PS and its concentration, different types of cell death can be induced. For example, erythrosine can induce an apoptotic response at low concentrations, but causes necrosis at high concentrations (GARG ET AL., 2012). Methylene blue has been reported to cause apoptotic death in V79 cells, but faster (3 h post-irradiation) at high concentrations and slower (within 48 h post-irradiation) at low concentrations (NOODT ET AL., 1998).

- **Incubation time before irradiation:** The cell death mechanism induced by PDT can also change depending on the incubation time. For example, CV-1 cells incubated with Photofrin® underwent necrosis when the incubation times were short, whereas at longer incubations apoptotic death was induced. This is probably due to a differential distribution of the PS: at short times Photofrin® was still at the plasma membrane, whereas at longer times it was present in several organelles (DELLINGER, 1996; HSIEH ET AL., 2003; SORIANO ET AL., 2013).

- **Irradiation dose:** It has been reported for several PSs, such as Aluminium phthalocyanine (AlPc), meso-tetrakis (p-methoxyphenyl) porphyrin (TMPP) and Foscan®, that low irradiation doses produce mainly apoptotic cell death, whereas high doses preferentially induce necrosis (Villanueva, 1993; Luo and Kessel, 1997; Marchal et al., 2005). For other PSs, for example, aluminium tetra sulfo-phthalocyanine (AlTSPc) or its zinc counterpart (ZnTSPc), there is an optimal light dose that, when exceeded, produces a photobleaching effect and a consequent decrease of cell death in UACC62 cells. Photobleaching consists in a photochemical degradation of the PS due to an excessive light exposition (Maduray et al., 2011; Maduray, Odhav and Nyokong, 2012; Yoon, Li and Shim, 2013).

I 1.4.2. Influence of the cell type

Several studies have demonstrated that the same PS can produce different effects in different cell lines, albeit the same experimental conditions were applied. In this sense, Palladium (II)-tetra phenyl-porphycene (PdTPPo) can cause an apoptotic response in HeLa cells, whereas it produces necrosis in A549 cells (Cañete et al., 2004). On the other hand, 5-ALA was reported to induce different responses at different times post-irradiation depending on the cell line (Wyld, Reed and Brown, 2001).

I 1.4.3. Photosensitizers vehiculization

Frequently, PSs need to be modified in order to achieve better physicochemical properties to be administered. For example, when the PS is poorly soluble in aqueous solutions, the use of organic solvents (like ethanol or dimethylsulfoxide) allows its dissolution in aqueous solvents (Vargas et al., 2004; Chin et al., 2008). Hydrophobic PSs can also be stabilized with molecules (like serum albumin) to prevent their aggregation (aggregated PSs are less efficient than monomeric species) (Alarcón et al., 2009).

On the other hand, the effect of many PSs can be enhanced when attached to vehicles by minimizing problems such as degradation or fast circulation clearance, and improving accumulation in the target tissues. This accumulation is also increased through the enhanced permeability and retention (EPR) effect that usually occurs in tumors (Jin and

ZHENG, 2011; MUEHLMANN ET AL., 2011). Some examples of vehicles that can be used are antibodies (VAN DONGEN, VISSER AND VROUENRAETS, 2004), liposomes (CALIXTO ET AL., 2016) or nanoparticles (RANA ET AL., 2007; CHUNG ET AL., 2013; CALIXTO ET AL., 2016) (see section 2.1.).

2. Nano- and microsystems as drug carriers and delivery agents in nanomedicine

Nowadays, nanotechnology has a huge impact on different fields, such as defense, aeronautics, energy, food safety, environmental science or biomedicine, among many others (SARGENT JR., 2014), due to the new possibilities that the use of nanotechnology has opened to overcome several limitations in science and technology and to facilitate research development (ALBANESE, TANG AND CHAN, 2012; ALAM ET AL., 2014). In the field of nanomedicine, the evolution of nanotechnology is allowing the renewal of imaging, diagnostic and therapeutic (theranostics) systems, focused mainly against cancer, with the help of new nanomaterials and devices (DAVIS, CHEN AND SHIN, 2008). A wide range of materials can be used to design nanoparticles (NPs) and microparticles (µPs) with a chemically modifiable surface, which allows to attach many ligands and use these devices as biosensors (RAY ET AL., 2012), imaging agents (MCCARTHY AND WEISSLEDER, 2008) or delivery vehicles (BROWN ET AL., 2010), among others.

NPs have unique physicochemical features that allow drug carrying and monitoring in real-time with high precision (YANG ET AL., 2012). Moreover, the surface of NPs can be coated with different agents to develop multifunctional or multimodal NPs (MMNPs), which can integrate several capabilities in a single entity such as imaging, monitoring, targeting or drug delivery (LIONG ET AL., 2008). For example, the attachment of an imaging agent will allow monitoring of the NPs; a specific targeting molecule will direct NPs to their target cells; a cell-penetrating agent will allow their entrance into the target cells; and several drugs could act in different ways to achieve the desired therapeutic effect (Figure 4). Moreover, the same particle can carry several chemotherapeutic, anti-angiogenic and gene therapy agents to exert the therapeutic effect synergistically (integrated theranostics) (FERNANDEZ-FERNANDEZ, MANCHANDA AND MCGORON, 2011).

Surface modifications can enhance or facilitate NPs circulation through the circulatory system, so that their circulation time, pharmacokinetics and extravasation through the vessel walls will ultimately depend on the particles design (DECUZZI ET AL., 2009; ARVIZO ET AL., 2011; TAN ET AL., 2013). Nevertheless, it has been reported that unmodified NPs and µPs already show a tendency to accumulate in tumoral tissues, rather than in normal ones, due to the abnormal architecture of blood vessels in the tumor region. This is known as the enhanced permeability and retention (EPR) effect (Figure 5). Moreover, the lack of an effective lymphatic drainage is frequent in tumor tissues. As a result, an altered transport dynamics is found in tumoral environments, which enhances the extravasation of macromolecules and particles and allows an increased retention (CHATTERJEE, FONG AND ZHANG, 2008; MAEDA, 2010; ACHARYA AND SAHOO, 2011).
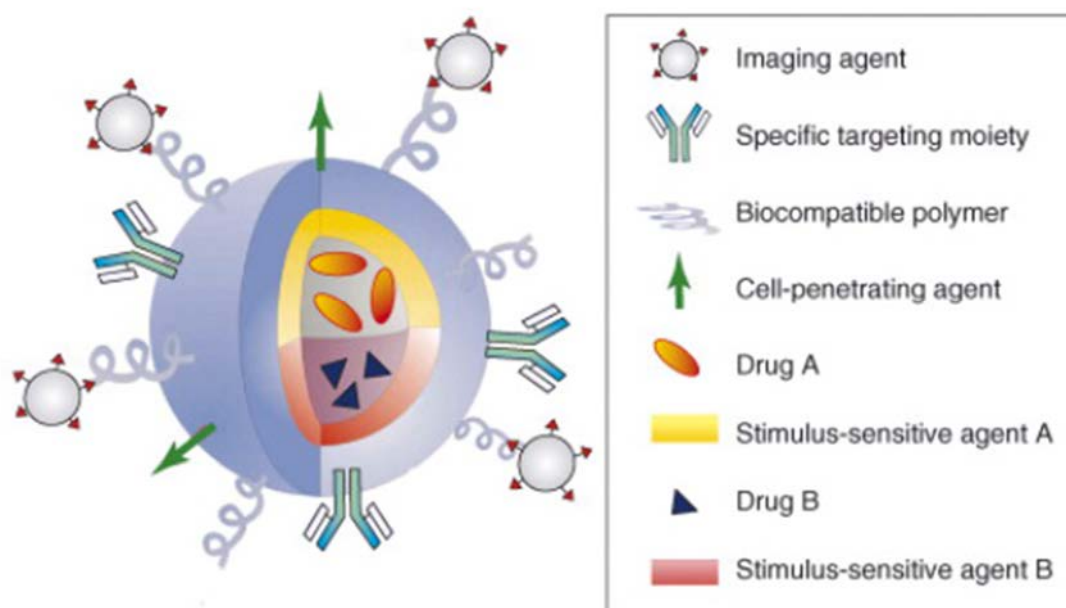
Figure 4. Potential particle modifications to construct a multifunctional device (SANVICENS AND MARCO, 2008).

2.1. Types of nano- and microsystems used as drug carriers

Several types of nano- and microsystems can be used as drug carriers. Some of the most relevant are summarized in Figure 6 and explained below:

- **Liposomes:** Liposomes were the first drug delivery system approved for clinical uses and, currently, several liposome-based nano-drugs have been approved for the clinical practice while others are already in the clinical trials phase (ALAM ET AL., 2015). Liposomes are vesicles composed of a central hydrophilic space (core) surrounded by single or multilamellar lipid bilayers with sizes between 30 nm and several micrometers. They are usually used to encapsulate lipophilic and/or hydrophilic molecules into their lipid layers and their core, respectively, to better reach their target site (ALLEN AND CULLIS, 2013). Liposomes can incorporate other molecules, such as polymers (ADLAKHA-HUTCHEON ET AL., 1999) or targeting molecules (WANG ET AL., 2014), in order to increase the circulation time or improve the drug delivery and, consequently, enhance the therapeutic effects.
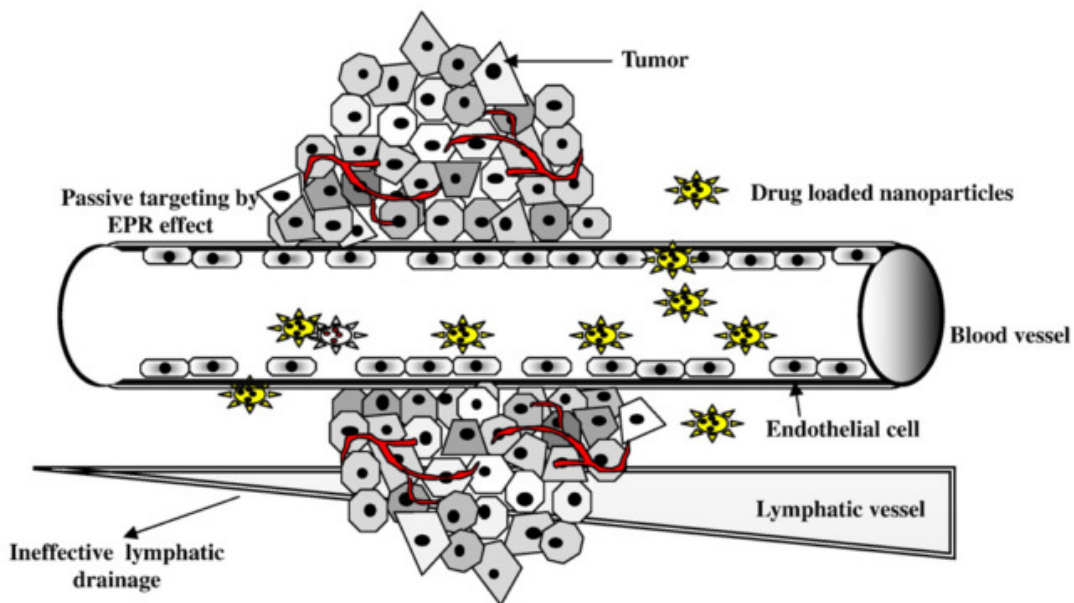

Figure 5. Enhanced permeability and retention (EPR) effect. Particles and other molecules tend to accumulate in tumoral tissues, collaterally protecting healthy cells from undesired effects. In order to grow, tumor cells stimulate angiogenesis, which usually results in new vessels with architecture abnormalities, like wide fenestrations or the absence of a smooth muscle cells layer (ACHARYA AND SAHOO, 2011).

- **Polymeric micelles:** These NPs, of 10 to 100 nm in diameter, consist of polymer chains with a hydrophobic or ionic core and a shell structure that can play various roles, such as drug-carriers or for imaging or diagnosis purposes. These carriers

have been used to encapsulate different lipophilic anticancer drugs to prevent their aggregation in aqueous solutions, which could cause embolism when administered intravenously (TORCHILIN ET AL., 2003).
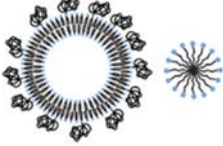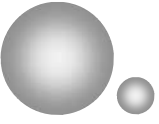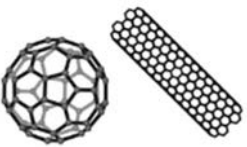
	Particle type	Composition/Structure	Applications
	Lipid	Liposomes, micelles	Drug delivery
	Polymer (particles and micelles)	PLGA, glycerol, chitosan, DNA; monomers, copolymers, hydrogels	Drug delivery; passive release (diffusion), controlled release (triggered), imaging
	Dendrimer	PAMAM, etc	Drug delivery
	Polystyrene	Nanoparticles, microparticles	Drug delivery
	Gold nanoparticles	Spheres, rods, shells	Hyperthermia therapy, drug delivery, imaging
	Silica	Spheres, shells, mesoporous	Contrast agents, drug delivery (encapsulation)
	Magnetic nanoparticles	iron oxide or cobalt-based; spheres,aggregates in dextran or silica	Contrast agents (MRI), hyperthermia therapy
	Quantum dots	CdSe, CuInSe, CdTe, etc	Optical imaging
	Carbon-based	Carbon nanotubes, buckyballs, graphene	Drug delivery, hyperthermia therapy

Figure 6. Classification of the principal nano- and microsystems that can be used as drug carriers (adapted from DAWIDCZYK, RUSSELL AND SEARSON, 2014).

- **Polymeric nanoparticles:** Biodegradable polymers like poly(lactic-co-glycolic acid) (PLGA), polyethylene glycol or chitosan, can be used for NP fabrication. For example, PLGA-NPs with a nuclear localization sequence attached have been used as doxorubicin carriers, improving its therapeutic efficacy against breast cancer cells (Misra and Sahoo, 2010).

- **Dendrimers:** Dendrimers are polymers of symmetrical and regularly branched macromolecules. They acquire spherical shapes and measure between 2 and 10 nm in diameter (Bosman, Janssen and Meijer, 1999). Multiple variants of dendrimers can be constructed, for example, having an isophyllic end-group like a carboxyl group that can make the dendrimer soluble in water. Dendrimers can carry drugs in their core cavities, which can be designed either hydrophilic or hydrophobic (Cheng et al., 2011). For instance, for cancer theranostics use, a multifunctional dendrimer with a covalent attachment of a cytotoxic drug created a prodrug, inactive until the drug release (Majoros et al., 2006).

- **Polystyrene nano- and microparticles:** Polystyrene is a widely used polymer fabricated through the polymerization of styrene monomers. Polystyrene NPs and μPs display high homogeneity, a low index of polydispersity and the ability to form stable colloids in biological environments (Loos et al., 2014). The main feature that make polystyrene particles so appropriate for nanomedicine uses is their easily modifiable surface (van Midwoud et al., 2012). In addition, their inertness and biocompatibility makes polystyrene particles a good choice for their use as drug carriers.

- **Gold nanoparticles (GNPs):** These can have different shapes (spheres, nanoshells, nanorods or nanocages) and can carry different molecules simultaneously, like therapeutic drugs and targeting agents. When GNPs interact with some molecules, their physicochemical properties can be altered producing detectable signals and enabling GNPs to act, for instance, as quenchers with higher efficiency than conventional organic quenching substances (Uehara, 2010). Due to their optical and electrical properties, GNPs can also be used for cell imaging, photothermal ablation or drug treatment, making them really

versatile and promising for cancer theranostics (HUANG AND EL-SAYED, 2011; KENNEDY ET AL., 2011; JAIN, HIRST AND O'SULLIVAN, 2012).

- **Silica particles:** Another widely used component is silica, normally developed for imaging and sensing because it is a good host for fluorescent dyes, metal ions and drugs due to its easily modifiable surface for biomolecules attachment (TALLURY, PAYTON AND SANTRA, 2008).

- **Mesoporous silicon particles:** Silicon has high biocompatibility and its pore size can be controlled through its electrochemical synthesis, making silicon NPs and μPs promising candidates as drug carriers and deliverers (ANGLIN ET AL., 2008). The pores are perfect to encapsulate several molecules such as drugs (SALONEN ET AL., 2005) or siRNA (TANAKA ET AL., 2010; MA ET AL., 2013; MENG ET AL., 2013). In addition, the silicon surface can be easily functionalized in order to attach other kind of molecules for other applications, such as targeting or sensitive drug release (YANG, GAI AND LIN, 2012).

- **Magnetic nanoparticles:** Magnetic NPs are usually made with the iron oxides magnetite (Fe_3O_4) or maghemite (γ-Fe_2O_3) and can be used to target chemotherapeutic drugs to tumors. They can be injected in the organism and retained at a specific site using an external magnetic field (HÄFELI, 2004). Magnetic NPs can also be used for cancer hyperthermia (JORDAN ET AL., 1999), photodynamic therapy (PENON ET AL., 2016) or as contrast agents for magnetic resonance imaging (QIAO ET AL., 2012). In addition, super-paramagnetic iron NPs present low cytotoxicity and their surface can be functionalized with several molecules for targeting and/or drug delivery (HUANG ET AL., 2011; YOFFE ET AL., 2012).

- **Quantum dots (QDs):** QDs are spherical NPs smaller than 100 nm in diameter. QDs consist of a crystalline semiconductor core coated by a shell with optical properties and covered by a cap to enable hydrosolubility (RHYNER ET AL., 2006). As they are highly resistant to photobleaching (NAGASAKI ET AL., 2004), they are

excellent for imaging purposes and, when functionalized, they can target the desired cells.

- **Carbon nanotubes (CNTs):** CNTs have a cylindrical structure made of rolled graphene sheet (single walled) or sheets (multiwalled), having 1 nm in diameter and between 1 and 100 nm in length. Graphene is a material constructed by hexagonal networks of carbon atoms, which confer high mechanical strength, thermal resistance and conductivity (electric and thermal) to CNTs. CNTs have a large surface to which many molecules can be attached (YANG ET AL., 2011). Moreover, multiwalled CNTs can be used for thermotherapies due to their high optical absorbance in the near-infrared (BURKE ET AL., 2009; DING ET AL., 2011).

I 2.2. Particle interactions with biological components

The described carriers should be designed and functionalized taking into account that they will interact with several biological components at different levels. In order to cause the desired effects, NPs and µPs should be able to reach their target cells and interact with them. But, in a pluricellular organism like the human body, several biological barriers would difficult or impede the free circulation of NPs and µPs, preventing the particles to reach their target. These barriers start at the systemic level, go through the organ level and finish at the cellular level (PETROS AND DESIMONE, 2010).

I 2.2.1. Barriers at the systemic and organ level

The initial barriers that NPs and µPs will encounter inside the body would depend on the administration way (oral, inhaled, topical, intravenous or intraperitoneal). To overcome these barriers, several strategies can be applied. For instance, size can be very relevant for a good pulmonary delivery (SUNG, PULLIAM AND EDWARDS, 2007), whilst an optimal carrier stability should be obtained to overcome the harassing conditions of the gastrointestinal tract (ROGER ET AL., 2010). For an intravenous administration, it is advisable to apply a preinjection of decoy carriers to saturate the phagocytic capacity of the cells of the reticulo-endothelial system (PETROS AND DESIMONE, 2010). On the other hand, the alteration of the carrier surface could reduce its opsonization, preventing the addition of removal marks. Alternatively, specific proteins, such as cell surface proteins,

could be attached to the carrier surface in order to cheat fagocytic cells (Petros and DeSimone, 2010).

Biological fluids contain several biomolecules which can interact with NPs and µPs in different ways. The adsorption of serum proteins and other molecules on particles, when they enter the circulatory system, can lead to the formation of a protein corona around the particles (Nel et al., 2009). This corona can influence the particles biodistribution (Monopoli et al., 2011; Bargheer et al., 2015), circulation time (Sakulkhu et al., 2014) and cellular uptake (Yan et al., 2013; Ritz et al., 2015). Also, the protein corona can reduce the specificity of NPs by masking the targeting molecules (Salvati et al., 2013).

2.2.2. Barriers at the cellular level

Once NPs or µPs reach their target cell, a new barrier emerges: the plasma membrane, which blocks diffusion of charged molecules and molecules bigger than about 1 kDa (Petros and DeSimone, 2010). Thus, endocytic mechanisms will be needed to allow the internalization of the particles.

Endocytic mechanisms have been traditionally divided into two groups: phagocytosis ("cell eating", involving the endocytosis of large particles) and pinocytosis ("cell drinking", involving smaller molecules, fluids and solutes), which will be explained in detail below (Figure 7).

Phagocytosis

This mechanism allows the internalization of large complexes (more than 200 nm), including microorganisms, foreign materials or dead cells. In multicellular organisms, it is normally restricted to specialized cells, such as macrophages and neutrophils of the reticulo-endothelial system, although other cells, such as fibroblasts, endothelial cells and epithelial cells, can also exhibit phagocytic skills under some conditions (El-Sayed and Harashima, 2013). Phagocytosis requires the stimulation of a cell-surface receptor to activate the phagocytic machinery through the "eat-me" signals present on the foreign body surface or by an "indirect" recognition due to its opsonization. Phagocytosis starts with the formation of surface protrusions promoted by actin

polymerization, which wrap and internalize the foreign body forming an endocytic vesicle in the cytosol, known as the phagosome.
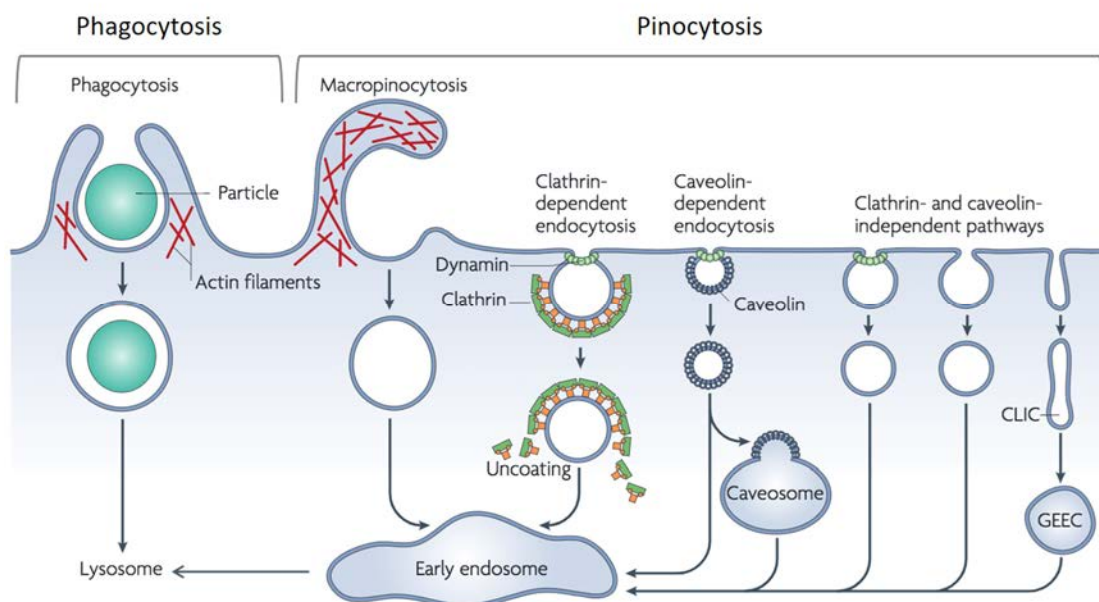

Figure 7. General view of the most relevant endocytic mechanisms (adapted from MAYOR AND PAGANO, 2007).

Usually, phagosomes follow the degradative endolysosomal pathway, so their contents end up in the lysosomes (phagolysosomes) where the internalized material is degraded. Lysosomes contain soluble hydrolytic enzymes that can digest many types of molecules. All are acid hydrolases whose major activity occurs at low pH. There are about 50 types of acid hydrolases and they are highly specialized in the hydrolysis of different molecules, such as lipids, proteins, DNA, RNA or polysaccharides (COOPER, 2008). Some indigestible substances remain in the lysosomes forming residual bodies that can be secreted by a process known as exocytosis (ALBERTS ET AL., 2014).

Pinocytosis

This endocytic mechanism occurs in all cell types and mainly involves the internalization of fluids and solutes, forming pinocytic vesicles. Pinocytosis can be classified as:

- **Macropinocytosis**: This process can be non-specific and starts with a cell-surface protusion called ruffle formed by the polymerization of actin microfilaments.

Then, the ruffle collapses engulfing the extracellular material into a vesicle called macropinosome. The presence of macropinosomes larger than 5 µm or even 10 µm in diameter has been reported (ARSIANTI ET AL., 2010; EL-SAYED AND HARASHIMA, 2013).

Depending on the cell type, macropinosomes can follow different pathways, although, in the majority of the situations, they mature similarly to classical endosomes. Macropinosomes start acidification while they acquire early endosome markers, like the early endosome antigen 1 (EEA1) and/or Rab5. Then, macropinosomes can continue reducing their pH while shrinking and acquiring late endosome markers, and fuse with other late endosomes or lysosomes (MERCER AND HELENIUS, 2012). On the other hand, macropinosomes can also recycle their content to the extracellular matrix through their fusion with the plasma membrane, as mainly occurs, for instance, in A531 human carcinoma cells (HEWLETT, PRESCOTT AND WATTS, 1994).

- **Clathrin-mediated endocytosis**: This is a receptor-mediated mechanism present in all eukaryotic cells. It involves a wide variety of membrane receptor proteins that can interact with several macromolecules to form a specific internalization complex. Clathrin-mediated endocytosis starts with a signal promoted by some of these macromolecules when binding specific transmembrane receptors, and it is followed by the recruitment of clathrin, a soluble intracellular protein that polymerizes on the inner hemimembrane of the plasma membrane (MCMAHON AND BOUCROT, 2011). Clathrin recruitment is leaded by the adaptor proteins, which bind on the one side to the receptor with the cargo and, on the other side, to clathrin, also mediating the selective gain of membrane and soluble cargo molecules into the vesicle (ALBERTS ET AL., 2014). Then, clathrin polymerization stabilizes the membrane curvature, which results in a clathrin-coated pit. Later, the protein dynamin polymerizes forming a coil that constricts the pit neck until the pinch off of the clathrin-coated pit occurs (EL-SAYED AND HARASHIMA, 2013). All this process takes place in a short period of time, since in about one minute a clathrin-coated vesicle is formed.

The resultant clathrin-coated vesicles have a mean size of 120 nm in diameter (TEKLE ET AL., 2008; WANG ET AL., 2010). Once they detach from the membrane, they lose their clathrin coat and can fuse one with another, or with vesicles resulting from other endocytic processes, to form an early endosome. In the early endosome the pH decreases until a range of 6.1-6.8 while the internalized molecules are sorted. Early endosomes have two distinguishable parts: a tubular side from where recycling endosomes are formed; and a bulbous, vacuolar region that drives the cargo to the degradative endolysosomal pathway. Non-recycled molecules remain in the bulbous region, which matures into a multivesicular body and, then, a late endosome, with a more acidic lumen where pH can reach values of 4.8 (EL-SAYED AND HARASHIMA, 2013). Finally, the late endosome fuses with a lysosome to form an endolysosome, where the cargo starts to be degraded at a pH of around 4.5, at which hydrolases can act (Figure 8).
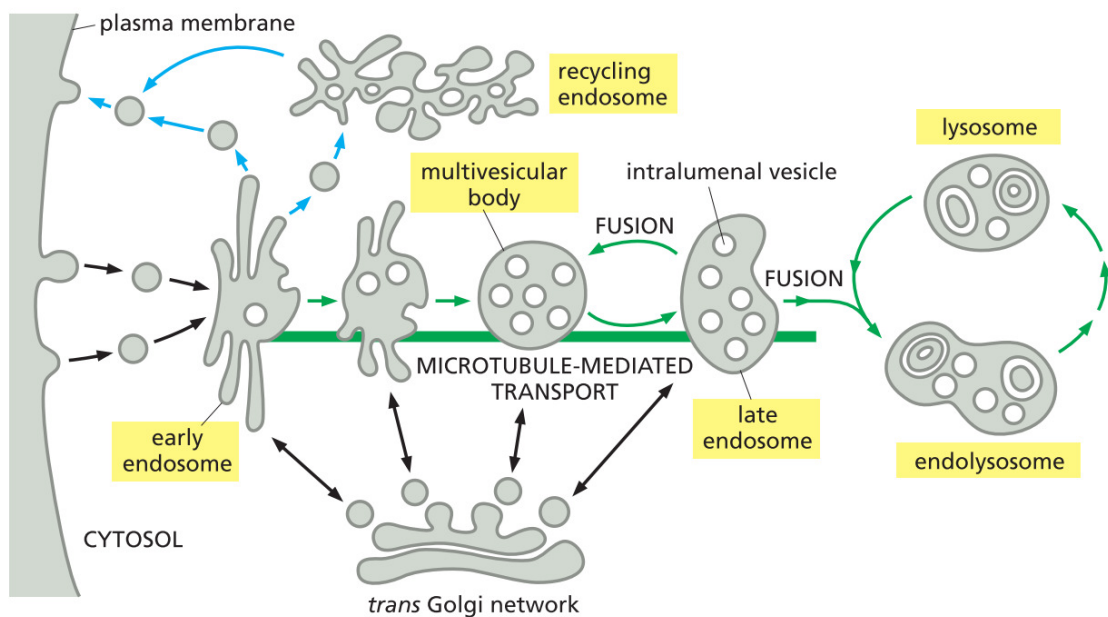

Figure 8. Endosome maturation from the plasma membrane until the lysosomes (ALBERTS ET AL., 2014).

As explained above, to internalize molecules by clathrin-mediated endocytosis a receptor is needed and will be present in the clathrin-coated vesicle membrane. From here, the receptor can either be recycled to the plasma membrane or

Photosensitizers and microparticles as tools against malignant cells

degraded in the lysosomes with the endocytic cargo. A well-known receptor endocytic pathway is that involving the LDL receptor. In the early endosome, the LDL receptor changes its conformation due to the low pH, releasing its ligand. Then, the empty receptor is recycled to the plasma membrane through recycling endosomes that emerge from the tubular region of the early endosome. Concurrently, the released LDL is leaded to the lysosome to be digested.

Other endocytic receptors, such as the transferrin receptor (TfR), are recycled to the plasma membrane together with their ligands. The TfR present in the plasma membrane binds transferrin with iron. When they arrive at the early endosome, iron is released from transferrin due to the low pH, but iron-free transferrin (apotransferrin) remains bound to its receptor. Then, the TfR-apotransferrin complex is recycled back to the plasma membrane from the tubular extensions of early endosomes. Once the complex returns to the neutral pH present in the extracellular medium, apotransferrin is released and the cycle can restart (ALBERTS ET AL., 2014).

Alternatively, endocytosed receptors can follow the degradative endolysosomal pathway together with their ligands, as is the case of the epidermal growth factor (EGF) receptor (EGFR). In this case, the EGF-EGFR complex does not dissociate in the early endosome, and both the receptor and the ligand end up in the lysosome, where they are degraded. This decreases the number of EGFR at the cell surface, in turn diminishing the cell ability to internalize EGF (ALBERTS ET AL., 2014).

- **Caveolin-mediated endocytosis**: This is another receptor-mediated mechanism of endocytosis, in this case, associated with the presence of caveolin, a dimeric membrane protein. The vesicles are thought to form from lipid rafts (membrane domains enriched in cholesterol and sphingolipids), where caveolin drives the formation of small invaginations called caveolae (CONNER AND SCHMID, 2003). The cytosolic side of caveolins is linked to large complexes of proteins that are likely stabilizing the membrane curvature. Contrary to clathrin-mediated endocytosis, caveolae usually remain static, unless their pinch off is induced by a signal that

causes caveolin phosphorilation (ALBERTS ET AL., 2014). The vesicles resulting from this endocytic mechanism have an approximated diameter of 60-80 nm (EL-SAYED AND HARASHIMA, 2013).

Different vesicles formed from caveolae can fuse to form a caveosome, which is able to avoid the endolysosomal pathway and transfer its cargo to the endoplasmic reticulum (ER) or even the Golgi apparatus, although it can also undergo the endolysosomal pathway. Alternatively, the initially formed vesicles can directly fuse with an endosome instead of the caveosome (PARTON AND SIMONS, 2007).

- **Clathrin- and caveolin-independent endocytosis**: There are several mechanisms that are still being unraveled. Some authors relate these mechanisms to lipid rafts with similar composition as caveolae (BAREFORD AND SWAAN, 2007; SANDVIG ET AL., 2008; EL-SAYED AND HARASHIMA, 2013). The formed vesicles normally undergo the degradative endolysosomal pathway, but more controlled studies are needed to better understand and describe these other endocytic mechanisms (EL-SAYED AND HARASHIMA, 2013).

I	2.2.3. Parameters influencing the interaction of particles with cells

There is a wide variety of physicochemical features that influence the exact way in which a particle interacts and penetrates into a cell, like particle size, shape, surface charge and modifications. In addition, the cell type also plays an important role.

Particle size influences the kinetics (CHITHRANI, GHAZANI AND CHAN, 2006) and the mechanism of endocytosis (REJMAN ET AL., 2004). However, there is not a consensual agreement on the minimum and maximum particle sizes that use each endocytic mechanism. In a study in non-phagocytic B16 cells, small particles (less than 200 nm) were preferentially endocytosed by clathrin-mediated endocytosis, whilst larger particles (from 200 nm to 1000 nm) were found more likely to enter via the caveolin-mediated endocytic pathway (REJMAN ET AL., 2004). Nonetheless, the relation between particle size and endocytic mechanism can vary among different cell lines (ZAUNER, FARROW AND HAINES, 2001).

Regarding particles shape, contradictory results have been published. For example, some studies report that spherical particles show the easiest entry into cells (CHITHRANI, GHAZANI AND CHAN, 2006; MURO ET AL., 2008), whilst others disagree, pointing that cylindrical shapes are a better choice (GRATTON, NAPIER, ET AL., 2008; GRATTON, ROPP, ET AL., 2008). Another study found that sharp-shaped NPs could escape from the endolysosomal system, whereas spherical NPs remained entrapped or were exocytosed (CHU ET AL., 2014). This variability could be due to the influence of other factors, such as the nature of the particle, its size or its surface charge, in addition to the cell type.

Probably due to the presence of negatively charged molecules at the surface of the plasma membrane, such as some glycoproteins or phospholipids, positively charged particles showed a better cellular intake than negatively charged ones (SINGH ET AL., 2000; MAO ET AL., 2005; HARUSH-FRENKEL ET AL., 2007; HAUCK, GHAZANI AND CHAN, 2008; THOREK AND TSOURKAS, 2008; ZHANG ET AL., 2013). It has also been reported that, depending on the density of the polycations, positively charged particles can induce membrane permeability by the formation of holes at the nanometric scale (CHEN ET AL., 2009).

Internalization can also be influenced by the modification of the particles surface. For example, attaching cationic polymers (CALVO, VILA-JATO AND ALONSO, 1997; LABALA ET AL., 2015) or peptides rich in cationic aminoacids (BROCK, 2014; COPOLOVICI ET AL., 2014) turns particles surface more positive and, thus, improves internalization. Particles can also be modified by conjugating a molecule that can be recognized by a plasma membrane receptor. Examples of such molecules are polyethylene glycols, which are recognized by LDL receptors (KIM ET AL., 2007), and transferrin or folate, which are recognized, in cancer cells, by the overexpressed receptors of transferrin (HÖGEMANN-SAVELLANO ET AL., 2003; TROS DE ILARDUYA AND DÜZGÜNEŞ, 2013) or folate (WONG AND CHOI, 2015), respectively. Monoclonal antibodies, like trastuzumab (SLAMON ET AL., 2001; LEWIS PHILLIPS ET AL., 2008) or lapatinib (GEYER ET AL., 2006) against the human epidermal growth factor receptor 2 (HER2 or ERBB2), overexpressed in several cancers (STUCHINSKAYA ET AL., 2011; SELIGER AND KIESSLING, 2013; AWADA ET AL., 2016), have also been used to biofunctionalize particles. These modifications do not only improve the internalization of the biofunctionalized particles, but they also allow to target them to specific cells. On the other hand, polymeric nanoparticles can release their cargo specifically in tumor environments

when using chemical bonds between the particle and its cargo sensitive to abnormal pH conditions, oxygen levels or enzymes that are overexpressed by tumoral cells (ALAM ET AL., 2015).

As already mentioned, the cell type can also influence the interaction with NPs and µPs. For example, the same µPs interacted in a different way with normal (MCF10A) and tumoral (SKBR3) breast epithelial cells, showing opposite responses to the same particle modifications: MCF10A showed more internalization of non-coated polystyrene µPs and less of polyethyleneimine (PEI)-coated ones, whilst SKBR3 preferred coated µPs over the naked ones (PATIÑO ET AL., 2015). In addition, the importance of the cell density has also been reported. For example, in KLN 205 cells, a mouse squamous carcinoma cell line, the internalization of polystyrene microspheres 560 nm in diameter was high (70%) when cells were actively growing, but there was not a detectable intake when cells were confluent. On the contrary, the same beads were almost equally (55-61%) internalized by growing or confluent ECV 304 cells, a derivative of the human bladder carcinoma cell line T24, highlighting the relevance of the cell line behavior in the presence of NPs or µPs (ZAUNER, FARROW AND HAINES, 2001).

I 2.2.4. Strategies for releasing endolysosomal contents into the cytosol

One of the major problems of nanomedicine is the fact that many therapeutic agents end their journey in the lysosomes. Their entrapment, accumulation and degradation is one of the major obstacles that impedes their action (SHETE, PRABHU AND PATRAVALE, 2014). Nevertheless, this limitation becomes an advantage when the final fate of the drug is the lysosomal compartment, as it is the case of some lysosomal diseases or Alzheimer therapies (BAREFORD AND SWAAN, 2007).

To free therapeutic agents from endolysosomal entrapment, the membrane of this compartment needs to be disrupted or permeabilized. To accomplish this, several approaches have been developed, including chemical, biological, and physicochemical escape enhancing strategies.

- **Chemical escape enhancers:** The use of highly positively charged molecules has shown their ability to surpass the endolysosomal barrier. This may occur due to

electrostatic interactions able to destabilize the endolysosomal membranes (YUHONG XU AND FRANCIS C. SZOKA ET AL., 1996), the proton-sponge effect (BOUSSIF ET AL., 1995), or a combination of both (SHRESTHA ET AL., 2012). The proton-sponge effect occurs when some cationic molecules, such as PEIs, which are rich in amino groups, buffer the endolysosomal pH through a massive accumulation of protons in their functional groups, behaving as "sponges" for protons. As the protons are recruited by the molecule, the proton pumps present in the endolysosomal membrane continue operating to increase the quantity of free protons inside the endolysosomal compartment. In parallel, there is an influx of Cl$^-$ to compensate the increasing number of positive charges inside the endolysosomes and to prevent the formation of a membrane potential. In the end, an osmotic swelling occurs due to an excessive entrance of water and endolysosomal disruption takes place, allowing the release of the contents into the cytosol (BOUSSIF ET AL., 1995) (Figure 9). Thus, coating or biofunctionalizing the particles surface with cationic molecules such as PEI may help to overcome the endolysosomal barrier, although this strategy may not be effective for the release of large µPs (PATIÑO ET AL., 2015).
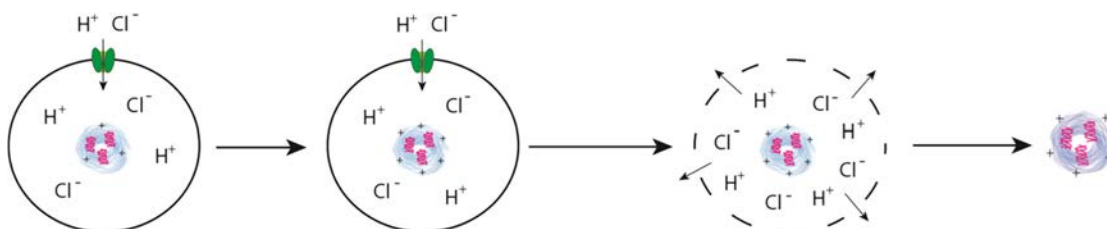

Figure 9. The proton sponge effect. The internalized molecule recruits positive charges that are compensated by an influx of Cl$^-$. Finally, an osmotic swelling occurs causing endolysosomal disruption and the release of endolysosomal contens into the cytosol (AGIRRE ET AL., 2014).

On the other hand, it has been described that polymers suffer a volumetrical expansion when they become highly protonated at low pH (umbrella hypothesis), which also contributes to the disruption of the endolysosomal membrane (NGUYEN AND SZOKA, 2012). Based on this, polymeric nanoparticles

with the skill of changing their size depending on their surrounding pH have been developed (Mura, Nicolas and Couvreur, 2013).

- **Biological escape enhancers:** Virus and bacterial toxins conform the most relevant biological escape enhancers. Viruses are naturally able to fuse with the plasma membrane, but can also be endocytosed. They have evolved to show specific viral fusion proteins and cell-penetrating peptides (CPPs) able to mediate endolysosomal escape (Fuchs, Weng and Gilabert-Oriol, 2016). For example, insulin or β-galactosidase, but also nucleic acids for gene therapy, have been delivered into the cytosol using CPPs derived from virus (Copolovici et al., 2014; Fuchs, Weng and Gilabert-Oriol, 2016). On the other hand, the exotoxins produced by some bacteria, such as the anthrax toxin from *Bacillus anthracis*, have similar effects, so that their truncated versions are also used for endolysosomal escape purposes (Fuchs, Weng and Gilabert-Oriol, 2016).

  Less studied are the eukaryotic escape enhancers, but they mainly comprise CPPs and pore forming proteins (Rosado et al., 2014; Zhang, Wang and Xu, 2016). The most studied eukaryotic CPP is penetratin, which corresponds to the binding domain of a *Drosophila* transcription factor. Penetratin has been used for cytosolic delivery of nucleic acids and toxins (Fuchs, Weng and Gilabert-Oriol, 2016).

- **Physicochemical escape enhancing strategies:** These are based on the physicochemical principles and reactions that can directly promote the contents release of the endolysosomal vesicles by membrane disruption. Some of these techniques include the use of ultrasounds (Omata et al., 2011), magnetic fields (Luo et al., 2012), plasmonic nanobubbles (Lukianova-hleb et al., 2012), pH-sensitive bonds (Alam et al., 2015) or photochemical internalization (PCI) (Berg et al., 1999; Weyergang et al., 2015). All these techniques need an external source, like a source of ultrasonic waves, a magnetic field or a specific wavelength light.
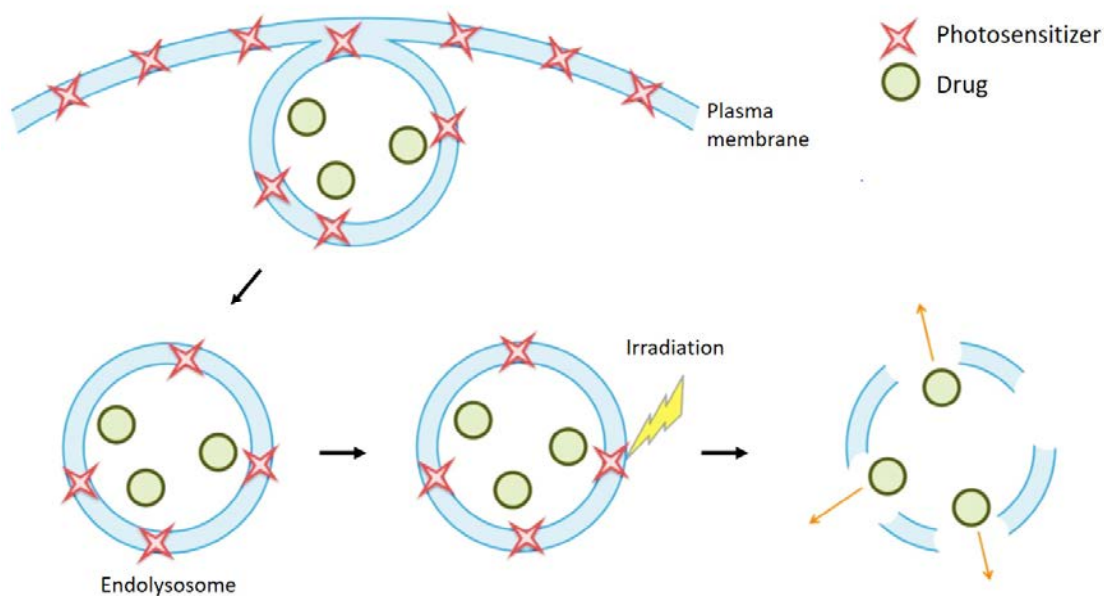
Figure 10. Photochemical internalization (PCI) mechanisms of action. A photosensitizer is integrated in the plasma membrane and consequently integrated in the endocytic vesicles. Then, irradiation excites the photosensitizer allowing the release of the endocytic contents (adapted from LIANG AND LAM, 2012).

PCI is based on the same principle as PDT: the activation of a PS by light and the subsequent formation of ROS. PSs used in PCI usually have a lipophilic or amphiphilic structure that allows their integration in the plasma membrane and their accumulation in the endolysosomal membranes after endocytosis. When the irradiation produces the PS excitation, the generated ROS induce lipid peroxidation that disrupts the endolysosomal membranes allowing their content to escape into the cytosol (Figure 10). The exact structure of the damaged membranes is still unknown (PRASMICKAITE ET AL., 2002). Using PCI, it has been reported that therapeutic drugs (WEYERGANG ET AL., 2011; LEE ET AL., 2013), DNA molecules for gene therapy (BOE AND HOVIG, 2013) or even NPs (SELBO ET AL., 2010) are able to escape from the endolysosomal system (BERG ET AL., 1999; NISHIYAMA ET AL., 2005; OHTSUKI ET AL., 2015). PCI-mediated release of endocytic content can last up to 6-8 h after irradiation, due to the fusion of new endocytic vesicles with the previously photodamaged ones (PRASMICKAITE ET AL., 2002).

PCI has demonstrated to be very effective for some applications, such as the better response in animal models treated with ribosome-inactivating protein

toxins (Selbo et al., 2001; Dietze et al., 2005), the improved therapeutic efficacy and specificity of saporin conjugated with EGF (Weyergang, Selbo and Berg, 2006) and of PCI targeted gene delivery vectors (Bonsted et al., 2008), or the improved cytotoxic effect of bleomycin both *in vivo* and *in vitro* (Berg, 2005).
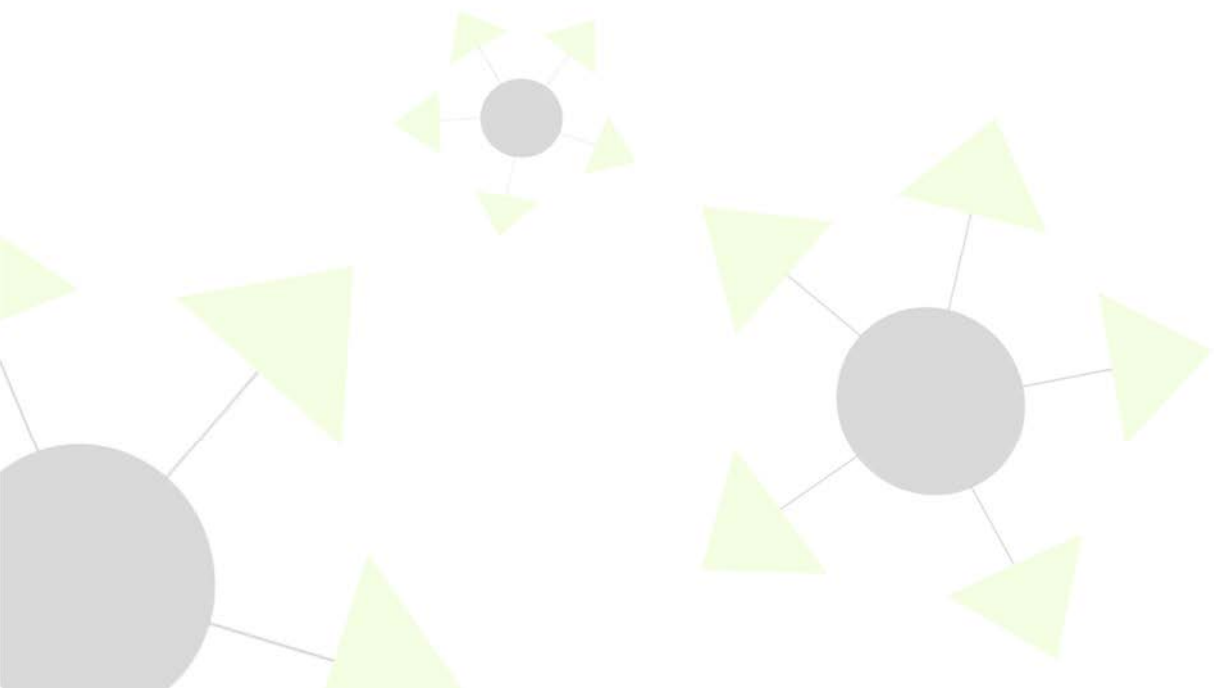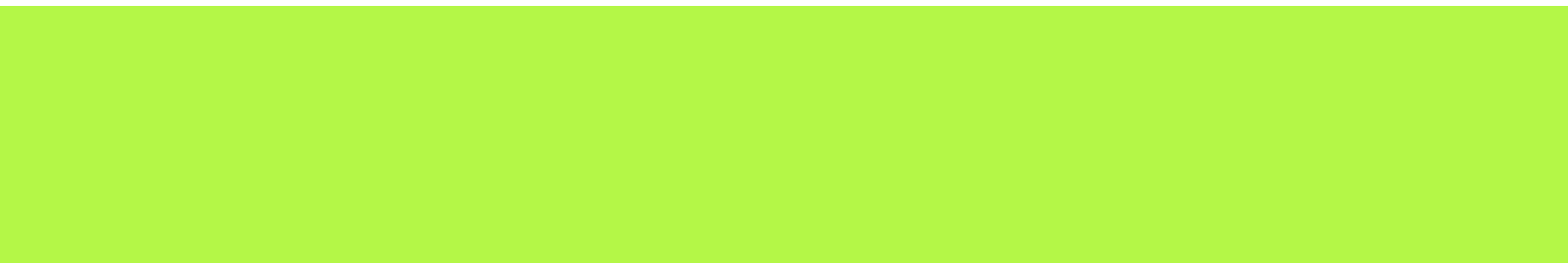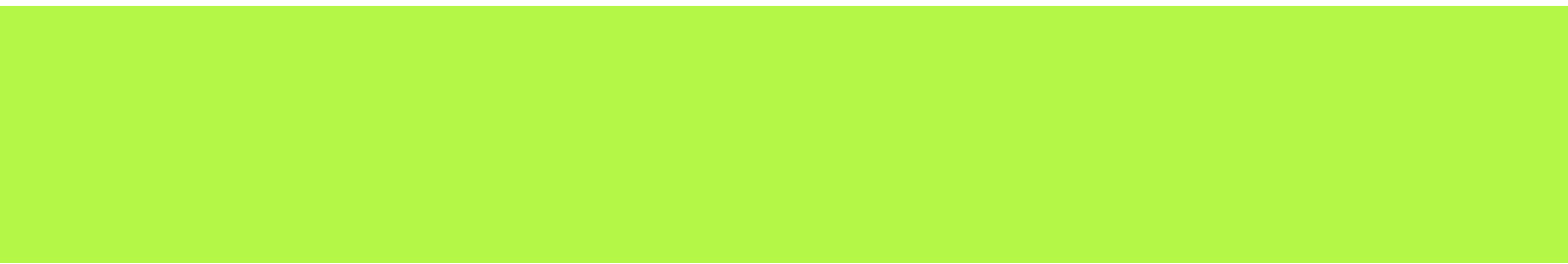
II

Objectives

The present Thesis is part of an interdisciplinary project aimed at selectively destroying malignant cells by using photodynamic treatments and/or biofunctionalized ⬚Ps. In this sense, the main objective is to specifically direct PSs or other therapeutic drugs to target tumoral cells by using biofunctionalized ⬚Ps as both targeting and delivery vehicles. This thesis represents the first step of the project and its specific objectives can be defined as follows:

1st. To evaluate the efficacy of two different PSs to induce cell death in photodynamic treatments of non-tumoral and tumoral human breast epithelial cells.

2nd. To assess the type of cell death mechanism induced by photodynamic treatments with the two photosensitizers in the two cell lines.

3rd. To evaluate the influence of µPs biofunctionalization with specific or non-specific molecules on cell targeting and µPs internalization by non-tumoral and tumoral human breast epithelial cells cultured in different conditions.

4th. To assess the effectivity of PCI for the release of µPs entrapped inside the endolysosomal compartment.

5th. To investigate the ultrastructural effects of PCI on the endolysosomal membranes.
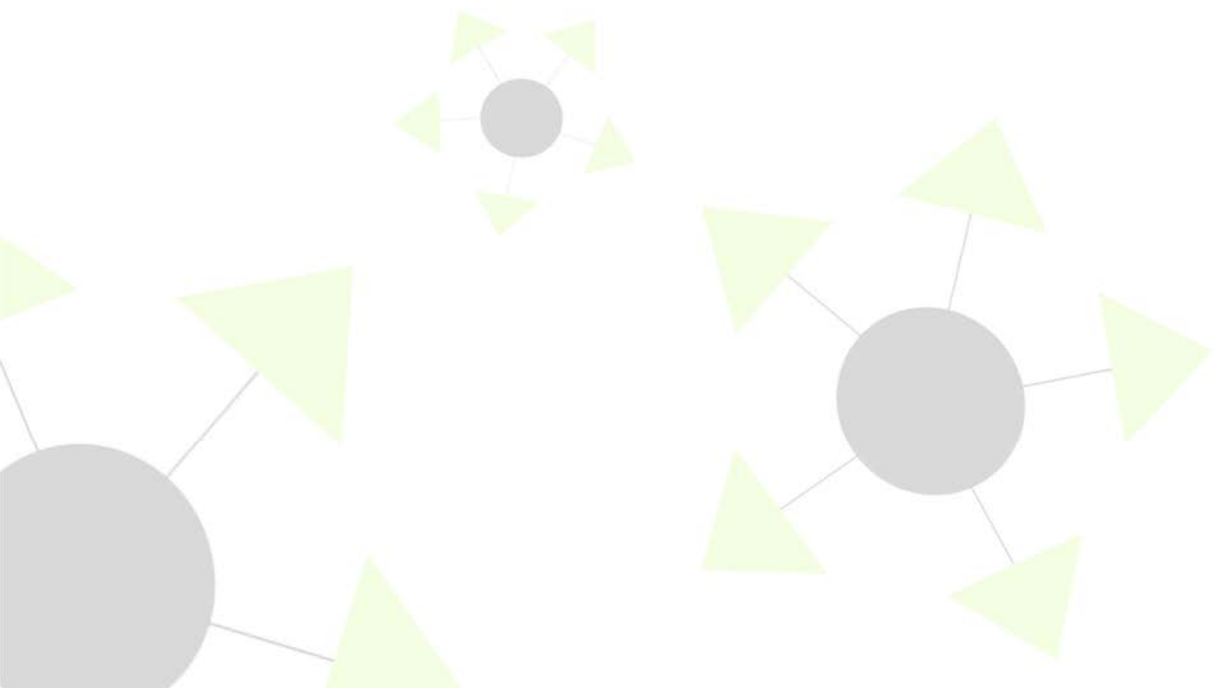
III

Results

Cell Death Mechanisms in Tumoral and Non-Tumoral Human Cell Lines Triggered by Photodynamic Treatments: Apoptosis, Necrosis and Parthanatos

J. Soriano[1], I. Mora-Espí[1], M. E. Alea-Reyes[2], L. Pérez-García[2,†], L. Barrios[1], E. Ibáñez[1] & C. Nogués[1]

[1]Departament de Biologia Cel·lular, Fisiologia i Immunologia, Universitat Autònoma de Barcelona, Spain.

[2]Departament de Farmacologia, toxicologia i Química Terapèutica and Institut de Nanociència i Nanotecnologia (IN2UB), Universitat de Barcelona, Spain.

[†] Present address: School of Pharmacy, The University of Nottingham, University Park, Nottingham, NG72RD, UK.

Abstract

Cell death triggered by photodynamic therapy can occur through different mechanisms: apoptosis, necrosis or autophagy. However, recent studies have demonstrated the existence of other mechanisms with characteristics of both necrosis and apoptosis. These new cell death pathways, collectively termed regulated necrosis, include a variety of processes triggered by different stimuli. In this study, we evaluated the cell death mechanism induced by photodynamic treatments with two photosensitizers, meso-tetrakis (4-carboxyphenyl) porphyrin sodium salt (Na-H2TCPP) and its zinc derivative Na-ZnTCPP, in two human breast epithelial cell lines, a non-tumoral (MCF-10A) and a tumoral one (SKBR-3). Viability assays showed that photodynamic treatments with both photosensitizers induced a reduction in cell viability in a concentration-dependent manner and no dark toxicity was observed. The cell death mechanisms triggered were evaluated by several assays and cell line-dependent results were found. Most SKBR-3 cells died by either necrosis or apoptosis. By contrast, in MCF-10A cells, necrotic cells and another cell population with characteristics of both necrosis and apoptosis were predominant. In this latter population, cell death was PARP-dependent and translocation of AIF to the nucleus was observed in some cells. These characteristics are related with parthanatos, being the first evidence of this type of regulated necrosis in the field of photodynamic therapy.

Introduction

Photodynamic therapy (PDT) is a therapeutic modality for the treatment of neoplastic and non-neoplastic diseases. It is based on the administration of a photosensitizer (PS) that accumulates in target tissues, followed by irradiation with visible light. The combination of PS, light and oxygen triggers photochemical processes leading to the formation of reactive oxygen species (ROS), which interact with cellular structures causing the selective destruction of the irradiated tissue[1,2]. Cell death triggered by PDT can occur through different mechanisms: apoptosis, necrosis, autophagy or mitotic catastrophe. The pathway that is activated after photodynamic treatments depends on the PS, treatment doses, subcellular localization of the PS and cell type[3–6]. Traditionally, necrosis has been considered an unregulated process independent of apoptosis.

However, recent studies have demonstrated novel mechanisms of cell death with characteristics of both apoptosis and necrosis, challenging this idea. The term "regulated necrosis" has been proposed by the Nomenclature Committee on Cell Death to comprise these mechanisms[7,8], which occur in response to numerous damaging situations such as alkylating damage of DNA, exposition to certain excitotoxins or pathogens, the binding of some ligands to membrane receptors or ROS exposition[9]. However, it is important to take into account that these triggers are not exclusive of regulated necrosis because, depending on the cellular context, they can induce other cell death mechanisms such as apoptosis.

Van den Berghe et al. defined regulated necrosis as a genetically controlled cell death process that eventually results in cellular leakage, and that is morphologically characterized by cytoplasmic granulation, as well as organelle and/or cellular swelling (oncosis)[10]. Multiple subroutines of regulated necrosis, such as necroptosis, parthanatos, ferroptosis, autosis, netosis or pyroptosis, share these features, but they are triggered by different stimuli and their underlying molecular pathways are different[10]. Parthanatos is one of the most studied mechanisms of regulated necrosis[11,12]. It is elicited by stimuli that induce DNA damage, such as ultraviolet irradiation, alkylating agents or ROS[13], which overactivate Poly (ADP-ribose) polymerase (PARP), an (ADP-ribosyl) transferase involved in DNA repair. This hyperactivation of PARP induces a massive PARtylation of proteins, depleting cells of NAD+ and ATP and leading to an energetic catastrophe. In addition, PARP hyperactivation produces PAR polymers that induce the release of the truncated form of apoptosis-inducing factor (AIF) from the outer mitochondrial membrane and its entry into the nucleus, where AIF induces nuclear fragmentation through a still unknown mechanism. In spite of the important role of ROS as an inductor of regulated necrosis, only a few studies have described regulated necrotic processes in response to photodynamic treatments[14–16]. The aim of this study was to evaluate the type of cell death mechanism induced by photodynamic treatment with two PSs, meso-tetrakis (4-carboxyphenyl) porphyrin sodium salt (Na-H$_2$TCPP) and its derivative zinc (II) meso-tetrakis (4-carboxyphenyl) porphyrin sodium salt (Na-ZnTCPP) (Fig. 1). Experiments were performed in two human breast epithelial cell lines, a non-tumoral (MCF-10A) and a tumoral one (SKBR-3).
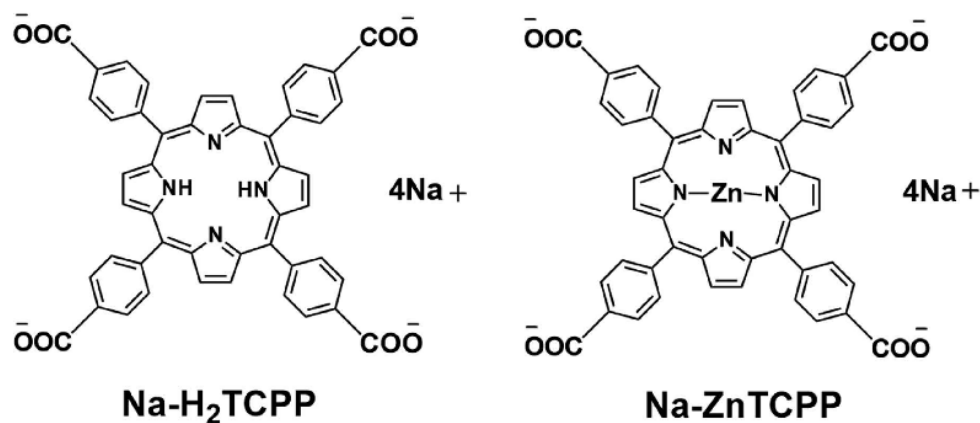
Figure 1. Structure of the porphyrins Na-H₂TCPP and Na-ZnTCPP.

Material and Methods

Porphyrins Na-H$_2$TCPP and Na-ZnTCPP. The structure of the Porphyrins Na-H$_2$TCPP and Na-ZnTCPP is shown in Fig. 1, and their synthesis has been reported elsewhere[28,29].

Cell culture. Experiments were conducted with two different human mammary epithelial cell lines, a non-tumorigenic (MCF-10A) and a tumorigenic one (SKBR-3). Both cell lines were purchased from American Type Culture Collection (ATCC, Manassas, VA, USA). The MCF-10A cell line was cultured in DMEM/F12 (Gibco, Paisley, United Kingdom) supplemented with 5% horse serum (Gibco), 20 ng/ml epidermal growth factor (Gibco), 0.5 mg/ml hydrocortisone (Sigma-Aldrich), 100 ng/ml cholera toxin (Sigma-Aldrich) and 10 μg/ml insulin (Gibco). The SKBR-3 adenocarcinoma cell line was cultured in McCoy's 5A modified medium (Gibco) supplemented with 10% fetal bovine serum (Gibco). Both cell lines were maintained at 37°C and 5% CO$_2$ (standard conditions).

For each experiment, cells were seeded in 24-well dishes, with or without coverslips, at a density of 50,000 cells/well. Treatments were performed 24 h after seeding.

Photodynamic treatments. Cells were incubated in serum-free medium with different concentrations of Na-H$_2$TCPP or Na-ZnTCPP (0.5, 1, 2 and 4 μM) for 3 h. Next, cells were washed thrice with Phosphate-Buffered Saline (PBS) and maintained in culture medium during irradiation and post-treatment. Irradiation was performed for 10 min using a

PhotoActivation Universal Light device (PAUL, GenIUL, Barcelona, Spain), in the range of 620–630 nm (red light) and with a mean intensity of 55 mW/cm^2.

MTT assay. Cell viability was determined 24 or 48 h after treatments by the 3-(4,5-dimethylthiazol-2-yl)-2,5diphenyltetrazolium bromide (MTT) assay (Sigma-Aldrich). The absorbance was recorded at 540 nm using a Victor 3 Multilabel Plate Reader (PerkinElmer, Waltham, MA, USA). To evaluate the toxicity of the PSs in absence of irradiation (Dark toxicity, DT), cells were also incubated with the maximum concentration of Na-H$_2$TCPP or Na-ZnTCPP (4 µM) and were kept in dark conditions. For each treatment, viability was calculated as the absorbance of treated cells in comparison with control cells. Three independent experiments were performed in each case.

Hoechst Staining and nuclear morphology analysis. Nuclear staining was performed 24 h after treatments. Cells grown on coverslips were fixed in cold methanol for 5 min, air dried and stained with 5 µg/ml Hoescht-33258 (H-33258, Life Technologies, Carlsbad, CA) for 3 min. Preparations were mounted in ProLong Gold (Life Technologies) and observed by fluorescence microscopy (Olympus IX70, Olympus, Hamburg, Germany). Previously described morphological criteria[14,30] were used to assess classic necrotic (small round shaped nuclei with highly condensed chromatin), regulated necrotic (nuclei with highly condensed chromatin spots, variable in number and shape) and apoptotic cells (nuclear shrinkage and fragmentation with apoptotic body formation). Hereafter, we will refer to the nuclear morphology of regulated necrotic cells as spotted nuclei.

TUNEL Assay. To detect DNA fragmentation, TUNEL assay was performed 5 h after the treatments. Cells grown on coverslips were fixed in 4% paraformaldehyde/PBS (Sigma-Aldrich) for 15 min at 4°C, washed thrice with PBS, permeabilized with 0.1% Triton X-100 (Sigma-Aldrich) in PBS for 2min and incubated with TUNEL reaction mixture (Roche, Indianapolis, IN, USA) for 1 h at 37°C. Cells were washed with PBS, mounted in ProLong Gold and observed under a Confocal Laser Scanning Microscope (CLSM, Olympus XT7).

Annexin V/Propidium Iodide Assay. Phosphatidylserine translocation and membrane integrity was evaluated using Annexin-V-FLUOS staining kit (Roche) 2 h after the

photodynamic treatments. The protocol was performed in accordance with manufacturer recommended conditions and samples were analyzed under a CLSM.

3-Aminobenzamide Treatments. Cells were incubated for 3 h in serum-free medium with different concentrations (0.5, 1 and 2mM) of a specific poly (ADP-ribose) polymerase (PARP) inhibitor, 3-aminobenzamide (3-AB, Sigma-Aldrich), in the presence or absence of 4 µM Na-H$_2$TCPP or Na-ZnTCPP. The samples were then washed thrice with PBS, irradiated for 10 min in the presence of 3-AB and incubated in the same medium without serum overnight. MTT assays were performed 24 h after irradiation.

Immunostaining. At 5 h of irradiation, cells grown on coverslips were fixed in 4% paraformaldehyde/PBS for 5 min, washed with PBS three times, permeabilized with 0.1% Triton X-100 in PBS and blocked with 5% BSA (Sigma-Aldrich) in PBS for 30 min. Cells were incubated for 1h at 37°C with either rabbit anti-apoptosis-inducing factor (AIF) polyclonal antibody (1:1000; Abcam, Cambridge, MA, USA. Ref: ab1998) or rabbit anti-active caspase 3 polyclonal antibody (1:1000; Sigma-Aldrich. Ref: C8487). Then, cells were washed with PBS three times and incubated 1 h at 37°C with Alexa 594-conjugated goat anti-rabbit IgG antibody (1:2000; Life Technologies. Ref: A-11012). Finally, cells were washed thrice with PBS, counterstained with 5 µg/ml H-33258 for 3 min, mounted in Prolong Gold and analyzed under a CLSM.

Statistical analyses. In order to quantify cell death morphologies, TUNEL positive nuclei, ANV/IP positive cells and active caspase-3 stained cells, three different and independent experiments were performed in each case and at least 250 cells were counted.

All graphics and statistical analyses were performed using GraphPad Prism version 6.00 for Windows, (GraphPad Software, La Jolla, California, USA). Analysis of variance (ANOVA) was run to test the effects of Na-H$_2$TCPP or Na-ZnTCPP on different cellular parameters. On the one hand, the results of TUNEL assay and active caspase-3 immunofluorescence assay were evaluated through one-way ANOVA. On the other hand, the effects of treatments with both PSs on cell viability, nuclear morphology or ANV/IP assay were determined through two-way ANOVA. In all cases, the minimal

significance level was set at P≤ 0.05. Data are shown as mean±standard error of the mean.

Significance is represented in the figures using an alphabetical superscript system on top of the columns. Letters shared in common between or among the groups would indicate no significant differences whereas different letters indicate statistically significant differences between groups.

Results

Cytotoxicity of photodynamic treatments. The phototoxic effect of Na-H_2TCPP and Na-ZnTCPP in MCF-10A and SKBR-3 cells is shown in Fig. 2. In absence of irradiation (dark toxicity, DT), the highest concentration of both PSs (4 µM) did not induce a significant decrease of cell viability at 24 h when compared with cells incubated without PSs. After 48 h, only MCF-10A cells treated with Na-H_2TCPP showed a significant decrease of cell survival.

On the contrary, 10 min of irradiation with red light lead to a decrease in cell survival, in a porphyrin concentration dependent manner when compared with cells incubated without PSs and irradiated too, and some differences between porphyrins and cell lines were observed. At 24 h post-irradiation, MCF-10A cells treated with the lower concentrations (0.5 or 1 µM) of Na-H_2TCPP or Na-ZnTCPP showed higher viability than SKBR-3 cells subjected to the same treatments. Treatments with the highest concentrations (2 and 4 µM) resulted in higher cytotoxicity and no significant differences between porphyrins or cell lines were observed. In SKBR-3 cell line the IC$_{50}$ at 24 h was four times lower when treated with Na-H_2TCPP and nearly thrice lower when treated with Na-ZnTCPP compared to MCF-10A line (Table 1).

At 48 h after photodynamic treatments, SKBR-3 cells treated with 0.5 µM Na-ZnTCPP showed a significantly lower viability than SKBR-3 cells treated with 0.5 µM Na-H_2TCPP or MCF-10A cells treated with both PSs at the same concentration. Cell viability was also lower for SKBR-3 cells treated with 1 or 2 µm Na-H_2TCPP than for MCF-10A cells subjected to the same treatments. Regarding treatments with the highest concentration (4 µM), no significant differences between porphyrins or cell lines were observed in cell

survival, which was between 10–20% in all the cases. Hereafter, all experiments were performed using a working concentration of 4 μM Na-H$_2$TCPP or Na-ZnTCPP, because this concentration showed the highest cytotoxicity in both cell lines.
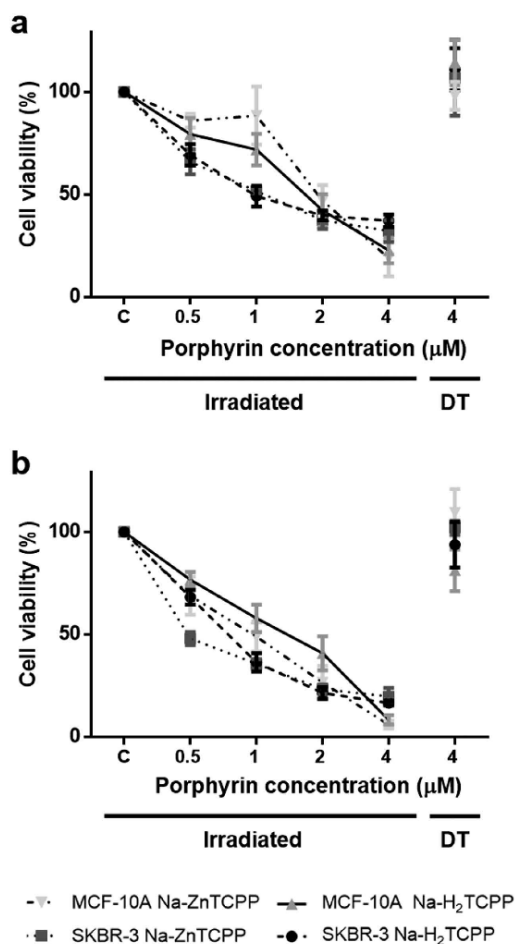

Figure 2. Viability of MCF-10A and SKBR-3 cells measured by MTT assay 24 (a) or 48 h (b) after photodynamic treatments. Cells were incubated with different concentrations of Na-H$_2$TCPP or Na-ZnTCPP and irradiated 10 min with red light or kept in absence of light in order to evaluate the dark toxicity (DT) of the photosensitizers.

	MCF-10A	SKBR-3
Na-H$_2$TCPP	2.255	0.518
Na-ZnTCPP	1.813	0.585

Table 1. IC$_{50}$ values of SKBR-3 and MCF-10A treated with Na-H$_2$TCPP and Na-ZnTCPP, at 24 h after irradiation.

Nuclear morphology after photodynamic treatments. Three different nuclear morphologies of cells stained with H-33258 24 h after irradiation were identified (Fig. 3): necrotic, apoptotic and spotted nuclei. In MCF-10A cells treated with Na-H$_2$TCPP, 28% of necrotic nuclei and 41% of spotted nuclei were observed. On the other hand, SKBR-3 cells incubated with Na-H$_2$TCPP showed 40% of necrotic nuclei and 26% of nuclei with the classical apoptotic morphology.

Similar results were observed in cells treated with Na-ZnTCPP, but in this case the percentage of necrotic nuclei was significantly higher (50% in SKBR-3 and 54% in MCF-10A cells) than the percentage of apoptotic (17% in SKBR-3) or spotted nuclei (19% in MCF-10A).

DNA fragmentation after photodynamic treatments. TUNEL assay was used to detect DNA fragmentation, characteristic of early stages of apoptotic processes (Fig. 4). MCF-10A cells treated with Na-H$_2$TCPP or Na-ZnTCPP showed 41% and 24% of TUNEL-positive nuclei, respectively, 5 h after treatments. However, SKBR-3 cells treated with the same PSs showed lower percentages of TUNEL-positive nuclei (12 and 11%, respectively). Live cells and cells with a necrotic morphology did not exhibit TUNEL-positive staining.

Phosphatidylserine translocation and plasma membrane integrity. At 2 h post-photodynamic treatments, cells were processed for Annexin V (ANV) and propidium iodide (PI) double staining (Fig. 5). ANV was used to detect the translocation of phosphatidylserine from the inner to the outer layer of the plasma membrane, an event that occurs during early apoptotic processes, whereas PI is an intercalating agent that only stains the nuclei of cells that have lost their plasma membrane integrity, as occurs in early necrotic process but not in early apoptosis. The majority of MCF-10A cells treated with either Na-H$_2$TCPP or Na-ZnTCPP showed a double positive staining, which corresponds to necrotic cell death (66% and 55%, respectively). By contrast, most of SKBR-3 cells showed a double negative staining when treated with both PSs and only a small percentage of ANV+/PI− (8% in both cases) or ANV+/PI+ cells (5% in cells treated with Na-H$_2$TCPP and 8% in cells treated with Na-ZnTCPP) was observed.
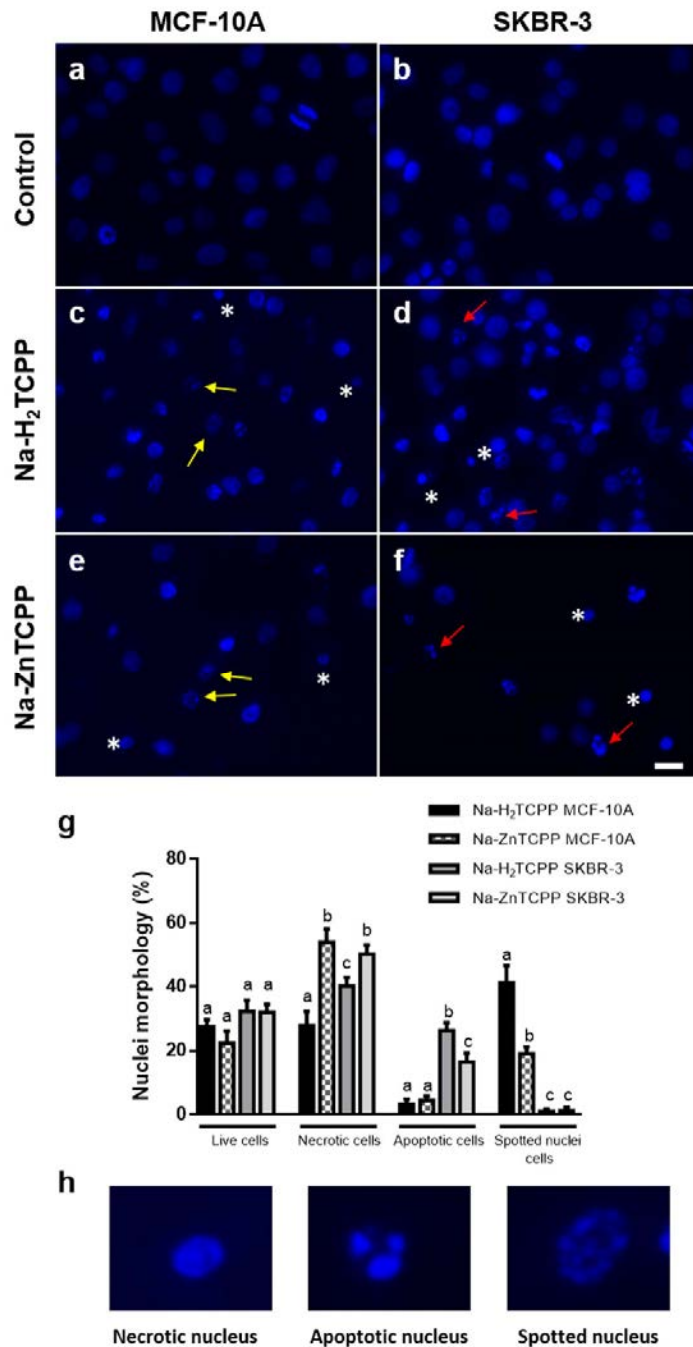
Figure 3. Nuclear morphology of Hoescht-33258 stained MCF-10A or SKBR-3 cells 24 h after photodynamic treatments. (a,b) Irradiated cells without photosensitizers (Control). (c,d) Cells treated with 4 µM Na-H$_2$TCPP. (e,f) Cells incubated with 4 µM Na-ZnTCPP. Asterisks, red arrows and yellow arrows point to some representative necrotic, apoptotic and spotted nuclei, respectively. Scale bar, 20 µm. (g) Percentage of live, necrotic, apototic and spotted nuclei cells observed 24 h after photodynamic treatments with the two photosensitizers at a 4 µM concentration. Different superscripts on top of the columns denote significant differences between groups not sharing the same superscript within the same nuclear morphology. (h) Detail of the three nuclear morphologies of cell death observed.
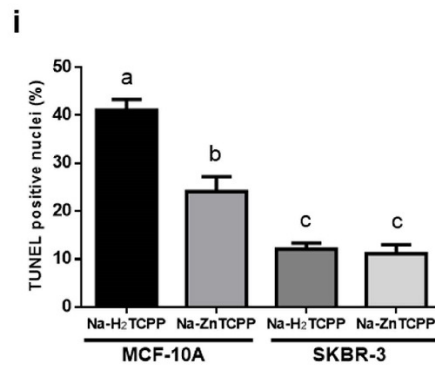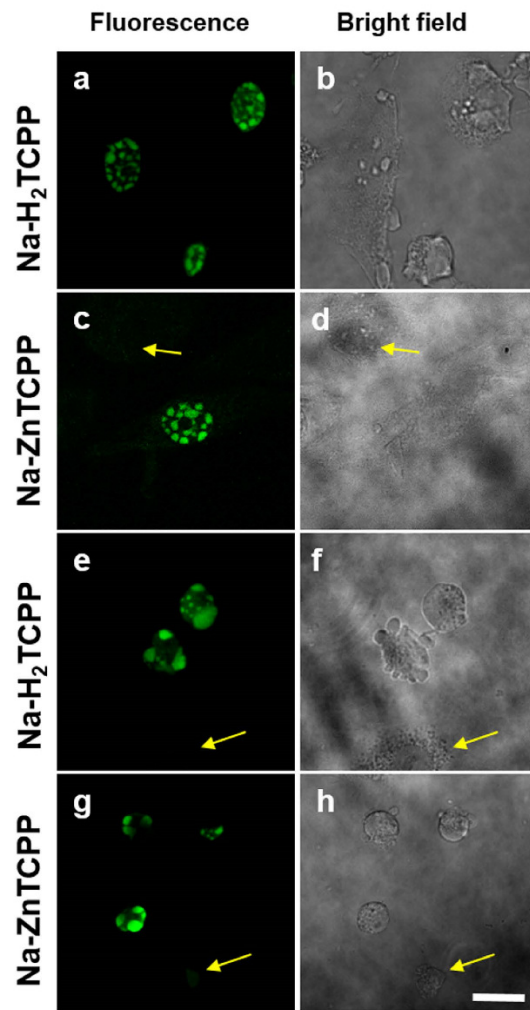
Figure 4. Cells processed for TUNEL assay 5 h after irradiation and observed under fluorescence and bright field microscope. (a,b) MCF-10A cells incubated with 4 µM Na-H$_2$TCPP. (c,d) MCF-10A cells treated with 4 µM Na-ZnTCPP. (e,f) SKBR-3 cells incubated with 4 µM Na-H$_2$TCPP. (g,h) SKBR-3 cells treated with 4 µM Na-ZnTCPP. Yellow arrows indicate TUNEL-negative cells. Scale bar, 20 µm. (i) Percentage of TUNEL positive cells observed 5 h after photodynamic treatments with 4 µM Na-H$_2$TCPP or Na-ZnTCPP. Different superscripts on top of the columns denote significant differences between groups not sharing the same superscript.
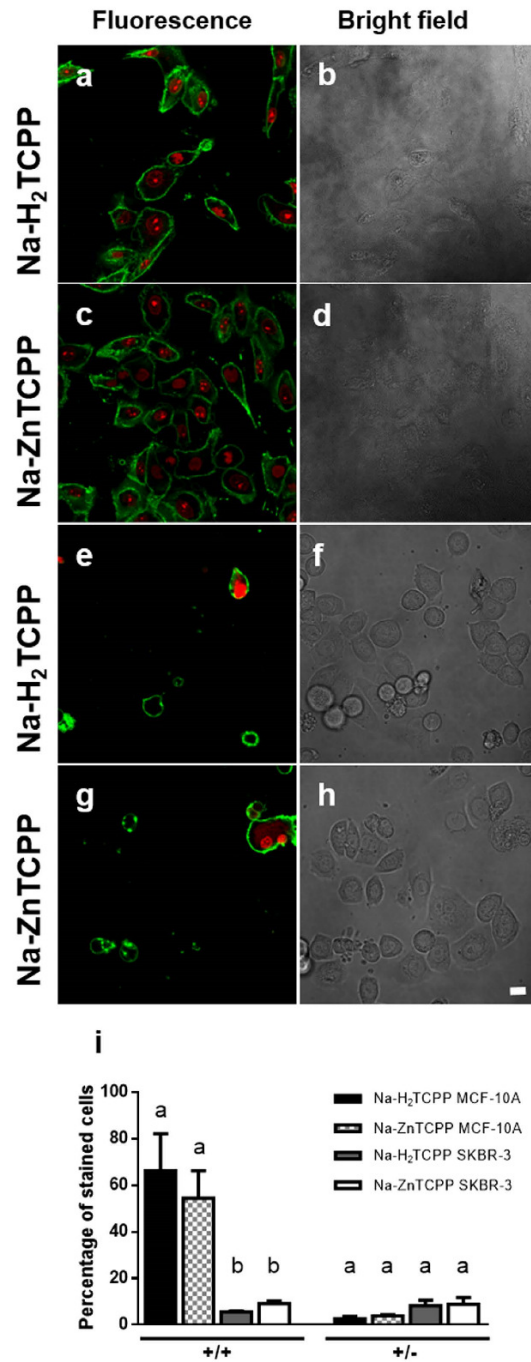
Figure 5. Cells processed with Annexin-V-FLUOS Staining Kit 2h after irradiation and observed under fluorescence or bright field microscope. (a,b) MCF-10A cells incubated with 4 µM Na-H$_2$TCPP. (c,d) MCF10A cells treated with 4 µM Na-ZnTCPP. (e,f) SKBR-3 cells incubated with 4 µM Na-H$_2$TCPP. (g,h) SKBR-3 cells treated with 4 µM Na-ZnTCPP. Green fluorescence corresponds to Annexin-V-FLUOS (ANV) and red fluorescence to propidium iodide (PI). Scale bar, 20 µm. (i) Percentage of ANV+/PI+ or ANV+/PI– cells observed 2h after photodynamic treatments with 4 µM Na-H$_2$TCPP or Na-ZnTCPP. Different superscripts on top of the columns denote significant differences between groups not sharing the same superscript within the cells +/+ and +/– for ANV/IP assay.

Caspase-3 activation after photodynamic treatments. Activation of caspase-3 is a hallmark of apoptosis, serving as a convergence point for different apoptosis signaling pathways. In the present study it was evaluated 5 h after irradiation by immunofluorescence staining (Fig. 6). SKBR-3 cells treated with Na-H$_2$TCPP or Na-ZnTCPP showed a positive staining of the cytoplasm in 26% and 16% of the cases, respectively. The majority of these positive cells also showed blebs on their plasma membrane and nuclear fragmentation, as expected for an apoptotic process. MCF-10A cells treated with Na-H$_2$TCPP or Na-ZnTCPP showed 40% or 37% of stained cells, respectively, with spotted nuclei but no plasma membrane blebs.

Effect of PARP-inhibition on the cytotoxicity of photodynamic treatments. The effect of different concentrations of 3-aminobenzamide (3-AB) on cells irradiated in the presence of Na-H$_2$TCPP or Na-ZnTCPP is shown in Fig. 7. In MCF-10A cells, the presence of 3-AB during photodynamic treatments increased cell viability in a concentration dependent manner. The highest 3-AB concentration tested (2mM) increased the survival of MCF-10A cells treated with Na-H$_2$TCPP from 35% to 80% and from 30% to 54% in the case of MCF-10A cells incubated with Na-ZnTCPP. By contrast, incubation with 3-AB did not significantly alter the cytotoxic effect of the photodynamic treatments in SKBR-3 cells.

Nuclear translocation of AIF. Translocation of AIF from mitochondria to the nucleus was assessed by immunofluorescence (Fig. 8). In control cells, AIF was apparently located inside the mitochondria. However, 5 h after irradiation MCF-10A cells treated with both PSs, showed a diffuse red fluorescence located in both the cytoplasm and the nucleus, which presented a spotted appearance. A similar result was observed in SKBR-3 cells. In both cell lines, cells with non-fragmented nuclei did not show AIF translocation.
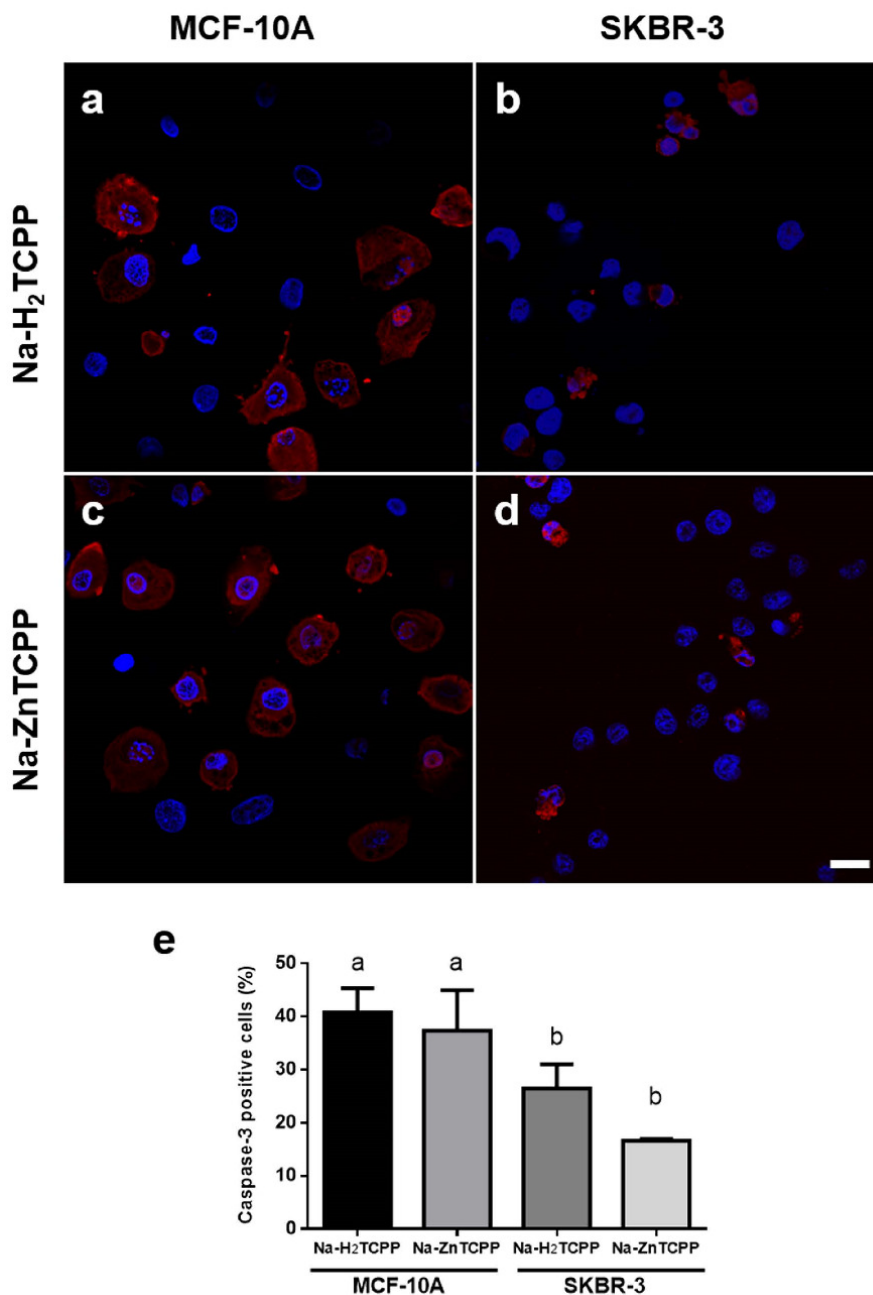
Figure 6. Cells processed for immunofluorescence staining of active caspase-3 (red) and counterstained with Hoescht-33258 (blue). (a) MCF-10A cells incubated with 4 µM Na-H$_2$TCPP and processed 5 h after irradiation. (b) SKBR-3 cells treated with 4 µM Na-H$_2$TCPP and processed 5 h after treatment. (c) MCF-10A cells incubated with 4 µM Na-ZnTCPP and processed 5 h after photodynamic treatment. (d) SKBR-3 cells treated with 4 µM Na-ZnTCPP and processed 5 h after treatment. Scale bar, 20 µm. (e) Percentage of active caspase-3 positive cells observed 5 h after photodynamic treatments. Different superscripts on top of the columns denote significant differences between groups not sharing the same superscript.
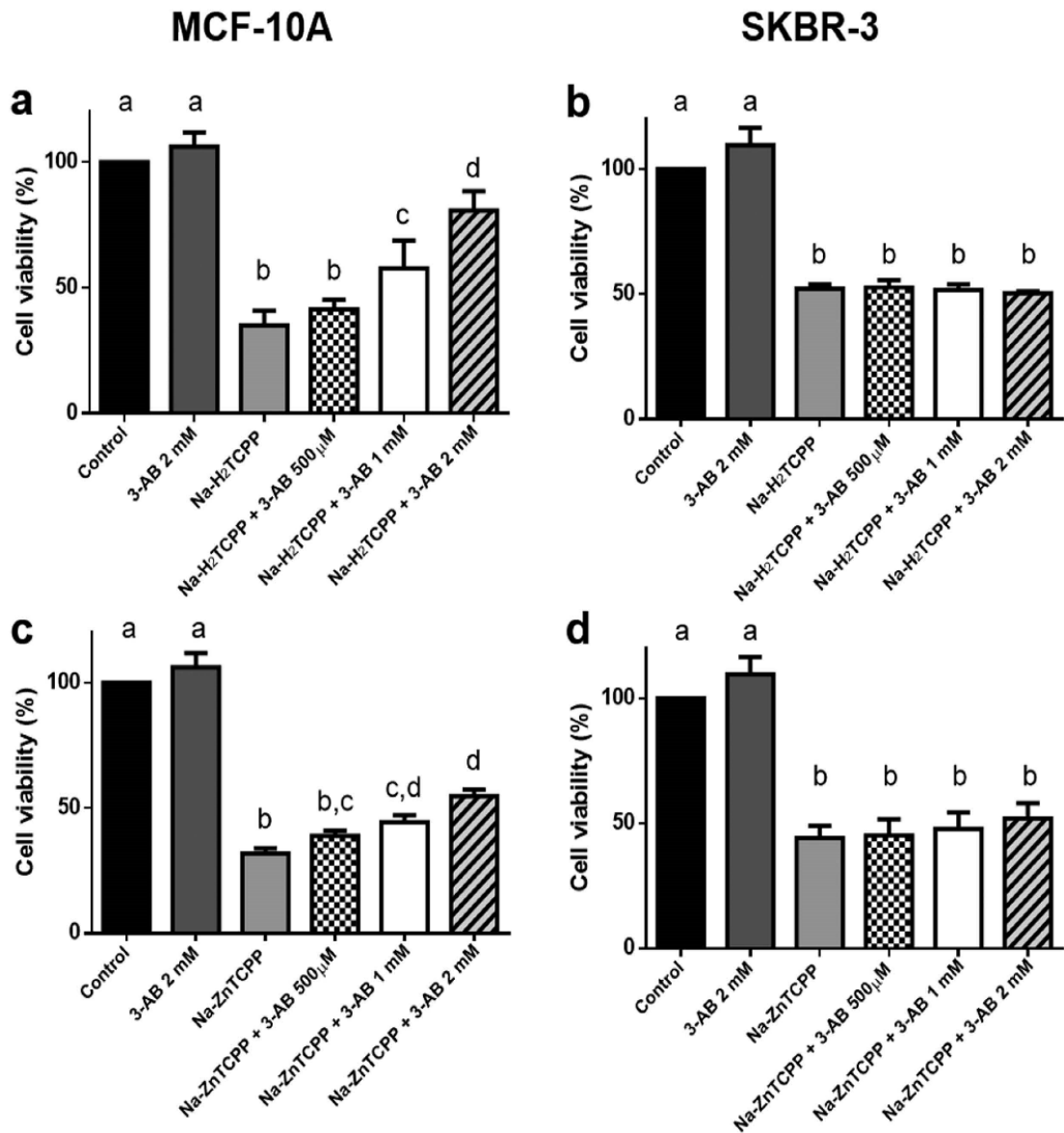
Figure 7. Viability of MCF-10A (a,c) and SKBR-3 cells (b,d) measured by MTT assay 24 h after photodynamic treatments in the presence of different concentrations of 3-Aminobenzamide and/or 4 µM Na-H$_2$TCPP (a,b) or 4 µM Na-ZnTCPP (c,d). Different superscripts on top of the columns denote significant differences between groups not sharing the same superscript.
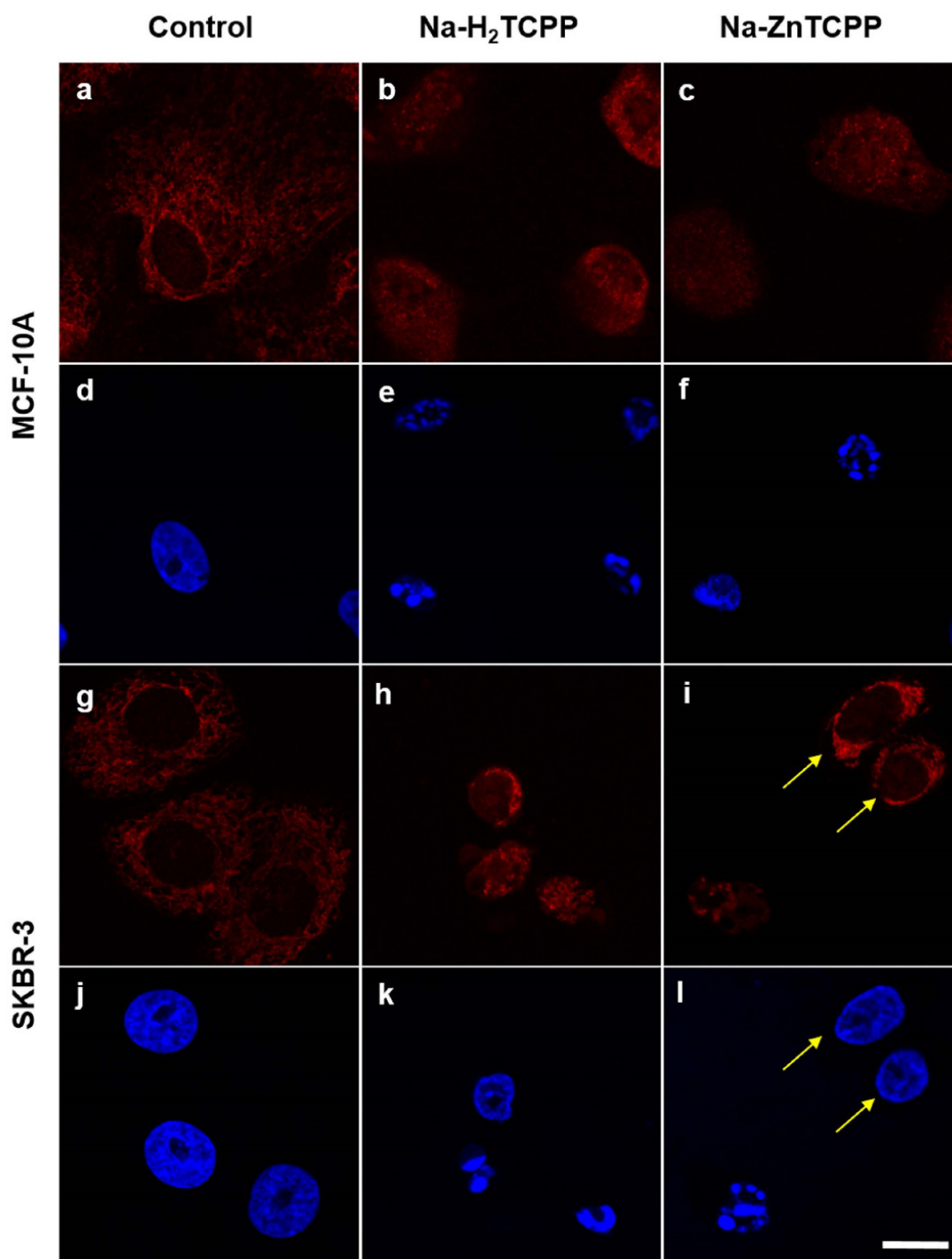
Figure 8. Cells incubated with Na-H$_2$TCPP or Na-ZnTCPP for 3 h, irradiated 10 min and processed 5 h after photodynamic treatments for immunofluorescence staining of AIF (red) and counterstained with Hoescht-33258 (blue). (a,d) MCF-10A control cells. (b,e) MCF-10A cells treated with 4 µM Na-H$_2$TCPP. (c,f) MCF-10A cells treated with 4 µM Na-ZnTCPP. (g,j) SKBR-3 control cells. (h,k) SKBR-3 cells treated with 4 µM Na-H$_2$TCPP. (i,l) SKBR-3 cells treated with 4 µM Na-ZnTCPP. Yellow arrows correspond to cells with unaltered nuclei. Scale bar, 20 µm.

Discussion

In the present study we compared the photodynamic effect of two different PSs on non-tumoral and tumoral breast epithelial cell lines. A concentration dependent reduction of cell viability was induced in both cell lines by the treatment with Na-H$_2$TCPP or Na-ZnTCPP and irradiation. However, the response to the treatment was different in both cell lines except for the highest concentration of the two PSs (4 µM), which triggered the death of most cells. At lower PSs concentrations, non-tumoral MCF-10A cells showed a higher resistance to photodynamic treatments than tumoral SKBR-3 cells. This result is of great interest for the development of selective photodynamic treatments, with less side effects in healthy tissues.

Notably, differences between cell lines in their response to photodynamic treatments, were also manifested as differences in nuclear morphologies. Specifically, SKBR-3 cells showed necrotic or apoptotic nuclei morphologies, whereas in MCF-10A cells the predominant morphologies were necrotic and spotted nuclei, which do not correspond with necrosis or apoptosis classical features. These results suggest that photodynamic treatments triggered different cell death pathways as a function of the cell line, as it has been described by other authors[3,4,17].

In order to determine the cell death mechanisms activated by photodynamic treatments, TUNEL and ANV/ PI assays and immunofluorescence staining of active caspase-3 were performed at short times after irradiation (5, 2 and 5 h, respectively).

Results showed significant differences between both cells lines when treated with Na-H$_2$TCPP. On the one hand, SKBR-3 cells presented small numbers of TUNEL-positive nuclei, with a staining pattern similar to that observed in apoptotic nuclei, ANV+/PI+ and ANV+/PI– cells, and caspase-3 positive cells. These results suggest that photodynamic treatments with Na-H$_2$TCPP induce a slow response in SKBR-3 cells that culminates in two different cell death mechanisms: necrosis and apoptosis. On the other hand, cell death events were triggered much faster in MCF-10A cells after photosensitization. At short times after irradiation, a high percentage of TUNEL-positive nuclei with a spotted staining pattern was found, as corresponds to an apoptotic process, but most of the cells

were ANV+/PI+, characteristic of necrosis. In addition, a high number of caspase-3 positive cells was observed 5 h after irradiation, which is traditionally considered an event exclusively associated with apoptosis. A recent study has demonstrated that the treatment of human-derived neuroblastoma cells with chelerythrine triggered a regulated form of necrotic cell death induced by an increase of ROS levels, which elicited an overactivation of caspases, caspase-3 included[18]. Given that PDT induces the formation of ROS, it is possible that a similar caspase-3 activation occurred under our experimental conditions. All these features (fragmented and condensed nuclei, early loss of membrane integrity but no blebbing and TUNEL positive staining) are considered characteristics of regulated necrosis[9].

Regulated necrosis includes a wide variety of cell death pathways that share characteristics of both apoptotic and necrotic processes. One of these pathways is parthanatos, which is characterized by nuclear fragmentation, early plasma membrane rupture, absence of membrane blebbing, mitochondrial depolarization, PARP-dependence and AIF translocation from the mitochondria to the nucleus (Table 2)[11,19]. In addition, caspase activation has been observed in this process, but it is not mandatory for the execution of parthanatos[11].

	Apoptosis	Necrosis	Parthanatos
Plasma Membrane	Blebbing	Swelling and lysis	Lysis but no blebbing
ANV/PI assay	+/−	+/+	+/+
TUNEL assay	+	−	+
Caspase-3 activation	+	−	+ (not mandatory)
PARP dependence	−	−	+
AIF	Translocation to the nucleus (not always)	No translocation	Translocation to the nucleus

Table 2. Main features of apoptosis, necrosis and parthanatos.

As some of these features correspond with the characteristics of the MCF-10A cells with spotted nuclei observed after treatements with Na-H$_2$TCPP, to confirm if parthanatos was involved in MCF-10A cell death, the PARP inhibitor 3-AB was used. Results showed that the presence of 3-AB increased the viability of MCF-10A cells treated with Na-

H$_2$TCPP, in a concentration dependent manner. Moreover, the higher concentration of 3-AB (2mM) increase cell viability from 35% to 80%, which corresponds with the percentage of spotted nuclei, TUNEL positive and active caspase-3 positive cells observed in the previous experiments. A similar rescue-effect has been previously reported in glioma cells treated with deoxypodophyllotoxin in the presence of 3-AB[20]. Contrarily, in SKBR-3 cells the presence of 3-AB did not modify the photodynamic effect of Na-H$_2$TCPP at any concentration, which supports the evidences of necrotic and apoptotic cell death in SKBR-3, because PARP is not involved in classic necrosis and its function is inhibited during apoptosis.

To further confirm that parthanatos was involved in cell death, AIF inmunostaining was performed 5 h after photodynamic treatments. In both cell lines treated with Na-H$_2$TCPP, AIF translocation from the mitochondria to the nucleus was observed in cells showing nuclear fragmentation. This event is associated with apoptotic cell death[21] and with parthanatos[11], but not with classic necrosis or other types of regulated necrosis.

Subcellular localization of the PSs could explain how parthanatos is triggered by photodynamic treatments, but under our experimental conditions it was not possible to visualize the PSs inside the cells. However, it has been described that H$_2$TCPP colocalizes with late endosomes and it is also diffusely distributed all over the cytoplasm and nucleoplasm in colon adenocarcinoma WiDr cells[22]. Taking into account this evidence, we can hypotesize that photoactivation of Na-H$_2$TCPP located in the nucleus of MCF-10A cells, could lead to a local increase of ROS, resulting in DNA damage and triggering PARP overactivation, the first step of parthanatos pathway. Nevertheless, SKBR-3 cells do not present the characteristics of parthanatos and a possible explanation for the different cell death mechanisms observed in both cells lines could be related to p53 expression. Recent studies have revealed that p53 is essential for PARP-mediated necrosis in response to DNA damage induced by ROS[23,24], suggesting that p53 regulates PARP activation by transcriptional and post-translational events, and even by direct interaction[25]. MCF-10A cells express wild type p53, whereas SKBR-3 cells possess the structural mutant p53-R175 h[26,27]. This mutation dramatically alters the conformation of p53, modifying its interactions with DNA and other proteins, which could explain why

different cell death mechanisms are activated in the two cell lines. However, further studies should be performed in order to elucidate the possible role of p53 in our photodynamic treatments.

Finally, regarding to treatments with Na-ZnTCPP we observed similar results to those obtained with Na-H$_2$TCPP, but the classical necrotic features prevailed over apoptotic (SKBR-3 cells) or regulated necrotic characteristics (MCF-10A cells).

Understanding the cell death mechanism/s induced by photodynamic treatments is important to develop more efficient and personalized treatments avoiding tumoral resistances. In this sense, our study demonstrates that the same photodynamic treatment can induce different cell death responses depending on the cell line studied. Moreover, the inhibition of PARP rescue most of the non-tumoral cells from cell death but has no significant effect on tumoral cells, which could be of great interest for the development of treatments with less side effects in healthy tissues. Finally, as far as we know, this study shows the first evidence of parthanatos induced by photosentization.

Acknowledgements

References

1. Benov, L. Photodynamic therapy: Current status and future directions. Med. Princ. Pract. 24, 14–28 (2015).

2. Agostinis, P. et al. Photodynamic Terapy of cancer: an update. CA Cancer J Clin. 61, 250–281 (2011).

3. Bastian, J. D., Egli, R. J., Ganz, R., Hofstetter, W. & Leunig, M. Differential response of porcine osteoblasts and chondrocytes in cell or tissue culture after 5-aminolevulinic acid-based photodynamic therapy. Osteoarthr. Cartil. 17, 539–546 (2009).

4. Yoon, J.-H. et al. The enhanced anti-cancer effect of hexenyl ester of 5-aminolaevulinic acid photodynamic therapy in adriamycinresistant compared to non-resistant breast cancer cells. Lasers Surg Med 44, 76–86 (2012).

5. Bacellar, I. O. L., Tsubone, T. M., Pavani, C. & Baptista, M. S. Photodynamic efficiency: From molecular photochemistry to cell death. Int. J. Mol. Sci. 16, 20523–20559 (2015).

6. Soriano, J. et al. Liposomal temocene (m-THPPo) photodynamic treatment induces cell death by mitochondria-independent apoptosis. Biochim. Biophys. Acta–Gen. Subj. 1830, 4611–4620 (2013).

7. Galluzzi, L. et al. Molecular definitions of cell death subroutines: recommendations of the Nomenclature Committee on Cell Death 2012. Cell Death Differ 19, 107–120 (2012).

8. Galluzzi, L. et al. Essential versus accessory aspects of cell death: recommendations of the NCCD 2015. Cell Death Differ. 1–16, doi: 10.1038/cdd.2014.137 (2014).

9. Vanlangenakker, N., Vanden Berghe, T. & Vandenabeele, P. Many stimuli pull the necrotic trigger, an overview. Cell Death Differ. 19, 75–86 (2012).

10. Van den Berghe, T., Linkermann, A., Jouan-Lanhouet, S., Walczak, H. & Vandenabeele, P. Regulated necrosis: the expanding network of non-apoptotic cell death pathways. Nat. Rev. Mol. Cell Biol. 15, 135–47 (2014).

11. Fatokun, A. A., Dawson, V. L. & Dawson, T. M. Parthanatos: Mitochondrial-linked mechanisms and therapeutic opportunities. Br. J. Pharmacol. 171, 2000–2016 (2014).

12. Sosna, J. et al. TNF-induced necroptosis and PARP-1-mediated necrosis represent distinct routes to programmed necrotic cell death. Cell. Mol. Life Sci. 71, 331–348 (2014).

13. Chiu, L. Y., Ho, F. M., Shiah, S. G., Chang, Y. & Lin, W. W. Oxidative stress initiates DNA damage MNNG-induced poly(ADPribose) polymerase-1-dependent parthanatos cell death. Biochem. Pharmacol. 81, 459–470 (2011).

14. Soriano, J., Villanueva, A., Stockert, J. & Cañete, M. Regulated Necrosis in HeLa Cells Induced by ZnPc Photodynamic Treatment: A New Nuclear Morphology. Int. J. Mol. Sci. 15, 22772–22785 (2014).

15. Coupienne, I., Fettweis, G., Rubio, N., Agostinis, P. & Piette, J. 5-ALA-PDT induces RIP3-dependent necrosis in glioblastoma. Photochem. Photobiol. Sci. 10, 1868 (2011).

16. Coupienne, I., Fettweis, G. & Piette, J. RIP3 expression induces a death profile change in U2OS osteosarcoma cells after 5-ALA-PDT. Lasers Surg Med 43, 557–564 (2011).

17. Yoo, J.-O., Lim, Y.-C., Kim, Y.-M. & Ha, K.-S. Differential cytotoxic responses to low- and high-dose photodynamic therapy in human gastric and bladder cancer cells. J. Cell. Biochem. 112, 3061–71 (2011).

18. Garcia-Belinchón, M. et al. An early and robust activation of caspases heads cells for a regulated form of necrotic-like cell death. J. Biol. Chem. 290, 20841–20855 (2015).

19. Aki, T., Funakoshi, T. & Uemura, K. Regulated necrosis and its implications in toxicology. Toxicology 333, 118–126 (2015).

20. Ma, D. et al. Deoxypodophyllotoxin triggers parthanatos in glioma cells via induction of excessive ROS. Cancer Lett. 371, 194–204 (2016).

21. Cregan, S. P., Dawson, V. L. & Slack, R. S. Role of AIF in caspase-dependent and caspase-independent cell death. Oncogene 23, 2785–2796 (2004).

22. Sobczyński, J., Kristensen, S. & Berg, K. The influence of Pluronics nanovehicles on dark cytotoxicity, photocytotoxicity and localization of four model photosensitizers in cancer cells. Photochem. Photobiol. Sci. 13, 8–22 (2014).

23. Montero, J., Dutta, C., van Bodegom, D., Weinstock, D. & Letai, A. p53 regulates a non-apoptotic death induced by ROS. Cell Death Differ. 20, 1465–74 (2013).

24. Ying, Y. & Padanilam, B. J. Regulation of necrotic cell death: p53, PARP1 and cyclophilin D-overlapping pathways of regulated necrosis? Cell. Mol. Life Sci. 73, 1–16 (2016).

25. Elkholi, R. & Chipuk, J. E. How do I kill thee? Let me count the ways: P53 regulates PARP-1 dependent necrosis. BioEssays 36, 46–51 (2014).

26. Tan, B. S. et al. Mutant p53-R273 h mediates cancer cell survival and anoikis resistance through AKT-dependent suppression of BCL2-modifying factor (BMF). Cell Death Dis. 6, e1826 (2015).

27. Liu, D. P., Song, H. & Xu, Y. A common gain of function of p53 cancer mutants in inducing genetic instability. Oncogene 29, 949–956 (2010).

28. Mojiri-Foroushani, M., Dehghani, H. & Salehi-Vanani, N. Enhancement of dye-sensitized solar cells performances by improving electron density in conduction band of nanostructure TiO2 electrode with using a metalloporphyrin as additional dye. Electrochim. Acta 92, 315–322 (2013).

29. Yuan, Y. et al. Enhanced visible-light-induced hydrogen evolution from water in a noble-metal-free system catalyzed by ZnTCPPMoS2/TiO2 assembly. Chem. Eng. J. 275, 8–16 (2015).

30. Rello, S. et al. Morphological criteria to distinguish cell death induced by apoptotic and necrotic treatments. Apoptosis 10, 201–8 (2005).

III

The importance of microparticle biofunctionalization with targeting molecules on cell internalization in static and fluidic culture conditions

Inmaculada Mora-Espí[1], Elena Ibáñez[1], Jorge Soriano[1], Carme Nogués[1], Thorarinn Gudjonsson[2,3], Leonardo Barrios[1]

[1]Unitat de Biologia Cel·lular, Departament de Biologia Cel·lular, Fisiologia i Immunologia, Facultat de Biociències, Universitat Autònoma de Barcelona, Bellaterra, 08193 Barcelona, Spain

[2]Biomedical Center, University of Iceland. Biomedical Center, University of Iceland, Reykjavík, Iceland

[3]Department of Anatomy, Faculty of Medicine, and Department of Laboratory Hematology, University Hospital, Reykjavik, Iceland

Abstract

Purpose: To determine whether microparticles can be specifically targeted to cells under fluidic conditions.

Methods: Two isogenic breast epithelial cell lines, a highly tumorigenic line overexpressing the HER2 oncogene (D492HER2) and a non-tumorigenic line expressing HER2 at much lower levels (D492) were used. Microparticles of 1 and 3 μm in diameter were functionalized with either a specific anti-HER2 antibody or an unspecific secondary antibody. Mono- and cocultures of both cell lines in static and fluidic conditions were performed and the cells with internalized microparticles were scored.

Results: The D492 cell line showed higher endocytic capacity than the D492HER2 cell line. For both cell lines, the percentage of cells with internalized microparticles was higher for microparticles functionalized with the anti-HER2 antibody than for those functionalized with the secondary antibody. The percentage of increase in internalization of microparticles biofunctionalized with the specific antibody, in relation to those functionalized with the unspecific antibody, was in general higher for the D492HER2 cell line.

Conclusion: The biofunctionalization of microparticles with a specific targeting molecule increases their internalization by cells. This effect is more pronounced in fluidic culture conditions, emphasizing the importance of targeting.

Introduction

Drug targeting has the potential to improve therapeutic efficacy and mitigate nonspecific effects of many drugs. In the last years, several types of drug delivery vehicles have been tested, including monoclonal antibodies,[1] peptides,[2] proteins,[3] lipoproteins,[4] carbohydrates[5] or polymeric nanoparticles.[6,7] Only a small number of studies involve the use of microparticles (μPs),[8–10] compared with the number of studies in which nanoparticles (NPs) are used.[11–15] However, in some cases, the larger size of μPs could be advantageous to prevent nonspecific interactions and internalization into normal non-phagocytic cells or for optimal tissue entrapment and transient retention.[16] Microparticle size and charge are important features to consider because they can

determine the way µPs interact with cells. Usually, small sizes and positively charged surfaces will favor cell intake.[9,10,17]

NPs and µPs surface can be physicochemically modified for cell targeting purposes. To target cancer cells, for instance, the drug carrier surface can be modified to increase its interaction with plasma membrane specific markers like the transferrin receptor,[18] the folate receptor[19] or the human epidermal growth factor receptor 2 (HER2, also known as ERBB2).[20,21] HER2 is a receptor tyrosine kinase overexpressed in some types of cancer, and it is considered as a marker of poor clinical outcome in breast and ovarian cancer.[22,23] Some treatments directed to this target have been already approved and are clinically used, like the anti-HER2 monoclonal antibody trastuzumab and the HER2 tyrosine kinase activity inhibitor lapatinib, but they have not always shown the expected good results.[21] Nonetheless, the use of trastuzumab conjugated with the cytotoxic drug emtansine (T-DM1) resulted in minimal growth inhibition of normal cells while clearly affecting HER2-positive tumor cells, both in vitro and in vivo, even in the case of cell lines previously described as trastuzumab resistant.[24]

Traditionally, in vitro studies on drug carriers and drug release have been performed in static monolayer cell cultures. Yet, studies in microfluidic environments, mimicking the circulatory system, are currently gaining interest.[15] Compared with static cultures, microfluidic studies allow better predictions on how a drug or a drug carrier, running in a circulating flow, interacts with cells.[25,26] On the other hand, because normal and tumoral cells are intermingled in vivo, cocultures of normal and tumoral cells can better simulate tissue conditions than monocultures.[27,28]

Hence, the aim of the present study was to evaluate the targeting efficiency of polystyrene µPs of 1 and 3 µm in diameter biofunctionalized with a specific targeting protein, an anti-HER2 antibody, or with a non-specific secondary antibody. The importance of targeting molecules was evaluated in different culture conditions: monoculture versus coculture conditions and static versus fluidic culture conditions. To carry out this study, two isogenic breast epithelial cell lines were used, one normal (D492)[29,30] and another tumorigenic, overexpressing HER2 (D492HER2)[31].

Material and methods

Biofunctionalization of polystyrene µPs

Carboxylate polystyrene µPs of 1 or 3 µm (µP-1 or µP-3) in diameter (Polybead® Carboxylate Microspheres. Polysciences, Inc, Warrington, PA) were biofunctionalized with two different targeting molecules: mouse Anti-c-ERBB2/c-Neu (Ab-5) clone TA-1 (Millipore, Darmstadt, Germany), from now on antiH, or Goat anti-Mouse IgG2a Secondary Antibody Alexa Fluor® 647 conjugate (Life Technologies, Carlsbad, CA), from now on secAb. Biofunctionalization was carried out using the PolyLink Protein Coupling Kit for COOH Microspheres (Polysciences) according to the manufacturer's instructions. Biofunctionalization was evaluated under a fluorescence inverted microscope (Olympus IX71, Olympus, Hamburg, Germany). Biofunctionalization of µPs with secAb (µP-secAb) was evaluated directly because of their far-red fluorescence emission. However, µPs biofunctionalized with antiH (µP-antiH) were incubated for 5 min with Chicken anti-mouse IgG (H+L) secondary antibody Alexa Fluor® 488 conjugate (1:500. Life Technologies) before the evaluation of green fluorescence emission.

ζ-potential analysis

Biofunctionalized and non-biofunctionalized µPs, were separately resuspended in H14 culture medium[30] and sonicated for 5 min (Fisherbrand FB15047, Fisher Scientific, Germany) to achieve a monodispersed sample. Then, their ζ-potential was measured with a Zetasizer Nano ZS (Malvern Instruments, Malvern, UK).

Cell lines

The isogenic breast epithelial cell lines D492 and D492HER2 were used in the study. D492 is a non-tumorigenic line with stem cell properties that expresses low levels of the HER2 oncogene[29,30]. D492HER2 was generated by overexpressing the HER2 oncogene in D492 and is highly tumorigenic[31]. Both cell lines constitutively express green fluorescent protein (GFP).

The cells were cultured in serum-free H14 culture medium[30] at 37°C and 5% CO_2 (standard conditions). As explained below, cell cultures were performed as follows: mono- or cocultures in static conditions and cocultures in fluidic conditions.

Cell cultures in static conditions

For monoculture experiments, cells were seeded at a density of 60,000 cells/well in 24-well plates (μ-Plate 24 Well ibiTreat: #1.5 polymer coverslip. Ibidi, Martinsried, Germany). For coculture experiments, 30,000 cells of each cell line (D492 and D492HER2) were seeded together in each well. In both cases, cells were maintained for 24 h in standard culture conditions prior to performing any experiment.

To analyze μP internalization, μPs (μP-antiH or μP-secAb) were sonicated for 5 min and then added to the cell cultures and incubated for further 24 h in standard culture conditions. In all the experiments, μPs were added at a proportion of 45 μP-1/cells or 5 μP-3/cells, to maintain a similar μP surface area.

Cell cultures in fluidic conditions

For these experiments, only cocultures were performed. Before seeding, channel slides (μ-Slides I 0.8mm ibiTreat, Ibidi) were coated with Bovine Collagen Type I (Advanced Biomatrix, San Diego, CA) to enhance cell adhesion. Then, 1.5×10^5 cells of each cell line (D492 and D492HER2) were seeded in H14 medium containing 2% penicillin-streptomycin (Biowest, Nuaillé, France) and incubated in standard culture conditions. After 24 h, the slides were connected to the microfluidic system consisting of a perfusion set (Perfusion Set Red ID 1.6 mm, Ibidi) filled with fresh H14 medium containing μPs (μP-1-secAb, μP-3-secAb, μP-1-antiH or μP-3-antiH) and a Fluidic Unit connected to an Ibidi Pump controlled with the PumpControl software (Ibidi). The microfluidic system was kept at 37°C and 5% CO_2. Cultures were maintained for 24 h under a unidirectional flow rate fixed at 4.32 ml/min with a shear stress of 1.50 dyn/cm² and a pressure of 7.9 mbar, as recommended by the manufacturer's.

Evaluation of microparticles internalization

After being cultured in either static or fluidic conditions, cells were washed three times with Phosphate Buffer Saline (PBS) at room temperature (RT), fixed for 15 min with 4% paraformaldehyde (Sigma-Aldrich, St Louis, MO) in PBS, and washed again with PBS (x3). Next, fixed cells were permeabilized with 0.1% Triton X-100 (Sigma-Aldrich) in PBS for 10 min at RT, washed with PBS (x3) and blocked with 3% bovine serum albumin (BSA) (Sigma-Aldrich) in PBS for 40 min. PBS with 3% BSA was also employed to dilute the antibodies used in this work.

Cells from monocultures were incubated with Alexa Fluor® 546 Phalloidin (1:40. Life Technologies) to label actin microfilaments and, in the case of samples with µP-antiH, also with goat anti-mouse IgG1 secondary antibody Alexa Fluor® 647 conjugate (1:150. Life Technologies) for 1 h at RT to detect µP-antiH.

To distinguish between D492 and D492HER2 in cocultures, cells were first incubated with rabbit anti-HER2 monoclonal antibody (1:200. Cell Signaling, Danvers, MA, USA) overnight at 4°C. Then, the samples were washed three times with PBS and incubated for 2.5 h at RT with Phalloidin conjugated with Alexa Fluor® 546 (1:80. Life Technologies) to label actin microfilaments, chicken anti-rabbit IgG (H+L) Alexa Fluor® 405 conjugate secondary antibody (1:150. Life Technologies) to label HER2 in the plasma membrane, and, only for cells incubated with µP-antiH, goat anti-mouse IgG1 secondary antibody Alexa Fluor® 647 conjugate (1:150. Life Technologies) to visualize µP-antiH.

Finally, cells were washed three times with PBS and maintained at 4°C in PBS until their evaluation under a confocal laser scanning microscope (CLSM. Olympus, Tokyo, Japan). Orthogonal projections of z-stacks of least 100 cells of each cell line were evaluated in each replicate.

Statistical analyses

At least three replicates of each experiment were performed. To compare µP internalization for each experimental condition and cell line, ANOVA with post-hoc Tukey HSD test was used. $P < 0.05$ was considered statistically significant.

Results

Microparticles characterization after biofunctionalization

Biofunctionalization of µPs was confirmed by two ways, microscopically and analyzing the ζ-potential. Under fluorescence microscopy, µP-secAb emitted far-red fluorescence and µP-antiH emitted green fluorescence after incubation with a secondary antibody Alexa® 488 conjugated (Figure 1A). Biofunctionalization was also confirmed by changes in the µP surface charge. Non-biofunctionalized polystyrene carboxylate µPs (µP-COOH) showed ζ-potential values of -32.3 mV and -33.3 mV, whereas µP-secAb and µP-antiH increased their ζ-potential to less negative values, ranging from -8.8 mV to -11.5 mV (Figure 1B).

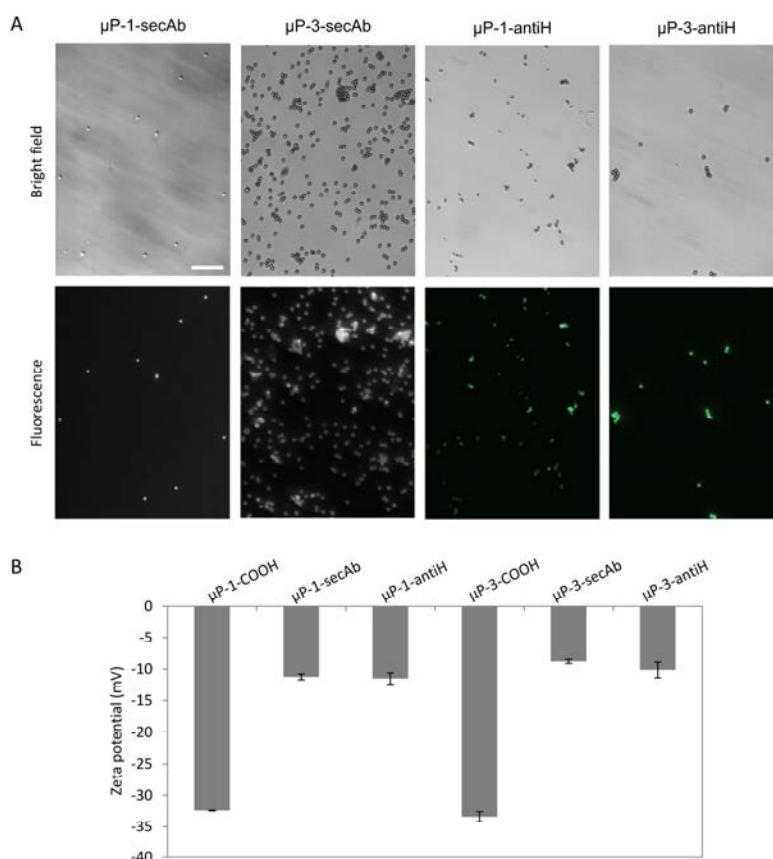Figure 1. Characterization of microparticles biofunctionalization. A) Images of microparticles biofunctionalized with a secondary antibody (µP-secAb) or an anti-HER2 antibody (µP-antiH) in bright field (upper panels) and fluorescence (lower panels) microscopes. B) Zeta potential before (COOH) and after biofunctionalization (µP-secAb and µP-antiH). The number in each type of µP refers to its diameter (1 or 3 µm). Scale bar: 30 µm.

Microparticles internalization by cells

The internalization of μPs by cells was evaluated through the orthogonal images captured on the CLSM in both static and fluidic culture conditions (Figures 2 and 3, respectively). Staining of actin filaments was useful to visualize the cell perimeter and, together with the orthogonal projections, allowed us to clearly distinguish between internalized and non-internalized μPs. From these images, the number of cells with at least one internalized μP were counted.

As can be seen in figure 4, in all culture conditions and for the same μP biofunctionalization (secAb or antiH), the percentage of D492 cells with internalized microparticles was always higher than for D492HER2 cells. Moreover, the percentage of cells with internalized μP-1 was always higher than for μP-3. In the majority of culture conditions, biofunctionalization with antiH also resulted in higher internalization rates than with secAb, being the differences significant in several cases.

When we compared, for the same cell line and μP biofunctionalization, the percentage of cells with internalized μP-1, we found that the differences between static mono- and coculture conditions were not significant. However, the percentages of cells with internalized μP were significantly lower in fluidic than in static cocultures.

In the case of μP-3, significantly higher percentages of internalization were observed with static coculture conditions when compared with static monoculture or fluidic coculture.

It is noteworthy that the percentage of increase in internalization of μP-1-antiH versus μP-1-secAb was higher for D492HER2 than for D492 cells. In static monocultures, the percentage of internalization using μP-1-antiH instead μP-1-secAb increased 22% for D492 cells and 77% for D492HER2 cells. A similar result was observed for static coculture conditions (increases of 35% and 99% for D492 and D492HER2 cells, respectively) and for fluidic culture conditions (increases of 100% and 164% for D492 and D492HER2 cells, respectively) (Figure 4). A similar trend was observed for μP-3, except for D492 cells static monoculture (Figure 4).
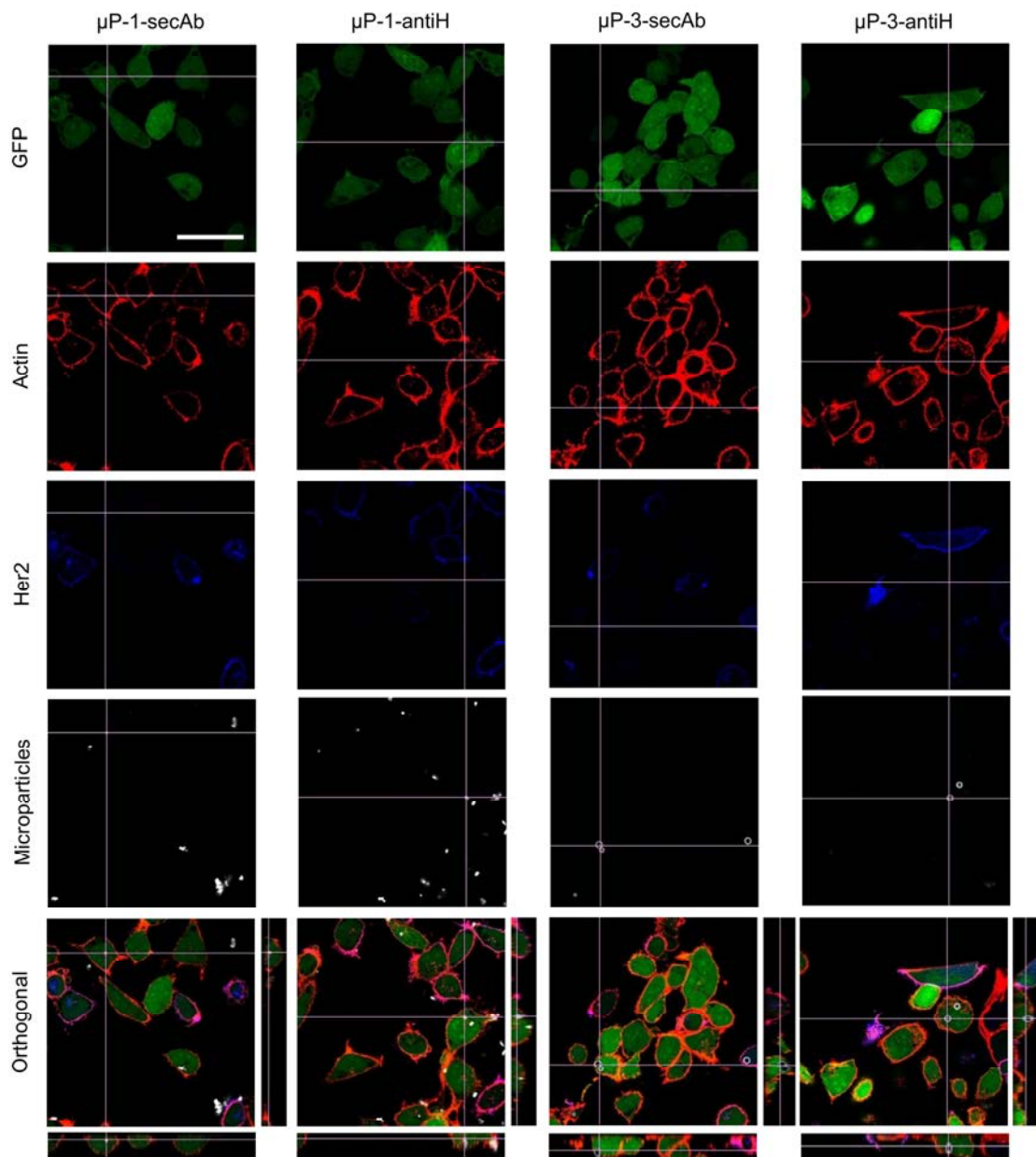
Figure 2. Immunofluorescence analysis by CLSM of cells cultured in static conditions. Confocal images of D492 and D492HER2 cells cocultured in static conditions and incubated with microparticles of 1 and 3 µm in diameter biofunctionalized with a secondary antibody (µP-1-secAb and µP-3-secAb) or an anti-HER2 antibody (µP1-antiH and µP-3- antiH). Scale bar: 30 µm.
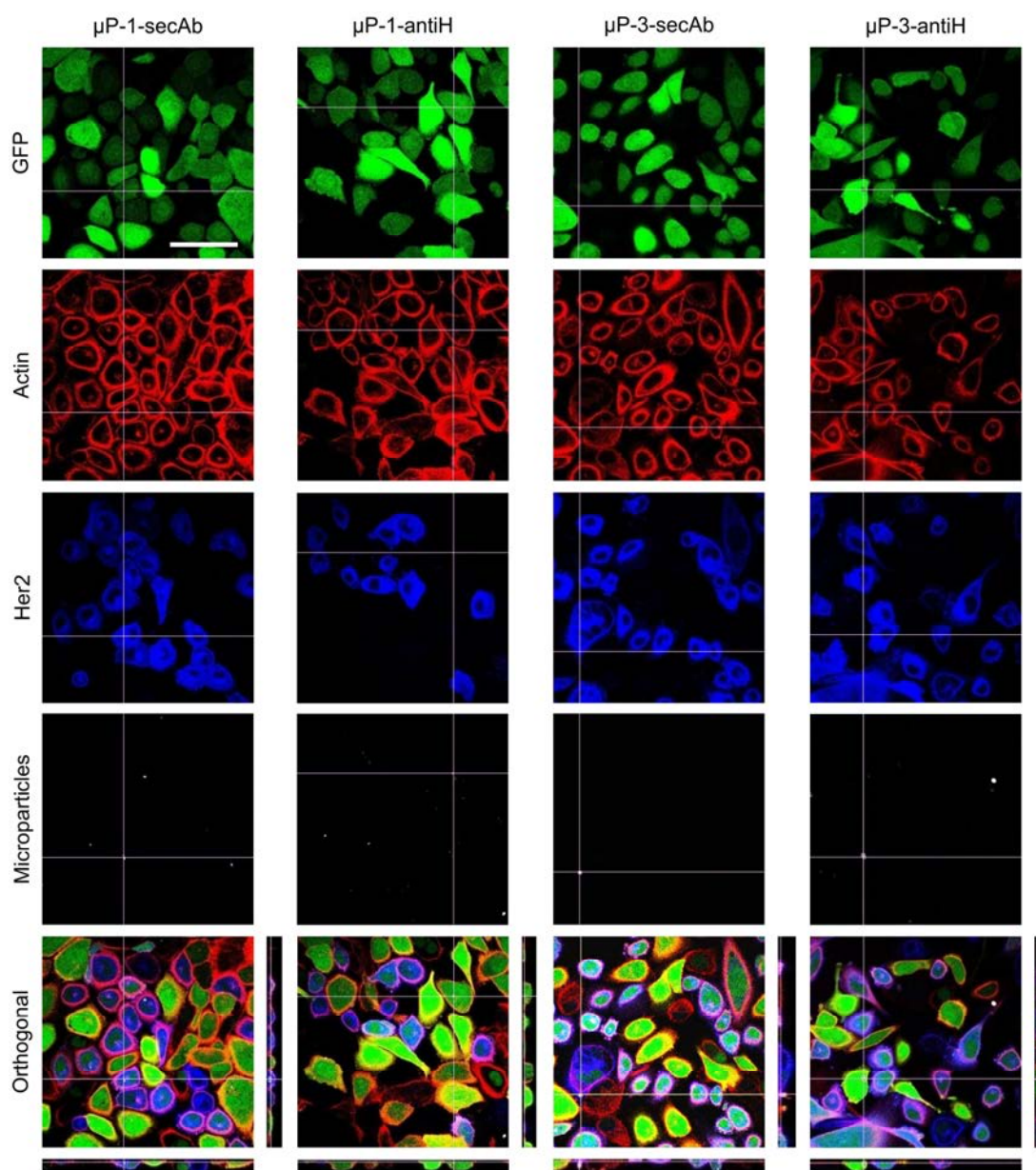
Figure 3. Immunofluorescence analysis by CLSM of cells cultured in fluidic conditions. Confocal images of D492 and D492HER2 cells cocultured in fluidic conditions and incubated with microparticles of 1 and 3 µm in diameter biofunctionalized with a secondary antibody (µP-1-secAb and µP-3-secAb) or an anti-HER2 antibody (µP1-antiH and µP-3- antiH). Scale bar: 30 µm.
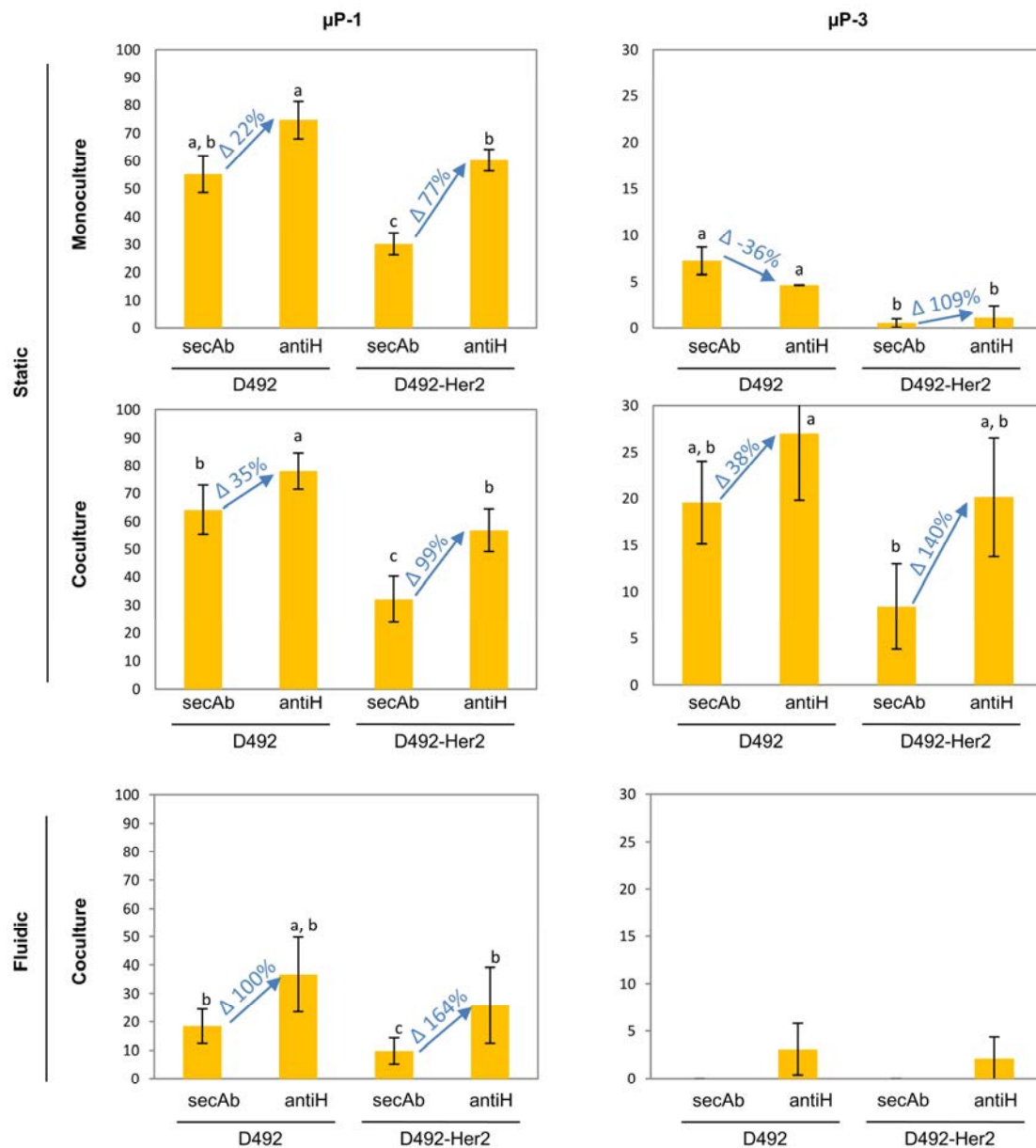
Figure 4. Microparticles internalization by mono- or cocultured D492 and D492HER2 cells in static and fluidic conditions. Percentages of cells with internalized microparticles of 1 and 3 μm in diameter biofunctionalized with a secondary antibody (μP-1-secAb and μP-3-secAb) or an anti-HER2 antibody (μP1-antiH and μP-3- antiH). Statistically significant differences are indicated with different letters on top of the bars. Percentages of increase of μPs internalization are indicated in blue together with blue arrows. Note: Y-axis represents the percentage of cells with internalized microparticles.

Discussion

Polystyrene μPs of 1 and 3 μm in diameter were successfully biofunctionalized with an anti-Her2 antibody or with a secondary antibody, as demonstrated by the detection of fluorescence under the microscope and of changes in their ζ-potential. The reduction in

µPs electronegativity could help in their interaction with the cell plasma membrane, which contains negatively charged saccharides. In fact, it has been described that positively or slightly negatively charged particles surfaces favor cell intake.[9,32–34]

To homogenize the total µP surface, we added 9 times more µP-1 (45/cell) than µP-3 (5/cell). We observed that µP-1 internalization was always higher than µP-3 internalization, suggesting that the total µP surface able to interact with the plasma membrane of cultured cells is not a key determinant of the µP internalization rate. Some authors have reported that larger µPs size is related with lower internalization rates.[10,17] Thus, the smaller size and the higher µP/cell ratio of µP-1 may explain their higher internalizations rates in both cell types.

The cell lines used in this study are isogenic breast epithelial cell lines. D492 was established by isolating suprabasal cells from reduction mammoplasty and subsequently immortalized using the E6 and E7 oncogenes from human papilloma virus [16.29,30] D492 has stem cell properties evaluated by the ability to generate luminal- and myoepithelial cells and in 3D culture to form branching ductal-alveolar like structures. In contrast, D492HER2 was generated by overexpressing the HER2 oncogene in D492[31]. Interestingly, D492 showed higher percentages of µPs internalization than D492HER2. A possible explanation could be the differences in phenotype between these cells. D492HER2 cells undergo epithelial to mesenchymal transition (EMT) and express mesenchymal marker that could reduce their ability to internalize µPs.[29,31] Higher rates of µP internalization have also been described in MCF10A breast epithelial normal cells than in SKBR3 breast epithelial tumoral cells, which also overexpress HER2.[9]

The molecules used to biofunctionalize the µPs also influenced internalization rates. In most cases, the percentage of cells, either D492 or D492HER2, with internalized µP-antiH was higher than with µP-secAb. This result was expected, because we hypothesized that a specific recognition between the cells and the µPs, as that afforded by antiH biofunctionalization, could result in an increase in µP internalization. Also as expected, the percentages of increase of µPs internalization obtained with antiH biofunctionalization were higher for D492HER2 cells, which overexpress HER2, than for D492 cells, which express HER2 at much lower levels.[31] These results clearly indicate

that when µPs are biofunctionalized with molecules that specifically interact with plasma membrane receptors their internalization can be improved, and that the level of improvement is related with the amount of receptors present on the cells surface.

When comparing monoculture and coculture in static conditions, we did not observe significant differences in the percentages of cells with internalized µP-1. However, for µP-3, there was a significant increase in the percentages of internalization for cocultures when compared with monocultures for both cell lines and both types of biofunctionalized µPs. The use of cocultures instead of monocultures has the advantage of a more accurate mimicking of tissue environment. In some studies, nanoparticles have been specifically functionalized to target cells cocultured with other cell types,[35–37] but the results have not been conclusive.

Finally, in relation to fluidic culture conditions, our results indicate that the percentage of cells with internalized µPs clearly decreased when compared with static conditions. As internalization requires the establishment of prior transient contacts between the plasma membrane and the µPs, it seems obvious that in fluidic conditions it may be more difficult to establish these contacts long enough to allow internalization. In agreement with this, another study found that at low shear stress conditions (1 dyn/cm^2) nanoparticles functionalized against a cell membrane receptor were able to adhere on cells, whereas no adhesion was observed at higher shear stress conditions (4.5 dyn/cm^2).[38] The results of this study also indicated a high impact of particle size on adhesion to cells in fluidic conditions. Likewise, in our study the decrease in µPs internalization in fluidic versus static conditions was more pronounced for µP-3 than for µP-1.

On the other hand, it has been described that the interaction between µPs and cells in the case of dynamic cultures is not only more difficult, but it also probably requires a more specific affinity to enable internalization. Thus, in these dynamic conditions, a specific targeting may be helpful to improve internalization rates. Our results agree with this idea because, for both cell lines, the increase of µPs-1-antiH internalization when compared with µPs-1-secAb was higher in fluidic than in static cocultures.

The present results, together with previous research, emphasize the relevance of cell type, specific targeting and culture conditions, like mono or coculture and static or fluidic, on the potential application of nano and microparticles for drug delivery to cancer cells.

Conclusions

The present study indicates that µPs biofunctionalization with appropriate targeting molecules improves the efficiency of internalization by target cells. Remarkably, in fluidic culture conditions (simulating the blood stream), the specificity of targeting is still more useful for µP internalization, emphasizing the importance of targeting not only to direct µPs to the appropriate cells but also to achieve reasonable internalization rates.

References

1.   Sato K, Nagaya T, Choyke PL, Kobayashi H. Near infrared photoimmunotherapy in the treatment of pleural disseminated NSCLC: Preclinical experience. Theranostics. 2015;5(7):698-709. doi:10.7150/thno.11559

2.   You H, Yoon HE, Jeong PH, Ko H, Yoon JH, Kim YC. Pheophorbide-a conjugates with cancer-targeting moieties for targeted photodynamic cancer therapy. Bioorganic Med Chem. 2015;23(7):1453-1462. doi:10.1016/j.bmc.2015.02.014

3.   Hamblin MR, Newman EL. Photosensitizer targeting in photodynamic therapy II. Conjugates of haematoporphyrin with serum lipoproteins. J Photochem Photobiol B Biol. 1994;26(2):45-56. doi:10.1016/1011-1344(94)07036-9

4.   Hamblin MR, Newman EL. Photosensitizer targeting in photodynamic therapy II. Conjugates of haematoporphyrin with serum lipoproteins. J Photochem Photobiol B Biol. 1994;26(2):147-157. doi:10.1016/1011-1344(94)07036-9

5.   Park SY, Baik HJ, Oh YT, Oh KT, Youn YS, Lee ES. A smart polysaccharide/drug conjugate for photodynamic therapy. Angew Chemie - Int Ed. 2011;50(7):1644-1647. doi:10.1002/anie.201006038

6.   Koopaei MN, Dinarvand R, Amini M, et al. Docetaxel immunonanocarriers as targeted delivery systems for HER 2-positive tumor cells: preparation, characterization, and cytotoxicity studies. Int J Nanomedicine. 2011;6:1903-1912. doi:10.2147/IJN.S23211

7.   Zheng Y, Yu B, Weecharangsan W, et al. Transferrin-conjugated lipid-coated PLGA nanoparticles for targeted delivery of aromatase inhibitor 7alpha-APTADD to breast cancer cells. Int J Pharm. 2010;390(2):234-241. doi:10.1016/j.ijpharm.2010.02.008

8.   Patiño T, Nogués C, Ibáñez E, Barrios L. Enhancing microparticle internalization by nonphagocytic cells through the use of noncovalently conjugated polyethyleneimine. Int J Nanomedicine. November 2012:5671. doi:10.2147/IJN.S34635

9.   Patiño T, Soriano J, Barrios L, Ibáñez E, Nogués C. Surface modification of microparticles causes differential uptake responses in normal and tumoral human breast epithelial cells. Sci Rep. 2015;5(May):11371. doi:10.1038/srep11371

10.   Zauner W, Farrow NA, Haines AM. In vitro uptake of polystyrene microspheres: effect of particle size, cell line and cell density. J Control Release. 2001;71(1):39-51. doi:10.1016/S0168-3659(00)00358-8

11.   Calero M, Gutiérrez L, Salas G, et al. Efficient and safe internalization of magnetic iron oxide nanoparticles: Two fundamental requirements for biomedical applications. Nanomedicine Nanotechnology, Biol Med. 2014;10(4):733-743. doi:10.1016/j.nano.2013.11.010

12.   Yang Q, Li L, Sun W, Zhou Z, Huang Y. Dual Stimuli-Responsive Hybrid Polymeric Nanoparticles Self-Assembled from POSS-Based Starlike Copolymer-Drug Conjugates for Efficient Intracellular Delivery of Hydrophobic Drugs. ACS Appl Mater Interfaces. 2016;8(21):13251-13261. doi:10.1021/acsami.6b02403

13.   Liu X, Wu F, Tian Y, et al. Size Dependent Cellular Uptake of Rod-like Bionanoparticles with Different Aspect Ratios. Sci Rep. 2016;6(October 2015):24567. doi:10.1038/srep24567

14.   Chatterjee DK, Fong LS, Zhang Y. Nanoparticles in photodynamic therapy: An emerging paradigm. Adv Drug Deliv Rev. 2008;60(15):1627-1637. doi:10.1016/j.addr.2008.08.003

15.	Chang J-Y, Wang S, Allen JS, et al. A novel miniature dynamic microfluidic cell culture platform using electro-osmosis diode pumping. Biomicrofluidics. 2014;8(4):044116. doi:10.1063/1.4892894

16.	Kutscher HL, Chao P, Deshmukh M, et al. Enhanced passive pulmonary targeting and retention of PEGylated rigid microparticles in rats. Int J Pharm. 2010;402(1-2):64-71. doi:10.1016/j.ijpharm.2010.09.020

17.	Gratton SEA, Ropp PA, Pohlhaus PD, et al. The effect of particle design on cellular internalization pathways. Proc Natl Acad Sci U S A. 2008;105(33):11613-11618. doi:10.1073/pnas.0801763105

18.	Tros de Ilarduya C, Düzgüneş N. Delivery of therapeutic nucleic acids via transferrin and transferrin receptors: lipoplexes and other carriers. Expert Opin Drug Deliv. 2013;10(November):1583-1591. doi:10.1517/17425247.2013.837447

19.	Wong PT, Choi SK. Mechanisms and implications of dual-acting methotrexate in folate-targeted nanotherapeutic delivery. Int J Mol Sci. 2015;16(1):1772-1790. doi:10.3390/ijms16011772

20.	Stuchinskaya T, Moreno M, Cook MJ, Edwards DR, Russell D a. Targeted photodynamic therapy of breast cancer cells using antibody-phthalocyanine-gold nanoparticle conjugates. Photochem Photobiol Sci. 2011;10(5):822-831. doi:10.1039/c1pp05014a

21.	Awada G, Gombos A, Aftimos P, Awada A. Emerging Drugs Targeting Human Epidermal Growth Factor Receptor 2 (HER2) In The Treatment Of Breast Cancer. Expert Opin Emerg Drugs. 2016;8214(February):14728214.2016.1146680. doi:10.1517/14728214.2016.1146680

22.	Slamon D, Clark G, Wong S, Levin W, Ullrich A, McGuire W. Human breast cancer: correlation of relapse and survival with amplification of the HER-2/neu oncogene. Science (80-). 1987;235(4785):177-182. doi:10.1126/science.3798106

23.   Slamon D, Godolphin W, Jones L, et al. Studies of the HER-2/neu proto-oncogene in human breast and ovarian cancer. Science (80-). 1989;244(4905):707-712. doi:10.1126/science.2470152

24.   Lewis Phillips GD, Li G, Dugger DL, et al. Targeting HER2-positive breast cancer with trastuzumab-DM1, an antibody-cytotoxic drug conjugate. Cancer Res. 2008;68(22):9280-9290. doi:10.1158/0008-5472.CAN-08-1776

25.   Calibasi Kocal G, Güven S, Foygel K, et al. Dynamic Microenvironment Induces Phenotypic Plasticity of Esophageal Cancer Cells Under Flow. Sci Rep. 2016;6(1):38221. doi:10.1038/srep38221

26.   Carvalho RM, Maia FR, Silva-Correia J, Costa BM, Reis LR, M. OJ. A semiautomated microfluidic platform for real-time investigation of nanoparticles' cellular uptake and cancer cells' tracking. Nanomedicine. 2017;12:581. doi:10.2217/nnm-2016-0344

27.   Tobar N, Guerrero J, Smith PC, Martínez J. NOX4-dependent ROS production by stromal mammary cells modulates epithelial MCF-7 cell migration. Br J Cancer. 2010;103(7):1040-1047. doi:10.1016/S1359-6349(10)71365-3

28.   Arrigoni C, Bersini S, Gilardi M, Moretti M. In vitro co-culture models of breast cancer metastatic progression towards bone. Int J Mol Sci. 2016;17(9). doi:10.3390/ijms17091405

29.   Sigurdsson V, Hilmarsdottir B, Sigmundsdottir H, et al. Endothelial induced EMT in breast epithelial cells with stem cell properties. PLoS One. 2011;6(9):1-11. doi:10.1371/journal.pone.0023833

30.   Gudjonsson T, Nielsen HL, Rønnov-jessen L, Bissell MJ, Petersen OW. Isolation, immortalization and Characterization of a Human Breast Epithelial Cell Line With Stem Cell Properties. Genes Dev. 2002:693-706. doi:10.1101/gad.952602.ture

31.   Ingthorsson S, Andersen K, Hilmarsdottir B, Maelandsmo GM, Magnusson MK, Gudjonsson T. HER2 induced EMT and tumorigenicity in breast epithelial progenitor cells

is inhibited by coexpression of EGFR. Oncogene. 2016;35(32):4244-4255. doi:10.1038/onc.2015.489

32.   Chithrani BD, Chan WCW. Elucidating the mechanism of cellular uptake and removal of protein-coated gold nanoparticles of different sizes and shapes. Nano Lett. 2007;7(6):1542-1550. doi:10.1021/nl070363y

33.   Dausend J, Musyanovych A, Dass M, et al. Uptake Mechanism of Oppositely Charged Fluorescent Nanoparticles in HeLa Cells. Macromol Biosci. 2008;8(12):1135-1143. doi:10.1002/mabi.200800123

34.   Fröhlich E. The role of surface charge in cellular uptake and cytotoxicity of medical nanoparticles. Int J Nanomedicine. 2012;7:5577. doi:10.2147/IJN.S36111

35.   Costa EC, Gaspar VM, Marques JG, Coutinho P, Correia IJ. Evaluation of Nanoparticle Uptake in Co-culture Cancer Models. 2013;8(7):1-13. doi:10.1371/journal.pone.0070072

36.   Gaspar VM, Costa EC, Queiroz JA, Pichon C, Sousa F, Correia IJ. Folate-Targeted Multifunctional Amino Acid-Chitosan Nanoparticles for Improved Cancer Therapy. Pharm Res. 2015;32(2):562-577. doi:10.1007/s11095-014-1486-0

37.   Akbari A, Lavasanifar A, Wu J. Interaction of cruciferin-based nanoparticles with Caco-2 cells and Caco-2/HT29-MTX co-cultures. Acta Biomater. 2017;64:249-258. doi:10.1016/j.actbio.2017.10.017

38.   Farokhzad OC, Khademhosseini A, Jon S, et al. Microfluidic System for Studying the Interaction of Nanoparticles and Microparticles with Cells. Anal Chem. 2005;77(17):5453-5459. doi:10.1021/ac050312q

Membrane disruption after photochemical internalization to release transferrin-biofunctionalized polystyrene microparticles

Inmaculada Mora Espí[1], Lleonard Barrios[1], Josep Nogués[2,3], Elena Ibáñez[1], Jorge Soriano[1] and Carme Nogués[1]

[1]Unitat de Biologia Cel·lular, Departament de Biologia Cel·lular, Fisiologia i Immunologia, Facultat de Biociències, Universitat Autònoma de Barcelona, Bellaterra, 08193 Barcelona, Spain

[2]Catalan Institute of Nanoscience and Nanotechnology (ICN2), CSIC and The Barcelona Institute of Science and Technology, Campus UAB, Bellaterra, 08193 Barcelona, Spain

[3]ICREA, Pg. Lluís Companys 23, E-08010 Barcelona, Spain.

Abstract

The use of therapeutic drugs is usually associated with issues related to being able to exert their effects specifically at the intended cells and sites of action. To circumvent this problem different strategies have been developed, involving, for example, drug carriers that can drive their cargo strictly to their target cells. This avoids the side effects connected with unspecific delivery, hence, allowing the use of lower drug doses. Another typical obstacle is the entrapment of the drug inside the endolysosomal compartment, which physically impedes its actuation by the impossibility of reaching its molecular site of action. To overcome this hurdle, photochemical internalization (PCI) has been proposed, since it is able to disrupt the endolysosomal membranes with the combined use of a photosensitizer and light in the presence of oxygen. However, the extent of PCI-induced membrane disruption and its capability to allow the release of microparticles is unknown. In the present study, polystyrene microparticles (1 and 3 μm in diameter) were biofunctionalized with transferrin to target SKBR3 cells, which overexpress the transferrin receptor in the plasma membrane. The evaluation of microparticle intake and intracellular fate evidenced that they were inside endolysosomes. To release the endolysosomal content, the photosensitive molecule Al (III) phthalocyanine chloride disulfonic acid was used in combination with red light (620-630 nm) to achieve the PCI-mediated endolysosomal membrane disruption. Several microscopy techniques (confocal laser scanning microscope, transmission electron microscopy (TEM) and scanning TEM (STEM) combined with energy dispersive x-ray) were applied to evaluate the ultrastructural effect of PCI on the endolysosomal membranes. The results showed that PCI produced a change in the ultrastructural state of endolysosomal membranes, which allows the release of soluble transferrin but no of the microparticles.

Introduction

The therapeutic effects of many drugs are limited due to several reasons, being the inefficient targeting to the desired cells and the trapping of the drug inside the endolysosomal compartment two of the most important[1,2]. Different drug carriers have been developed to direct the drugs to the target cells, such as monoclonal antibodies against specific molecules expressed only in the target cells[3], low-density lipoproteins

that interact with plasma membrane receptors[4] or nano- and microparticles that can carry several targeting molecules[5,6]. Micro- and nanoparticles allow integrating different functions other than targeting, such as biosensing[7], cell-tagging and tracking[7–10], or drug delivery[11–14].

Once the drug arrives at its target cell it usually needs to be internalized to reach its molecular site of action. The plasma membrane is a natural barrier that regulates the selective entrance of molecules and particles into the cell. Large molecules and particles are normally internalized by endocytosis[15], a process by which cells can internalize molecules of different sizes by wrapping them with plasma membrane, resulting in the formation of a vesicle containing the endocytosed material[16]. Consequently, endocytosed drugs cannot properly perform since they are trapped inside the endolysosomal compartment, which prevents their contact with their final molecular target.

To overcome the endolysosomal barrier, different approaches have been developed that can be classified into three main endolysosomal escape enhancers groups: 1) chemical enhancers, such as polyethylenimines (PEIs), which can buffer the endolysosomal pH by a massive accumulation of protons in their functional groups, acting as a "sponge" for protons. Proton accumulation is followed by an influx of Cl- ions to compensate the increase of positive charges inside the vesicle. Eventually these processes cause osmotic swelling and endolysosomal disruption that allows the release of the content into the cytosol by the "proton-sponge effect"[17]; 2) biological enhancers, like those involving virus and bacteria toxins, which present specific fusion proteins and cell-penetrating peptides able to mediate endolysosome scape[18]; and 3) physicochemical enhancing techniques, which are based on the physical principles and chemical reactions that can directly trigger the delivery of the content of the endolysosomal compartment by its membrane disruption. Some of these techniques include the use of ultrasounds[19], magnetic fields[20], plasmonic nanobubbles[21] or photochemical internalization[22,23].

Photochemical Internalization (PCI), developed by Berg et al., is based on Photodynamic Therapy[22,23]. In this approach, endolysosomal membranes are disrupted when exposed

to light of a particular wavelength that excites a photosensitizer (PS) previously integrated in the membranes. In the presence of oxygen, the excited PS induces the production of reactive oxygen species (ROS), which ultimately cause the disruption of the endolysosomal membranes and the release of the organelle contents into the cytosol[24]. It has been described that using PCI therapeutic drugs[25,26], DNA molecules for gene therapy[27] or even nanoparticles[28] are able to escape from the endolysosomal system[22,24,29]. Thus, PCI is a promising technique in the field of nanomedicine since it can potentiate therapeutic drug effects[22,24,25,30]. However, it must be taken into account that photodynamic therapy effects can be different for different cell lines[31].

Due to the lack of systematic studies on the mechanisms of endolysosomal membrane disruption, it is not yet clear how macromolecules can actually escape from the endolysosomal compartment after PCI. In one of these few studies, Ohtsuki et al. reported that the photoinduced endosomal disruption started with a ROS-induced membrane destabilization that allowed protons to flow to the cytosol, raising the pH of the endosome. This led to the endosomal membrane disruption, although the exact mechanism remains unclear[24].

Importantly, hitherto only molecules and nanoparticles have been reported to be able to escape from the disrupted endolysosomal vesicles[28]. Thus, given the great potential of microparticles in biomedical applications, the aim of the present study was to assess whether PCI can also allow the release of microparticles and, more specifically, how endolysosomal membranes are affected. To this end, microparticles of 1 and 3 μm in diameter were biofunctionalized with transferrin and targeted to SKBR3 cells, which overexpress transferrin receptors. To check the microparticles fate, lysosome-associated membrane protein 1 (LAMP1) immunofluorescence was performed and evaluated under a confocal laser scanning microscope (CLSM). Finally, to evaluate the disruption of the endolysosomal membranes after PCI, transmission electron microscopy (TEM) and scanning TEM (STEM) combined with energy dispersive x-ray (EDX) analysis were used.

Material and methods

Cell cultures

The breast epithelial cancer cell line SKBR3 (ATCC, Manassas, VA), which overexpresses transferrin receptors in the plasma membrane, was used in this work. Cells were cultured in McCoy's 5A modified medium (Gibco, Paisley, UK) supplemented with 10% fetal bovine serum (Gibco) and maintained at 37°C and 5% CO_2. Unless specified, all the experiments were performed 24 h after seeding.

Biofunctionalization of polystyrene microparticles

Carboxylated polystyrene microparticles of 1 or 3 µm (µP-1 or µP-3) in diameter (Polybead® Carboxylated Microspheres. Polysciences Inc, Warrington, PA) were biofunctionalized with Transferrin from human serum-Alexa Fluor® 488 conjugate (Tf-A488. Life Technologies, Carlsbad, CA) using the PolyLink Protein Coupling Kit for COOH Microspheres (Polysciences) and according to manufacturer's instructions.

The success of the biofunctionalization was evaluated in two ways. First, biofunctionalized microparticles were examined under a fluorescence inverted microscope (Olympus IX71, Olympus, Hamburg, Germany) to detect green fluorescence. Second, changes in zeta potential were also used to corroborate Tf-A488 biofunctionalization. The biofunctionalized microparticles were resuspended in serum-free culture medium, sonicated for 5 min (Fisherbrand FB15047, Fisher Scientific, Germany) to achieve a monodisperse suspension and their zeta potential was measured using a Zetasizer Nano ZS (Malvern Instruments, Malvern, UK). The results of the Tf-A488 biofunctionalized microparticles (µP-Tf-A488) were compared with those obtained for non-biofunctionalized microparticles in the same conditions. All the measurements were carried out in triplicate.

For the experiments, the biofunctionalized µP-1 or µP-3 were sonicated for 5 min before their incubation with cells in serum-free medium. To preserve the ratio between microparticles surface and cells, µP-1 or µP-3 were added in a proportion of 45 or 5 microparticles/cell, respectively.

Photochemical Internalization

Al (III) Phthalocyanine chloride disulfonic acid (AlPc. Frontier Scientific Inc, Logan, UT) was used as PS at different concentrations (0, 1 and 2 µg/ml). The photodynamic excitation was performed by 30 s of irradiation with red light, in the range of 620-630 nm, with a mean intensity of 55 mW/cm^2 (PhotoActivation Universal Light device, GenIUL, Barcelona, Spain). A negative control not exposed to irradiation was always performed as a dark toxicity (DT) control.

To optimize experimental conditions, PCI was first evaluated on cells without microparticles using a solution of Tf-A488. Cells were seeded in 35 mm diameter dishes (Nalge Nunc Int, Roskilde, Denmark) at a density of 3 x 10^5 cells/dish. The next day, cells were incubated for 20 h in serum-free medium with 20 µg/ml Tf-A488 and 0, 1 or 2 µg/ml AlPc. Next, cells were washed thrice with phosphate-buffered saline (PBS) and incubated for 4 h in a fresh medium. Then, cells were irradiated and immediately observed under a fluorescence microscope (Olympus IX71). Images were captured 0 and 7 min after irradiation, and the number of discrete green dots, corresponding to endosomes or lysosomes with entrapped Tf-A488, was quantified at both time points. The number of discrete green dots was divided between the total number of cells to normalize the result. The number of green dots at time 0 min was considered as the 100% of intact endolysosomes and used to calculate the reduction in the percentage of discrete green dots at 7 min in each replicate. The highest concentration of AlPc tested (2 µg/ml) was selected for the subsequent experiments.

In experiments with microparticles, cells were seeded in 24-well dishes with coverslips at a density of 50,000 cells/well. Three days after seeding, cells were incubated with 2 µg/ml AlPc and either µP-1-Tf-A488 or µP-3-Tf-A488 in a serum-free medium for 3 h at 37°C. Then, cells were washed thrice with PBS and incubated in fresh medium for 4 h before irradiation. After irradiation, cells were cultured for 1 h before further processing. Cells without µP-Tf-A488 and with/without AlPc were used as controls.

The cytotoxicity of the microparticles and AlPc in dark conditions and after irradiation was evaluated. Cells were seeded in 24-well dishes at a density of 50,000 cells/well, incubated with or without µP-1-Tf-488 and with or without 2 µg/ml AlPc and irradiated

for 30 s or kept in dark conditions. After 24 and 72 h of irradiation, cell viability was determined by the MTT (3-(4,5-dimethylthiazol-2-yl)-2,5-diphenyltetrazolium bromide) assay (Sigma-Aldrich, St Louis, MO), reading the 540 nm absorbance using a Victor 3 Multilabel Plate Reader (PerkinElmer, Waltham, MA).

All photodynamic experiments were performed in triplicate.

Immunofluorescence detection of LAMP1

Cells incubated with microparticles were fixed for 15 min with 4% paraformaldehyde (PFA. Sigma-Aldrich) in PBS, washed three times with PBS, permeabilized with 0.1% Triton X-100 (Sigma-Aldrich) in PBS for 10 min, washed again with PBS (x3) and blocked with 5% bovine serum albumin (BSA. Sigma-Aldrich) for 40 min. Next, cells were incubated for 1 h with mouse anti-LAMP1 monoclonal antibody (1:250. BD Biosciences, Franklin Lakes, NJ) at room temperature. Then, cells were washed thrice with PBS and incubated for 1 h at room temperature with goat anti-mouse IgG2a Alexa Fluor® 647 conjugate secondary antibody (1:150. Life Technologies) and Phalloidin Alexa Fluor® 594 conjugate (1:80. Life Technologies) to detect the actin cytocortex. Finally, cells were washed three times with PBS, mounted in ProLong Gold (Life Technologies) and analyzed under a CLSM (Olympus IX81. Olympus, Tokyo, Japan). Three replicates were done for each condition and a minimum of 115 cells per replicate were evaluated to assess the microparticle-cell interaction and the influence of irradiation on the disappearance of the LAMP1 positive signal around the internalized microparticles.

Sample preparation for TEM

Cells incubated with µP-3-Tf-A488 were fixed for 25 min in 2% PFA and 2.5% glutaraldehyde in 0.1 M cacodylate buffer. They were post-fixed with 1% osmium tetroxide for 2 h and dehydrated in a graded ethanol series (15 min in 30%, 30 min in 50%, 30 min in 90%, 30 min in 95% and twice 30 min in 100%), before embedding the samples in Epon resin. Polymerization was performed at 60°C for 48 h. Ultrathin sections of 70 nm were obtained using a Leica ultracut microtome (Leica Microsystems, Wetzlar, Germany) and placed on 200 mesh copper grids. Finally, samples were contrasted with

a 2% uranyl acetate solution for 30 min and subsequently with a Reynolds lead citrate solution for 5 min and observed under a TEM Jeol JEM-1400 (Jeol Ltd, Tokyo, Japan).

STEM high angle annular dark field (HAADF) and EDX analyses

Cells incubated with µP-3-Tf-A488 were processed as for conventional TEM experiments. However, in this case, ultrathin sections were placed on carbon-coated titanium or gold grids and were not contrasted. Cells with internalized microparticles were located and images were captured using HAADF-STEM [FEI Tecnai G2 F20 microscope operated at 200 kV and equipped with an EDX super ultra-thin window X-ray detector (FEI, Hillsboro, OR)]. For each microparticle, four equidistant transects were analyzed, acquiring STEM-EDX osmium (Os) content line profiles. Each transect was oriented from inside the microparticle to the cytoplasm, perpendicularly to with microparticle edge. Since Os tends to interact with biological membranes, an increase in the number of Os counts (i.e., intensity of the Os peak in the EDX spectrum; see Suppl. Fig. 1), indicates the presence of a lipid bilayer. For each transect analyzed, the region corresponding to the particle showed virtually no Os counts compared with the rest of the transect and was considered as background. On the other hand, in the cytoplasmic region the Os signal was usually somewhat higher than the background. To compute the width of the Os peak taking into account these two different Os level signals (particle and cytoplasm), the mean value of Os counts in the cytoplasmic region was subtracted in this region to level off the signal in the particle and cytoplasmic regions. Subsequently, the remaining Os peak was fitted to a Lorentzian curve (Suppl. Fig. 2). The width of the membrane was determined as full-width at half-maximum of the peak.

In order to obtain an average width of the membrane for the non-irradiated and irradiated cells, four transects for each particle (N=8 for each experimental condition) were analyzed. The results for each condition were grouped in intervals of 5 nm and the corresponding distributions were fitted to a log-norm function.

Statistical analysis

Normality was checked by the Kolmogorov-Smirnov test with the Lilliefors correction, and homogeneity of variances with the Levene test. The Chi-square test was used for

LAMP1 immunofluorescence and for TEM evaluation results comparisons. The ANOVA test with Tukey's multiple comparison test was used for PCI optimization and cytotoxicity evaluation results. The values with $p < 0.05$ were considered statistically significant.

Results

PCI-mediated release of soluble transferrin from the endolysosomal compartment

Regarding PCI optimization, cells incubated with 20 µg/ml Tf-A488 showed green discrete fluorescent dots corresponding to endosomes or lysosomes containing Tf-A488, regardless of the AlPc concentration used (Fig. 1a). In cells without AlPc, the number of discrete green dots was maintained after irradiation. By contrast, green fluorescence rapidly diffused to the cytosol after irradiation of cells incubated with AlPc (Fig. 1a and suppl. movies 1-3), resulting in a significant reduction in the number of discrete green dots at 7 min after irradiation (Fig. 1b). No significant differences were detected between the two AlPc concentrations used, and the highest concentration of AlPc tested (2 µg /ml) was selected to perform the subsequent experiments.

Microparticles biofunctionalization and internalization

Microparticles biofuctionalized with Tf-A488 showed green fluorescence (Fig. 2a). Biofunctionalization also produced electrochemical changes in the microparticles surface, as detected by the decrease in the negativity of the Zeta potential (Fig. 2b). Non-biofunctionalized microparticles showed highly negative Zeta potential values (-32.3 mV for µP-1 and -33.3 mV for µP-3) that decreased to less negative values (between -9.7 mV and -7.4 mV) after biofunctionalization.

When the biofunctionalized microparticles were added to the cell cultures, 27.1% of cells internalized one or more µP-1-Tf-A488. However, the microparticle intake decreased to 13.8% for µP-3-Tf-A488 (Fig. 3).
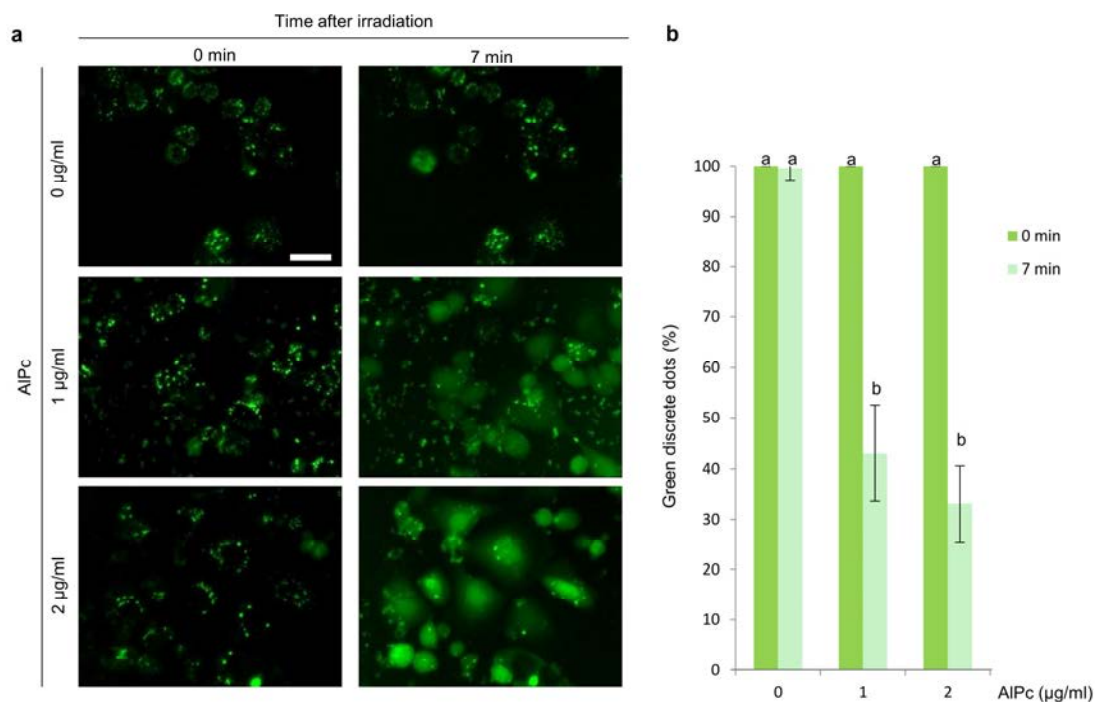
Figure 1. Transferrin-A488 release by photochemical internalization. a) Images of cells incubated with 20 μg/ml Tf-A488 and different concentrations of AlPc (0, 1 and 2 μg/ml) captured at 0 or 7 min after irradiation with a 620-630 nm wavelength. Discrete green dots correspond to Tf-A488 entrapped inside endosomes or lysosomes. Scale bar: 30 μm. b) Normalized percentage of discrete dots at 0 or 7 min after irradiation. Different letters on top of the columns denote significant differences between the two time-points for each AlPc concentration.
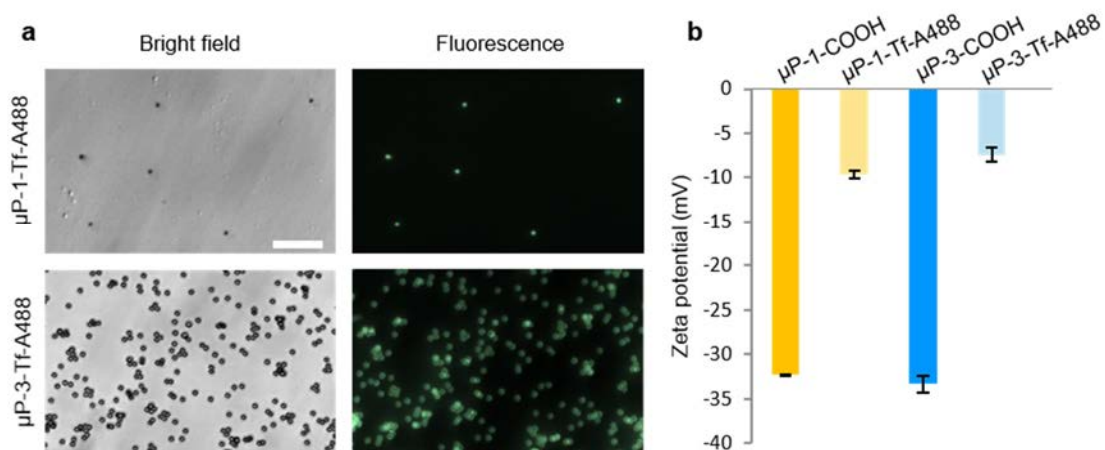

Figure 2. Microparticles biofunctionalization with transferrin-A488. a) Images of biofunctionalized μP-1-Tf-A488 and μP-3-Tf-A488 under bright field (left) and fluorescence (right). Scale bar: 30 μm. b) Zeta potential of carboxylated (COOH) and biofunctionalized (Tf-A488) microparticles.
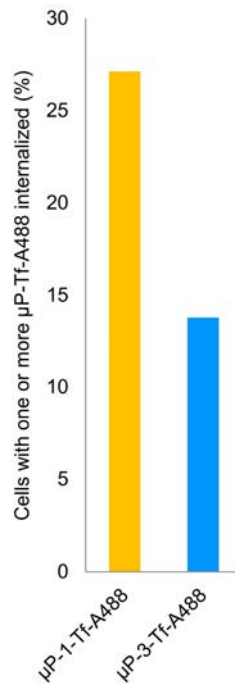
Figure 3. µP-Tf-A488 internalization. Percentage of SKBR3 cells with internalized µP-Tf-A488 particles (1 or 3 µm).

Cytotoxicity evaluation of the microparticles and the PCI treatment

Cell viability was not significantly affected by the presence of microparticles and/or AlPc, neither on the cells irradiated nor on the ones maintained in dark conditions. This lack of cytotoxicity was observed at both 24 and 72 h after irradiation (Suppl. Fig. 3). Note that since microparticle internalization was higher when using µP-1 than µP-3, and the lack of toxicity of µP-3 has been reported in a previous work[32] only µP-1 were used in this analysis.

Endolysosomal membrane disruption after microparticles internalization and PCI treatment

Cells incubated with biofunctionalized microparticles and AlPc were irradiated and, after 1 h, subjected to different techniques to assess the integrity of the membrane surrounding the internalized microparticles. First, LAMP1 immunodetection was used to score the number of internalized microparticles surrounded by endolysosomal

membranes (Fig. 4a). In DT conditions, most of the internalized µP-1-Tf-A488 (90.0%) and µP-3-Tf-A488 (85.4%) were clearly surrounded by a positive LAMP1 signal, indicating that the presence of an endolysosomal membrane around the microparticles. Nevertheless, after irradiation, the co-localization of LAMP1 signal with µP-1-Tf-A488 and µP-3-Tf-A488 significantly decreased to 31.0% and 35.7%, respectively (Fig. 4b).
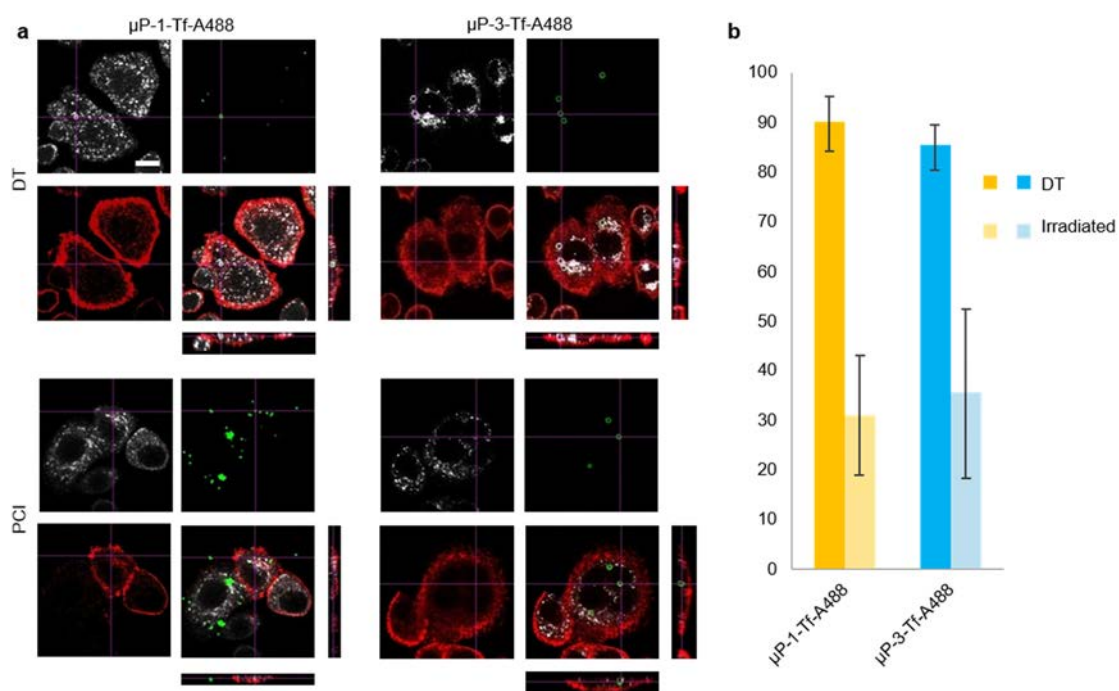

Figure 4. µP-Tf-A488, LAMP1 and actin co-localization analysis. (a) Orthogonal images of control (DT) and irradiated (PCI) samples incubated with µP-1-Tf-A488 or µP-3-Tf-A488 and 2 µg/ml AlPc. LAMP1 signal appears in white, µP-Tf-A488 in green and actin in red. Scale bar: 15 µm. (b) Percentage of µP-Tf-A488 co-localizing with the LAMP1 signal.

In addition, ultrastructural studies were performed in the cells incubated with µP-3-Tf-A488. In particular, a TEM analysis of the integrity of the membranes surrounding the microparticles was performed on 50 and 46 internalized µP-3-Tf-A488 in DT and irradiated cells, respectively. The number of microparticles surrounded by either a "well-defined" or a "blurred" membrane was recorded (Fig. 5a). As shown in Fig. 5b, the number of internalized microparticles surrounded by well-defined membranes was significantly higher in the DT samples than in the irradiated ones.
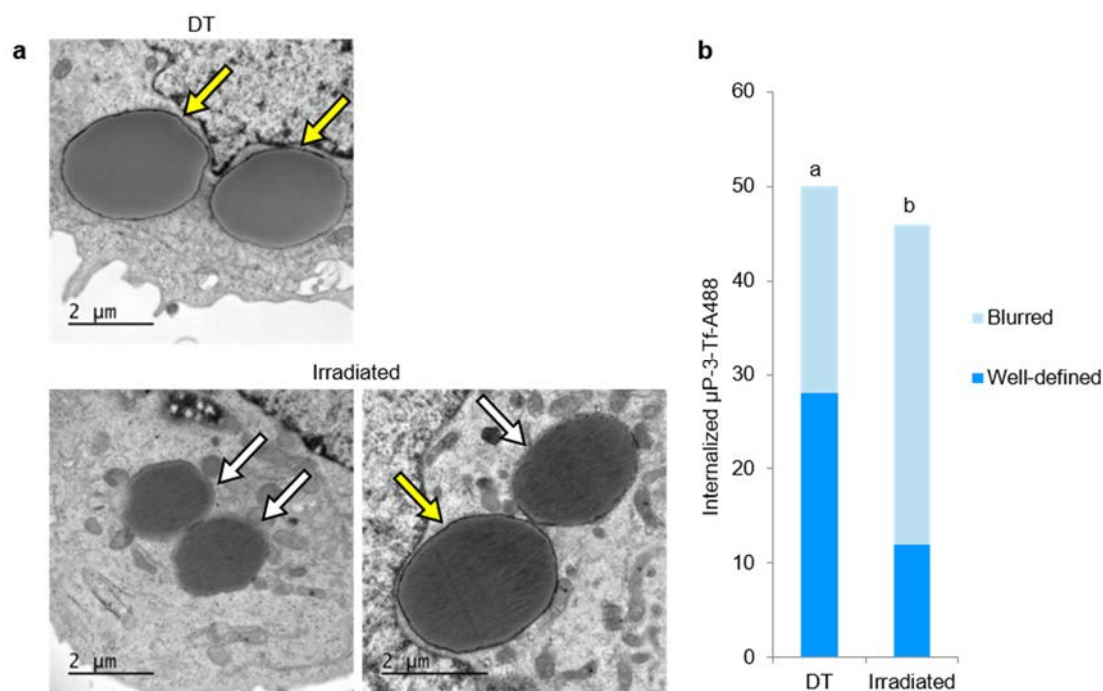
Figure 5. TEM evaluation of membranes surrounding internalized µP-3-Tf-A488. a) Internalized µP-3-Tf-A488 in non-irradiated cells (DT) or in irradiated cells incubated with 2 µg/ml AlPc with well-defined (yellow arrows) or blurred (white arrows) surrounding membranes. b) Number of internalized µP-3-Tf-A488 in control (DT) or irradiated cells surrounded by either well-defined or blurred membranes.

Finally, HAADF-STEM was used to confirm LAMP1 immunodetection and TEM results, as in the STEM images (Fig. 6) membranes appear more distinct than in conventional TEM (Fig. 5). This is due to the large atomic number of Os (Z = 76) and the imaging technique in HAADF-STEM, which is mostly sensitive to Z^2. In fact, well-defined and blurred membranes could be easily distinguished in STEM images (Fig. 6b, f). Furthermore, the 3D image of the HAADF-STEM intensity also clearly evidenced the difference in membrane integrity between the well-defined (DT) and blurred (irradiated) membranes (Fig. 6d, h).

To quantify membrane width more accurately, STEM-EDX was used to analyze the effect of PCI by collecting Os profiles of the membranes surrounding the microparticles (Fig. 6c, g). As it can be clearly seen in Fig. 7, the width distribution of the Os peaks was shifted towards higher values (i.e., the membranes were broader) in the irradiated samples compared with the non-irradiated ones. This suggests that irradiation causes a certain

degree of membrane disruption, in agreement with the confocal and TEM data, that is compatible with a PCI effect.
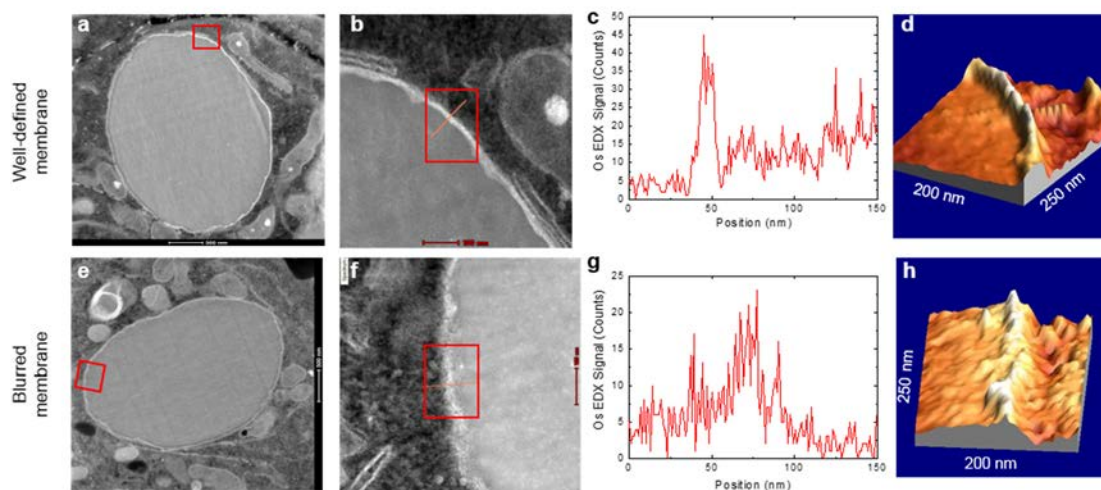
Figure 6. Membrane disruption evaluation by STEM HAADF-EDX. (a,e) Image of a microparticle inside an endolysosome. (b,f) Detail of the membrane surrounding the microparticle of the areas highlighted in (a,e), with the transect (line) and area (rectangle) analyzed. (c,g) Os EDX-counts profile. (d,h) 3D image of the membrane. The upper panel corresponds to a microparticle surrounded by an intact membrane (DT), with a clear Os EDX-peak and a well-defined 3D image of the membrane. The bottom panel corresponds to a blurred membrane (irradiated), with a considerably broader Os EDX-peak and a 3D image of the membrane.
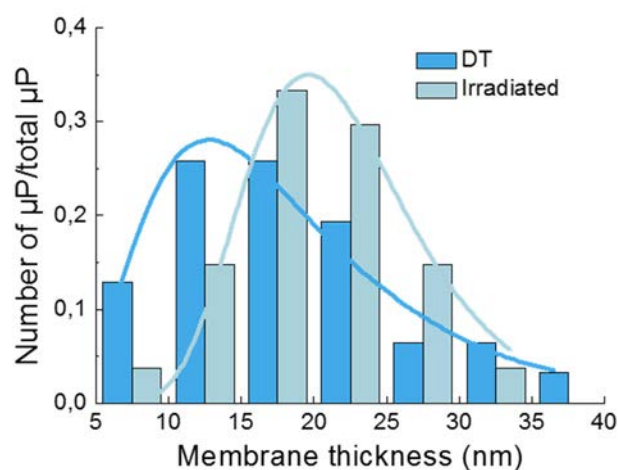
Figure 7. Distribution of membrane thickness for the non-irradiated (dark blue) and irradiated (light blue) samples. The lines are fits to log-normal distributions. The means of the log-normal distribution were 16.6 ±0.5 nm for dark toxicity (DT) and 21.2±0.3 nm for irradiated samples.

Discussion

The therapeutic effects of many drugs are conditioned on their ability to recognize and enter their target cells, in order to reach their site of action and mediate their effects. However, the performance of many drugs is usually limited due to their inefficient targeting and/or endolysosomal escape. Antibody-targeted delivery of therapeutic drugs to the desired cells is a promising concept that has been developed in the last decades. For enhanced efficiency, the combination of this approach with endolysosomal release systems, such as PCI, has been proposed. Several targeting molecules have been successfully used to direct therapeutic drugs or drug carriers before performing PCI, such as a chimeric construct with vascular endothelial growth factor and gelonin for vascular targeting[33], or antibodies against HER2 receptor[23], epidermal growth factor receptor[34] or EpCAM[35] to target cancer cells. Interestingly, targeting molecules have been bound to different types of drug carriers such as polymeric micelles[36] or nanoparticles[37] to transport the drugs, showing enhanced therapeutic activity, reduced side effects and allowing to reduce the drug concentration due to their high specificity against the target cells[26,37].

Compared to nanoparticles, microparticles may be advantageous for more specific targeting, since not all the cell types can internalize micrometric particles[38]. Although several reports agree that sizes between 30 and 50 nm are optimal for cell uptake[39], it must be emphasized that nanoparticles can easily be non-specifically uptaken by non-targeted cells, leading to undesired secondary effects. In this regard, it has been reported that particles with sizes in the microscale show a higher targeting ability than those in the nanoscale[40]. In addition, the smaller nanoparticles may have increased cytotoxicity[41–43]. However, despite the potential of microparticles for biomedical purposes relatively few studies have been carried out to evaluate their internalization and posterior endolysosome release.

To analyze if PCI could assist in the release of large devices, in this study polystyrene microparticles of 1 and 3 μm in diameter were biofunctionalized with transferrin. We have previously demonstrated that the biofunctionalization of 3 μm poly-Si/Cr/Au chips with transferrin increased more than twice their internalization in SKBR3 cells, likely due

to the overexpression of the TfR in their plasma membrane[44]. In the present study, we found that the biofunctionalization reduced the negative charge of the microparticles, which could further help to increase their cell-intake since it has been reported that positive or slightly negative charges facilitate endocytosis in most cell types[45,46]. In a previous work, less than 5% of SKBR3 cells were able to internalize non-functionalized μP-3 of a similar negative charge than the TF-biofunctionalized μP-3 used in the present study, which were uptaken by more than 10% of the cells. This corroborates the important role of transferrin as targeting molecule in this cell line.

Prior to performing microparticle internalization and release, the PCI technique was optimized using transferrin in solution. To be able to follow the transferrin, it was used combined with Alexa 488 (Tf-A488), similar to what other authors have done to follow the immunotoxin MOC31-gelonin during PCI[26]. Concerning the PS, Al (III) phthalocyanine chloride disulfonic acid (AlPc) was chosen for the present study due to its appropriate characteristics (e.g., hydrosolubility and amphiphilicity) for PCI[47–49]. Different concentrations of the AlPc were tested (1 and 2 μg/ml), none of which produced cytotoxic effects neither in DT nor after irradiation, in agreement with other studies[50–53]. Moreover, μP-3 have been previously described as non-cytotoxic[32] and our results also indicate that the biofunctionalization of the microparticles with Tf-A488 does not have cytotoxic effects. To elucidate the effect of the PCI on the membranes, we first corroborated that, in dark conditions, internalized μP-Tf-A488 were indeed located inside the endolysosomal system using LAMP1 immunodetection. Interestingly, the percentage of microparticles surrounded by a LAMP1 positive signal significantly decreased after irradiation, suggesting that microparticles could have been released into the cytosol by the PCI process. Nevertheless, the remaining presence of some LAMP1 positive signal around some internalized microparticles indicates that the disruption of the endolysosomal membrane does not lead to its complete disintegration under the current conditions.

According to different reports, the PCI-induced membrane disruption, visualized as endolysosomal cargo diffusion, is due to lipid peroxidation[22,24–26,36,37,54]. To our knowledge, little research has been carried out using electron microscopy to assess the extent of membrane disruption[55,56] and none to evaluate the ultrastructural changes

resulting from PCI-induced membrane disruption. In the present study, TEM evaluation of the irradiated samples showed that membranes surrounding microparticles were frequently diffuse (probably damaged). By contrast, non-irradiated samples showed a well-defined structure of the membranes surrounding microparticles. To better understand these differences, a STEM-EDX analysis was performed. This approach allows determining the chemical elements present in a sample, and it can be used to quantify the relative abundance of a specific element at any point of a particular position of the sample under study. Despite its potential, STEM-EDX has been rarely used in cell biology. For example, it has been previously used to determine the location of specific ions in mouse induced pluripotent stem cells and mesenchymal stem cells[57], the interaction of quantum dots with human oral epithelial cells[58] or to locate ZnO nanoparticles in breast cancer cells[59].Given the great potential of this methodology to track high-Z atoms, we used it to evaluate PCI-induced endolysosomal membrane disruption. The tendency of osmium (Os) to interact with biological membranes has been used for decades to fix cell membranes and to enhance their contrast for electron microscopy studies[60]. Importantly, since Os does not react with polystyrene microparticles (Suppl. Fig. 4), EDX is not only particularly suitable to determine the presence/absence of membranes surrounding microparticles, but also to infer their integrity. An increase in the Os level (Os peak) around the microparticle allows confirming the presence of a membrane and to actually measure its width. Thus, the width of the Os peak can be used as an indicator of the intactness of a membrane. In our study, the width of the Os peaks in the irradiated samples was larger than in the non-irradiated ones, which is in accordance with the images obtained in traditional TEM where membranes in irradiated samples appeared to be more diffuse. These results are also in agreement with those obtained using confocal analysis, where the absence of LAMP1 signal around microparticles in irradiated samples indicates a membrane disruption. It is important to emphasize that in all the microparticles analyzed an Os signal, although with variable width, was always present around them. Most probably, the disruption of the membrane induced by PCI corresponds to a reorganization of the lipid bilayer sufficient to release molecules in suspension such as Tf-A488 (present work), or nanoparticles[61], but not sufficient to completely liberate a 3 μm microparticle into the cytosol. For this reason, the PCI treatment could be eventually complemented

with the use of pH-sensitive bonds between the therapeutic drug and the microparticle. In the lysosomal acidic environment, these bonds would be readily cleaved, allowing the release of the drug and its escape to the cytosol due to the membrane disruption.

Conclusions

In the present study, we aimed at using PCI-mediated endolysosomal membrane disruption to release microparticles entrapped in the endolysosomal compartment. The results show that while soluble Tf-A488 is released into the cytosol, µP-3-Tf-A488 remained inside the endosomes. In order to identify how PCI affects the endolysosomal membranes different microscopy techniques were used. LAMP1 immunodetection results suggested a complete disruption of the endolysosomal membrane in most of the irradiated cells. However, ultrastructural studies showed that the endolysosomal membrane was always present around the microparticle, although showing a variable width. PCI-mediated endolysosomal membrane disruption seems to consist in a partial disorganization, but not in a complete disappearance of the membrane. Thus, PCI could potentially be a good candidate to overcome endolysosomal entrapment of therapeutic drugs carried by microparticles only if it is complemented with the use of pH-sensitive bonds.

Acknowledgements

References

1.   Lloyd, J. B. Lysosome membrane permeability: implications for drug delivery. Adv. Drug Deliv. Rev. 41, 189–200 (2000).

2.   Shete, H. K., Prabhu, R. H. & Patravale, V. B. Endosomal Escape: A Bottleneck in Intracellular Delivery. J. Nanosci. Nanotechnol. 14, 460–474 (2014).

3.   Ye, Q. et al. Generation and functional characterization of the anti-transferrin receptor single-chain antibody-GAL4 (TfRscFv-GAL4) fusion protein. BMC Biotechnol. 12, 91 (2012).

4.   de Vries, H. E., Moor, A. C., Dubbelman, T. M., van Berkel, T. J. & Kuiper, J. Oxidized low-density lipoprotein as a delivery system for photosensitizers: implications for photodynamic therapy of atherosclerosis. J. Pharmacol. Exp. Ther. 289, 528–534 (1999).

5.   Calixto, G. M., Bernegossi, J., de Freitas, L. M., Fontana, C. R. & Chorilli, M. Nanotechnology-Based Drug Delivery Systems for Photodynamic Therapy of Cancer: A Review. Molecules 21, 342 (2016).

6.   Cheng, R., Meng, F., Deng, C., Klok, H. A. & Zhong, Z. Dual and multi-stimuli responsive polymeric nanoparticles for programmed site-specific drug delivery. Biomaterials 34, 3647–3657 (2013).

7.   Khlebtsov, N. et al. Analytical and Theranostic Applications of Gold Nanoparticles and Multifunctional Nanocomposites. Theranostics 3, 167–180 (2013).

8.   Fernandez-Rosas, E. et al. Intracellular polysilicon barcodes for cell tracking. Small 5, 2433–9 (2009).

9.   Novo, S. et al. Direct embryo tagging and identification system by attachment of biofunctionalized polysilicon barcodes to the zona pellucida of mouse embryos. Hum. Reprod. 28, 1519–27 (2013).

10.   Novo, S. et al. Traceability of human sperm samples by direct tagging with polysilicon microbarcodes. Reprod. Biomed. Online 31, 162–170 (2015).

11.   Morales-Cruz, M. et al. Activation of caspase-dependent apoptosis by intracellular delivery of cytochrome c-based nanoparticles. J. Nanobiotechnology 12, 33 (2014).

12.   Méndez, J. et al. Delivery of Chemically Glycosylated Cytochrome c Immobilized in Mesoporous Silica Nanoparticles Induces Apoptosis in HeLa Cancer Cells. Mol. Pharm. 11, 102–111 (2014).

13.   Song, Y., Li, Y., Xu, Q. & Liu, Z. Mesoporous silica nanoparticles for stimuli-responsive controlled drug delivery: advances, challenges, and outlook. Int. J. Nanomedicine Volume 12, 87–110 (2016).

14.   Yingchoncharoen, P., Kalinowski, D. S. & Richardson, D. R. Lipid-based drug delivery systems in cancer therapy: What is available and what is yet to come. Pharmacol. Rev. 68, 701–787 (2016).

15.   Petros, R. A. & DeSimone, J. M. Strategies in the design of nanoparticles for therapeutic applications. Nat. Rev. Drug Discov. 9, 615–627 (2010).

16.   Bareford, L. M. & Swaan, P. W. Endocytic mechanisms for targeted drug delivery. Adv. Drug Deliv. Rev. 59, 748–758 (2007).

17.   Boussif, O. et al. A versatile vector for gene and oligonucleotide transfer into cells in culture and in vivo: Polyethylenimine. Proc. Natl. Acad. Sci. U. S. A. 92, 7297–7301 (1995).

18.   Fuchs, H., Weng, A. & Gilabert-Oriol, R. Augmenting the Efficacy of Immunotoxins and Other Targeted Protein Toxins by Endosomal Escape Enhancers. Toxins (Basel). 8, 200 (2016).

19.   Omata, D. et al. Bubble Liposomes and Ultrasound Promoted Endosomal Escape of TAT-PEG Liposomes as Gene Delivery Carriers. Mol. Pharm. 8, 2416–2423 (2011).

20.   Luo, Z. et al. Redox-Responsive Molecular Nanoreservoirs for Controlled Intracellular Anticancer Drug Delivery Based on Magnetic Nanoparticles. Adv. Mater. 24, 431–435 (2012).

21.   Lukianova-hleb, E. Y., Belyanin, A., Kashinath, S., Wu, X. & Lapotko, D. O. Biomaterials Plasmonic nanobubble-enhanced endosomal escape processes for selective and guided intracellular delivery of chemotherapy to drug-resistant cancer cells. Biomaterials 33, 1821–1826 (2012).

22.   Berg, K. et al. Photochemical internalization: A novel technology for delivery of macromolecules into cytosol. Cancer Res. 59, 1180–1183 (1999).

23.   Weyergang, A. et al. Photochemical activation of drugs for the treatment of therapy-resistant cancers. Photochem. Photobiol. Sci. 14, 1465–75 (2015).

24.   Ohtsuki, T. et al. The molecular mechanism of photochemical internalization of cell penetrating peptide-cargo-photosensitizer conjugates. Sci. Rep. 5, 18577 (2015).

25.   Lee, C.-S., Park, W., Park, S. & Na, K. Endolysosomal environment-responsive photodynamic nanocarrier to enhance cytosolic drug delivery via photosensitizer-mediated membrane disruption. Biomaterials 34, 9227–36 (2013).

26.   Weyergang, A., Selbo, P. K., Berstad, M. E. B., Bostad, M. & Berg, K. Photochemical internalization of tumor-targeted protein toxins. Lasers Surg. Med. 43, 721–733 (2011).

27. Boe, S. L. & Hovig, E. Enhancing nucleic acid delivery by photochemical internalization. Ther. Deliv. 4, 1125–1140 (2013).

28. Selbo, P. K. et al. Photochemical internalization provides time- and space-controlled endolysosomal escape of therapeutic molecules. J. Control. release 148, 2–12 (2010).

29. Nishiyama, N. et al. Light-induced gene transfer from packaged DNA enveloped in a dendrimeric photosensitizer. Nat. Mater. 4, 934–941 (2005).

30. Kamoshima, Y., Terasaka, S., Kuroda, S. & Iwasaki, Y. Morphological and histological changes of glioma cells immediately after 5-aminolevulinic acid mediated photodynamic therapy. Neurol. Res. 33, 739–746 (2011).

31. Wyld, L., Reed, M. W. & Brown, N. J. Differential cell death response to photodynamic therapy is dependent on dose and cell type. Br. J. Cancer 84, 1384–1386 (2001).

32. Patiño, T., Soriano, J., Barrios, L., Ibáñez, E. & Nogués, C. Surface modification of microparticles causes differential uptake responses in normal and tumoral human breast epithelial cells. Sci. Rep. 5, 11371 (2015).

33. Veenendaal, L. M. et al. In vitro and in vivo studies of a VEGF121/rGelonin chimeric fusion toxin targeting the neovasculature of solid tumors. Proc. Natl. Acad. Sci. U. S. A. 99, 7866–71 (2002).

34. Fretz, M. M., Hogset, A., Koning, G. A., Jiskoot, W. & Storm, G. Cytosolic delivery of liposomally targeted proteins induced by photochemical internalization. Pharm. Res. 24, 2040–2047 (2007).

35. Lund, K. et al. The novel EpCAM-targeting monoclonal antibody 3–17I linked to saporin is highly cytotoxic after photochemical internalization in breast, pancreas and colon cancer cell lines. MAbs 6, 1038–1050 (2014).

36. Lu, H. L., Syu, W. J., Nishiyama, N., Kataoka, K. & Lai, P. S. Dendrimer phthalocyanine-encapsulated polymeric micelle-mediated photochemical

internalization extends the efficacy of photodynamic therapy and overcomes drug-resistance in vivo. J. Control. Release 155, 458–464 (2011).

37.   Yang, Q., Li, L., Sun, W., Zhou, Z. & Huang, Y. Dual Stimuli-Responsive Hybrid Polymeric Nanoparticles Self-Assembled from POSS-Based Starlike Copolymer-Drug Conjugates for Efficient Intracellular Delivery of Hydrophobic Drugs. ACS Appl. Mater. Interfaces 8, 13251–13261 (2016).

38.   Zauner, W., Farrow, N. A. & Haines, A. M. . In vitro uptake of polystyrene microspheres: effect of particle size, cell line and cell density. J. Control. Release 71, 39–51 (2001).

39.   Shang, L., Nienhaus, K. & Nienhaus, G. Engineered nanoparticles interacting with cells: size matters. J. Nanobiotechnology 12, 5 (2014).

40.   Barua, S. et al. Particle shape enhances specificity of antibody-displaying nanoparticles. Proc. Natl. Acad. Sci. 110, 3270–3275 (2013).

41.   Pan, Y. et al. Size-Dependent Cytotoxicity of Gold Nanoparticles. Small 3, 1941–1949 (2007).

42.   Karlsson, H. L., Gustafsson, J., Cronholm, P. & Möller, L. Size-dependent toxicity of metal oxide particles—A comparison between nano- and micrometer size. Toxicol. Lett. 188, 112–118 (2009).

43.   Coradeghini, R. et al. Size-dependent toxicity and cell interaction mechanisms of gold nanoparticles on mouse fibroblast. Toxicol. Lett. 217, 205–216 (2013).

44.   Patiño, T. et al. Polysilicon-chromium-gold intracellular chips for multi-functional biomedical applications. Nanoscale 8, 8773–8783 (2016).

45.   Gratton, S. E. A. et al. The effect of particle design on cellular internalization pathways. Proc. Natl. Acad. Sci. U. S. A. 105, 11613–11618 (2008).

46.   Thompson, D. B., Villaseñor, R., Dorr, B. M., Zerial, M. & Liu, D. R. Cellular uptake mechanisms and endosomal trafficking of supercharged proteins. Chem. Biol. 19, 831–843 (2012).

47.   Alonso, L. et al. Photodynamic evaluation of tetracarboxy-phthalocyanines in model systems. J. Photochem. Photobiol. B Biol. 161, 100–107 (2016).

48.   Christie, C. et al. Synergistic chemotherapy by combined moderate hyperthermia and photochemical internalization. Biomed. Opt. Express 7, 1240 (2016).

49.   Selbo, P. K., Rosenblum, M. G., Cheung, L. H., Zhang, W. & Berg, K. Multi-Modality Therapeutics with Potent Anti-Tumor Effects: Photochemical Internalization Enhances Delivery of the Fusion Toxin scFvMEL/rGel. PLoS One 4, e6691 (2009).

50.   Kim, H. R. C., Luo, Y., Li, G. & Kessel, D. Enhanced apoptotic response to photodynamic therapy after bcl-2 transfection. Cancer Res. 59, 3429–3432 (1999).

51.   Shiraishi, T. & Nielsen, P. E. Photochemically enhanced cellular delivery of cell penetrating peptide-PNA conjugates. FEBS Lett. 580, 1451–1456 (2006).

52.   Andrzejak, M., Santiago, M. & Kessel, D. Effects of Endosomal Photodamage on Membrane Recycling and Endocytosis. Photochem. Photobiol. 87, 699–706 (2011).

53.   Abrahamse, H. & Hamblin, M. R. New photosensitizers for photodynamic therapy. Biochem. J. 473, 347–364 (2016).

54.   Selbo, P. K., Kaalhus, O., Sivam, G. & Berg, K. 5-Aminolevulinic Acid-based Photochemical Internalization of the Immunotoxin MOC31-gelonin Generates Synergistic Cytotoxic Effects In Vitro. Photochem. Photobiol. 74, 303 (2001).

55.   Zhou, X. & Huang, L. DNA transfection mediated by cationic liposomes containing lipopolylysine_ characterization and mechanism of action. Biochim. Biophys. Acta - Rev. Cancer 1189, 195–203 (1994).

56.   Bieber, T., Meissner, W., Kostin, S., Niemann, A. & Elsasser, H. I ntracellular route and transcriptional competence of polyethylenimine – DNA complexes. J. Control. Release 82, 441–454 (2002).

57.   Egusa, H. et al. Comparative Analysis of Mouse-Induced Pluripotent Stem Cells and Mesenchymal Stem Cells During Osteogenic Differentiation In Vitro. Stem Cells Dev. 23, 2156–2169 (2014).

58.   Cepeda-Pérez, E. et al. SERS and integrative imaging upon internalization of quantum dots into human oral epithelial cells. J. Biophotonics 9, 683–693 (2016).

59.   Othman, B. A. et al. Correlative Light-Electron Microscopy Shows RGD-Targeted ZnO Nanoparticles Dissolve in the Intracellular Environment of Triple Negative Breast Cancer Cells and Cause Apoptosis with Intratumor Heterogeneity. Adv. Healthc. Mater. 5, 1310–1325 (2016).

60.   Rivlin, P. K. & Raymond, P. A. Use of osmium tetroxide-potassium ferricyanide in reconstructing cells from serial ultrathin sections. J. Neurosci. Methods 20, 23–33 (1987).

61.   Yu, H. et al. Overcoming endosomal barrier by amphotericin B-loaded dual pH-responsive PDMA- b-PDPA micelleplexes for siRNA delivery. ACS Nano 5, 9246–9255 (2011).

Supporting material

1. Correlation between Os peaks and presence of a lipid membrane
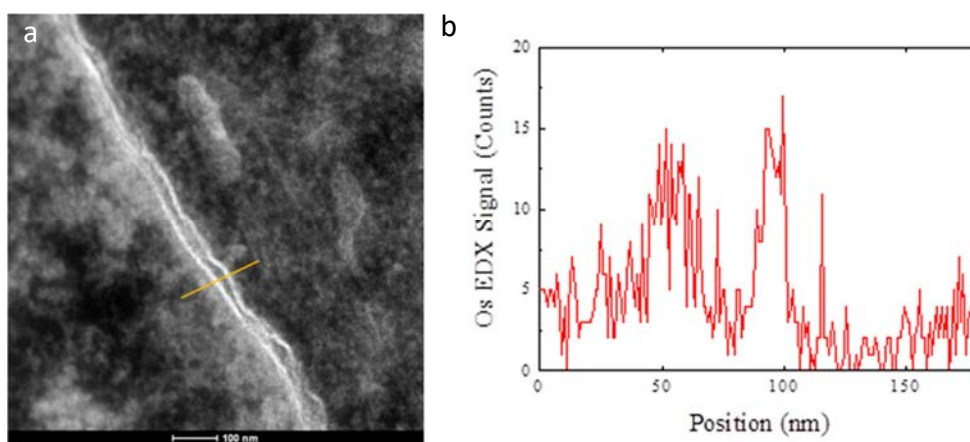
Supplementary figure 1. (a) TEM image of a nuclear envelope showing the inner and outer membranes. The yellow line indicates the transect analyzed. (b) STEM-EDX Os content profile obtained along the transect where two different Os peaks, corresponding to the inner and outer membrane, can be observed. Abbreviations: N, nucleus; C, cytoplasm.

2. Methodology to compute the width of the Os peak
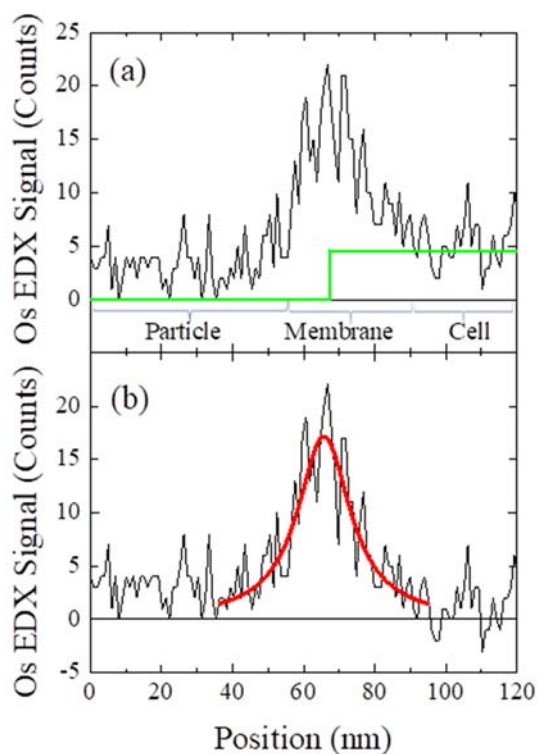
Supplementary figure 2. (a) Os EDX signal (black) and its background signal (green). (b) Background-corrected Os EDX signal (black) with a fit to a Lorentzian function (red). Note: Cell refers to cytoplasm.

3. Cell viability in the presence of µP-1-Tf-A488 and AlPc, alone or combined
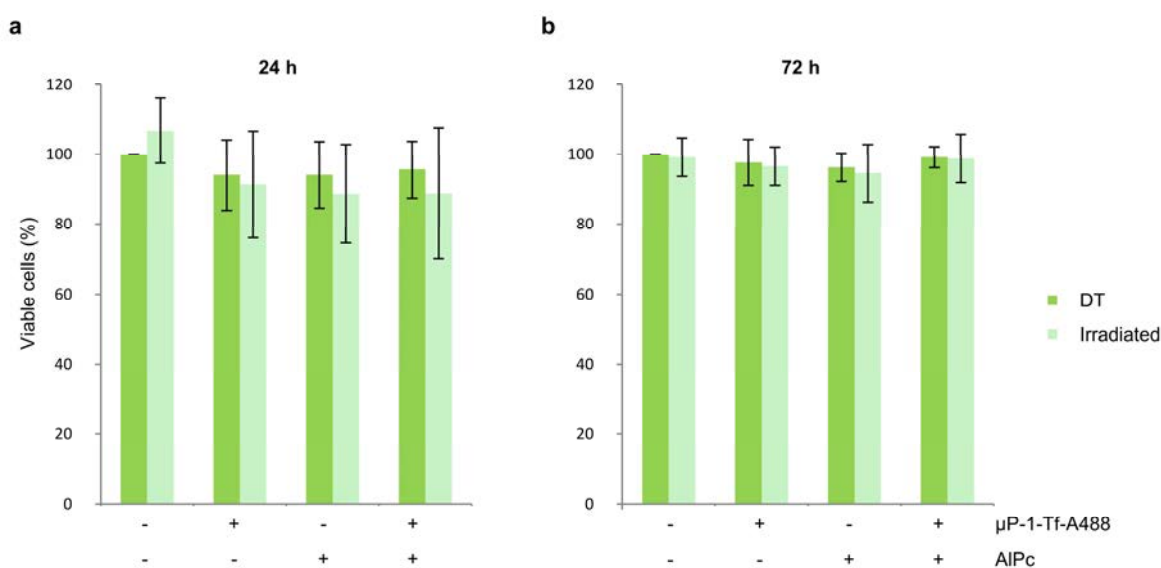
Supplementary figure 3. Cell viability in the presence of µP-1-Tf-A488 and AlPc, alone or combined. MTT assay was performed at 24 h (a) and 72 h (b) after irradiation or in dark conditions (DT). Cytotoxicity of microparticles and AlPc, alone and combined, was evaluated in irradiated and DT cultures. The percentage of viable cells was normalized to the DT controls. Abbreviations: Tf, Transferrin from human serum Alexa Fluor® 488 conjugate; µP-1-Tf-A488, 1 µm diameter µP biofunctionalized with Tf-A488; AlPc, Al (III) phthalocyanine chloride disulfonic acid; DT, dark toxicity.

4. EDX counts of free and internalized particles
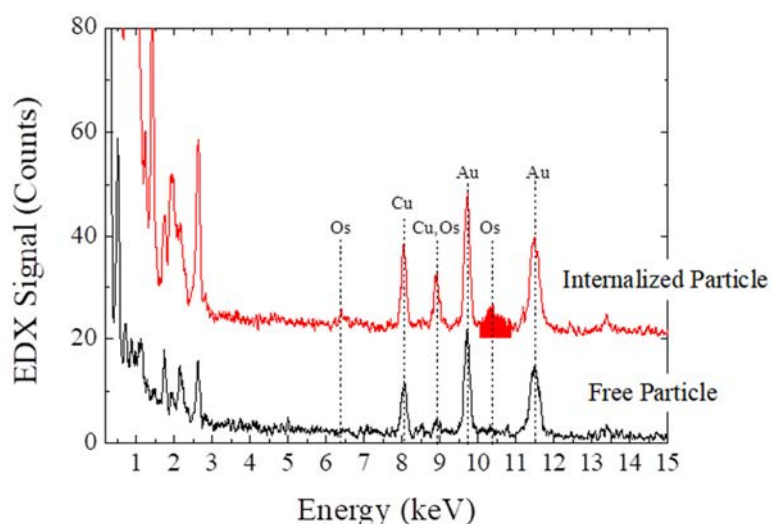
Supplementary figure 4. EDX signal of the microparticle edge of a free microparticle (outside the cell) and an internalized one (inside an endolysosome). The Os peak is only observed in internalized microparticles.

5. Transferrin-A488 release by photochemical internalization in vivo.

Movies of cells incubated with different concentrations of AlPc (0, 1 and 2 µg/ml) and 0.02 mg/ml Tf-A488 captured during 7 minutes after irradiation (620-630 nm) where discrete green dots (endolysosomes) gradually disappear in samples incubated with AlPc.

Supplementary movie 1. Control

Supplementary movie 2. 1 µg/ml AlPc

Supplementary movie 3. 2 µg/ml AlPc

Abbreviations: Tf-A488, Transferrin from human serum Alexa Fluor® 488 conjugate; AlPc, Al(III) Phthalocyanine chloride disulfonic acid.

IV

Discussion

The last advances in biomedicine have opened new approaches to overcome some of the major limitations of the current therapies. In the cancer field, the majority of strategies are designed to destroy malignant cells with the minimum effects on the healthy ones. For this purpose, several strategies have been developed, like those involving physicochemical methods, such as PDT, which has increased its effectivity in the last decades, while reducing its undesired side effects (MILLA SANABRIA ET AL., 2013; YOON, LI AND SHIM, 2013; ONISZCZUK ET AL., 2016).

Nowadays, several PSs have been approved for the clinical treatment of cancer through PDT, but research still continues for the design of new PSs with optimized properties. In this sense, the main goals of the **first work** were to evaluate the effectivity of two PSs to induce cell death in tumoral (SKBR3) and non-tumoral (MCF10A) human breast epithelial cell lines, and to characterize the type of cell death induced. The two PSs evaluated were meso-tetrakis (4-carboxyphenyl) porphyrin sodium salt (Na-H$_2$TCPP), and its newly developed zinc derivative (Na-ZnTCPP) (MARÍA E. ALEA-REYES ET AL., 2017). Porphyrins are able to induce the formation of ROS and it has been reported that the addition of bivalent cations, like Zn^{2+}, to form a metalloporphyrin, results in more efficient PSs for PDT uses than metal-free porphyrins (YU ET AL., 2015).

Whilst in dark conditions both PSs were not cytotoxic, after irradiation cell viability decreased in a concentration-dependent manner in both cell lines. At low concentrations (0,5 and 1 μM) of any of the two PSs, MCF10A cells proved to be slightly more resistant to induced cell death than SKBR3 cells, an interesting result towards the development of more selective treatments against tumors. Indeed, other studies using other PSs, such as ALA or zinc tetrasulfophthalocyanines, have also shown less cell death triggered by photodynamic treatments in non-tumoral than in tumoral cell lines, encouraging PDT research to fight against cancer (WYLD, REED AND BROWN, 2001; MADURAY ET AL., 2011).

Concerning the cell death mechanism induced, differences were found depending both on the cell lines and the PS used. Na-ZnTCPP induced mostly necrosis, regardless of the cell line used. However, Na-H$_2$TCPP induced necrotic and apoptotic nuclear morphologies in SKBR3 cells, but necrotic and spotted nuclei in MCF10A cells. Spotted

nuclei were also detected in MCF10A cells exposed to Na-ZnTCPP, but at much lower percentage since necrotic nuclei were largely predominant in this case. An extensive analysis using several assays allowed us to conclude that these spotted nuclei corresponded to cells that died by parthanatos, a type of regulated necrosis that had never been described in PDT. Parthanatos is characterized by nuclear fragmentation, early rupture of the plasma membrane without blebbing, mitochondrial depolarization, PARP-dependence, AIF translocation from mitochondria to the nucleus and, sometimes, caspase activation (FATOKUN, DAWSON AND DAWSON, 2014; AKI, FUNAKOSHI AND UEMURA, 2015). Interestingly, inhibition of PARP increased MCF10A cells viability from 35% to 80% in photodynamic treatments with Na-H$_2$TCPP, but was not able to rescue SKBR3 cells. Thus, the fact that, even with the same PS, the cell death mechanism induced by photodynamic treatments differs between tumoral and non-tumoral cells could be exploited for the design of more selective treatments with less injuries to healthy cells.

Traditionally, apoptosis has been the objective sought in cancer therapies, since it does not elicit an aggressive immune response in the patient because apoptotic cells are rapidly recognized and cleared by phagocytic cells. By contrast, necrosis has been usually related with an accidental and aggressive cell death that may lead to a high local inflammation due to the attraction of professional and non-professional phagocytes that secrete inflammatory factors or cytokines (GARG ET AL., 2010). In this sense, necrosis might cause major side effects, making this cell death mechanism an option to avoid unless local inflammation and immune system activation are sought, as for example in some metastatic lesions, where inflammation allows the recruitment of immune cells (KORBELIK, 1996; GARG ET AL., 2010). In this line of reasoning, Na-H$_2$TCPP could constitute a better PS option for PDT in tumors in which inflammation is undesired, such as brain tumors, because it induces less necrotic responses than Na-ZnTCPP. This differential response may be due to the addition of Zn^{2+} to the porphyrin, which could induce a higher production of ROS, leading to a necrotic response (HAMPTON AND ORRENIUS, 1997; HIGUCHI ET AL., 1998). However, one must be cautious since PSs may induce different cell death mechanisms depending on the cell line/type, so that the low necrotic response to Na-H$_2$TCPP observed in our two cell lines may not be universal. For instance, it has been reported that cells of the murine melanotic melanoma B16F1 cell line die mainly by

necrosis, with no significance appearance of apoptosis, after photodynamic treatment with H$_2$TCP (FABRIS ET AL., 2007).

In summary, the first work evidenced the importance of the PS, its concentration and the cell type in photodynamic treatments. Non-tumoral cells showed slightly higher viability than tumoral cells at low PS concentrations and the different cell death mechanism induced in both types of cells opens the door to treatments to selectively prevent cell death in non-malignant cells (i.e. the use of PARP inhibitors when cell death occurs by parthanatos in the non-tumoral cells but not in the tumoral ones). However, despite these positive results, a higher specificity of the treatments should be pursued to prevent undesired side effects in PDT. With this aim, PDT could be combined with the use of nano- and microsystems designed to direct the PSs specifically to the desired cells.

Various studies have highlighted the importance of targeting molecules on the cell surface to enhance interaction and internalization of drug carriers, like µPs and NPs, by the target cells (LIONG ET AL., 2008; ACHARYA, DILNAWAZ AND SAHOO, 2009; KOOPAEI ET AL., 2011). In this sense, and as a first step towards the development of multifunctional µPs with targeting and drug delivery abilities, the **second work** was aimed at evaluating HER2 as target molecule in tumoral cells, and studying the relevance of cell culture conditions in cell targeting with antiH-biofunctionalized µPs.

HER2 is a transmembrane tyrosine kinase from the ErbB receptor family with a highly conserved extracellular domain that is expressed in the plasma membrane of normal epithelial cells in low amounts but overexpressed in some types of cancer cells. This confers HER2 a special interest as a target molecule for cancer research and clinical treatments.

To study the suitability of HER2 as a target to direct µPs to tumoral cells, the isogenic breast epithelial cell lines D492 (GUDJONSSON ET AL., 2002; SIGURDSSON ET AL., 2011) and D492HER2 (INGTHORSSON ET AL., 2016) were selected. D492HER2 cells overexpress HER2, which confers them tumorigenic features (INGTHORSSON ET AL., 2016). As expected, µP-1 were uptaken by a higher percentage of cells than µP-3 regardless of the cell line, type of biofunctionalization or culture condition, and internalization was generally higher for

µP-antiH than for µP-secAb in both cell lines and in all culture conditions. However, it was surprising to find that internalization of µP-antiH occurred in a lower percentage of D492HER2 than D492 cells, given that D492HER2 cells overexpress the target molecule. This could be related with the general increased internalization capacity observed for D492 cells when compared with their HER2-overexpressing counterparts, which may arise from their different differentiation status (INGTHORSSON ET AL., 2016). A possible explanation could be that D492HER2 expresses mesenchymal marker that may reduce their ability to internalize µPs. Differences in µP internalization have also been reported for MCF10A breast epithelial normal cells when compared with SKBR3 breast epithelial tumoral cells, which also overexpress HER2 (PATIÑO ET AL., 2015). Nonetheless, when percentages of increase in internalization rates, rather than the absolute percentages, are considered in comparing µP-antiH and µP-secAb internalization, then it is clear that biofunctionalization of µPs with the anti-HER2 antibody results in a higher increase in internalization than biofunctionalization with a non-specific antibody, demonstrating that HER2 is a suitable target for directing µPs to tumoral cells.

On the other hand, it is worth noting that static or microfluidic cell culture conditions clearly affected µPs internalization rates, emphasizing the importance of using culture models more similar to *in vivo* conditions. The longer time to interact with cells, as would occur in static conditions, is likely to be responsible for the higher µPs internalization rates when compared with microfluidic ones. In static cultures, the µPs added to the culture medium readily deposit on the cells facilitating the interaction between the µPs and the plasma membrane, regardless of the specificity of the targeting molecule. By contrast, in fluidic cultures, the µPs move along the flow and only when there is a specific recognition of the target molecule the µPs would be retained on the cell surface and internalized. In this sense, the presence of the anti-HER2 antibody on the µPs surface may explain the higher increase in internalization rates observed in microfluidic cultures between µP-secAb and µP-antiH in both cell lines when compared with the increase observed in static conditions. This may also explain why only µP-3 biofunctionalized with anti-HER2 were internalized by D492 and D492HER2 cells in microfluidic cultures.

As a whole, the second work highlights the importance of HER2 targeting to direct µPs to tumoral cells, especially in fluidic culture conditions. Eventually, the

biofunctionalization of µP with an anti-HER2 antibody and a PS may help to direct the PS specifically to tumoral cells, reducing the side effects of PDT.

On the other hand, NPs and µPs can also be used as targeting and delivery vehicles for therapeutic drugs other than PSs to destroy malignant cells. However, one of the major problems of this strategy is the entrapment of the vehicle and the carried drug inside the endolysosomal system, preventing the therapeutic drug to reach its intracellular target site. Moreover, endolysosomal retention can also result in the destruction of the therapeutic molecule by enzymatic digestion. To circumvent these obstacles, different approaches and techniques have been developed in the last years, such as PCI. This technique, born from PDT, has demonstrated its usefulness for the release of different molecules from the endolysosomal compartment to the cytosol, which could be helpful for gene therapy, vaccination or cancer treatment (BERG ET AL., 1999; WEYERGANG ET AL., 2015; KARIMI ET AL., 2016; MARTINEZ DE PINILLOS BAYONA ET AL., 2016). PSs used in PCI have the ability to integrate in the plasma membrane, which will eventually be internalized through endocytic processes and become part of the endolysosomal membrane. This is an important feature, as in PCI, in contrast to traditional PDT, the goal of PS excitation is not to directly kill the cell but to disrupt its endolysosomal membranes, allowing the release of the endolysosomal contents into the cytosol.

Despite PCI has been successfully used to release several molecules and even NPs from endolysosomes (SELBO ET AL., 2010), its ability for the release of larger particles is unknown and the ultrastructural consequences of PCI on biological membranes has never been described in detail. In this line, the **third work** evaluated whether PCI allows µPs to escape from the endolysosomal compartment and characterized the ultrastructural changes elicited by PCI in endolysosomal membranes using different microscopy techniques. For these purposes, SKBR3 cells were incubated with µPs of 1 and 3 µm in diameter biofunctionalized with Tf, since it was previously demonstrated that SKBR3 cells, as many other tumoral cells, overexpress the TfR (HÖGEMANN-SAVELLANO ET AL., 2003; KOLHATKAR, LOTE AND KHAMBHATI, 2011) and that functionalization of multi-material polysilicon-Cr-Au intracellular chips with Tf led to a higher internalization by SKBR3 cells (PATIÑO ET AL., 2016).
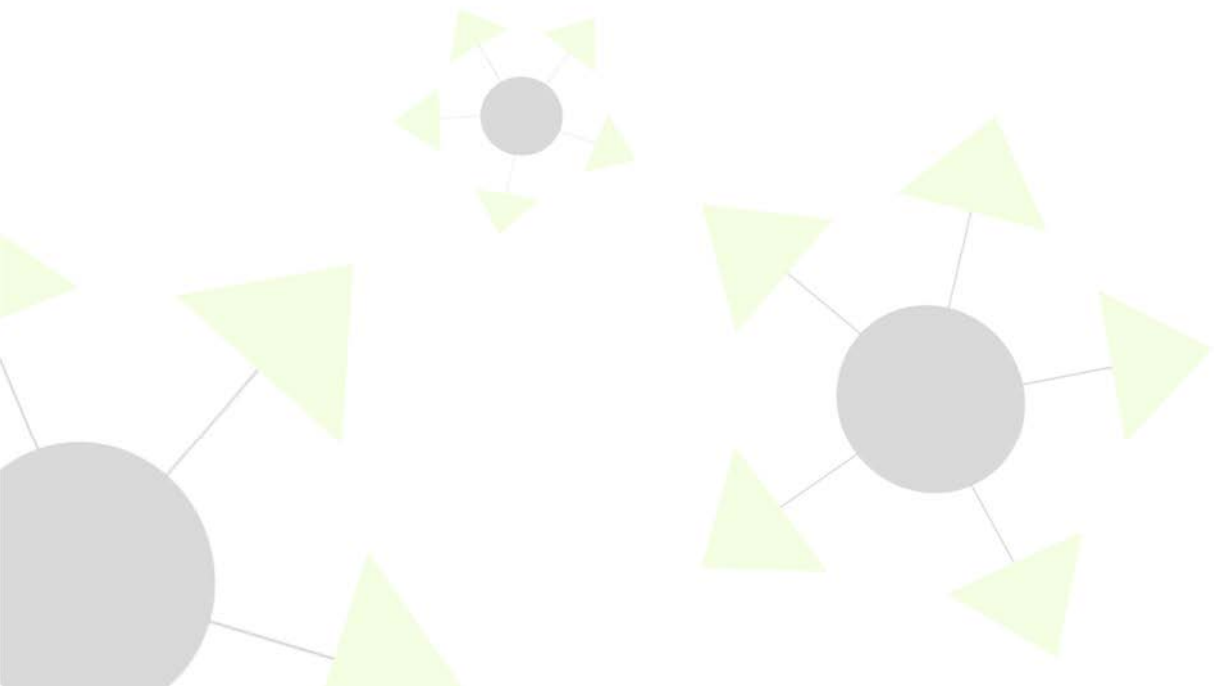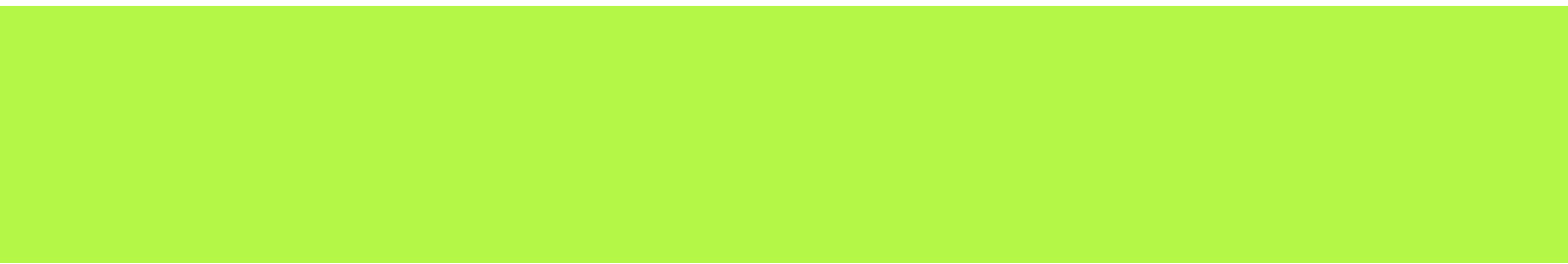
In order to test PCI, the photosensitizer AlPc was chosen since it is able to integrate in the biological membranes and has been previously used for PCI with good results (SELBO ET AL., 2010). Our first results showed that AlPc was not cytotoxic, neither in dark conditions nor after irradiation, and that it was useful for the release of soluble Tf-A488 from the endolysosomes after irradiation. However, the disruption of endolysosomal membranes achieved with the PCI treatment was not enough to completely liberate μPs-Tf-A488, since some remains of the endolysosomal membranes could still be detected around the μPs-Tf-A488.

It is worth noting the contribution of several microscopy techniques used in our study to gain a better understanding of the PCI-induced endolysosomal membranes disruption. First, colocalization of μPs and LAMP1 fluorescent signals under CLSM, confirming the location of μPs inside the endolysosomal compartment, significantly decreased after irradiation. This result indicated some sort of disruption of the endolysosomal membranes as a consequence of PCI, but it was not possible to conclude whether μPs lacking a surrounding LAMP1 signal were indeed free in the cytosol or were still surrounded by damaged endolysosomal membranes. In this sense, it is important to bear in mind that damage to LAMP1 due to PCI could have precluded its recognition by the antibody, producing a lack of signal even though the membrane was still present. Therefore, to further investigate the extent of endolysosomal membranes disruption, electron microscopy techniques were next used. Standard TEM showed that some μPs were surrounded by a well-defined membrane, whereas others, especially in the irradiated samples, were encircled by a blurred membrane. These blurred membranes could correspond to those without LAMP1 positive signal in previous colocalization CLSM experiments. Finally, the use of HAADF-STEM in combination with EDX, a technique that allows analyzing the presence and amount of different elements at any point of a sample, evidenced the difference in membrane integrity between the well-defined and the blurred membranes, in light of the different width of the Os peaks.

Further research is needed to specifically assess the extent of biochemical and ultrastructural damage suffered by the endolysosomal membranes as a result of PCI, and to optimize this technique to achieve their complete disintegration. Alternative ways to attain the final goal of liberating the carried drug should also be explored,

especially if a complete disintegration of the endolysosomal membranes through PCI proves to be not possible. For instance, the use of pH-sensitive bonds between the drug and its carrier, that would break once the functionalized µP reaches the endolysosomal compartment, would allow the detachment of the drug from the µP and its release into the cytosol through the PCI-induced disrupted membranes even if the µP could not be liberated.

In summary, the three works of the present thesis provide useful knowledge towards the optimization of two different strategies to specifically destroy cancer cells: PDT and the use of µPs as vehicles to target and deliver therapeutic drugs to malignant cells. Combining the obtained knowledge, new microdevices able to target and kill cancer cells more specifically could be designed and tested. Nonetheless, translation of the in vitro studies to the clinical practice should be carefully approached.
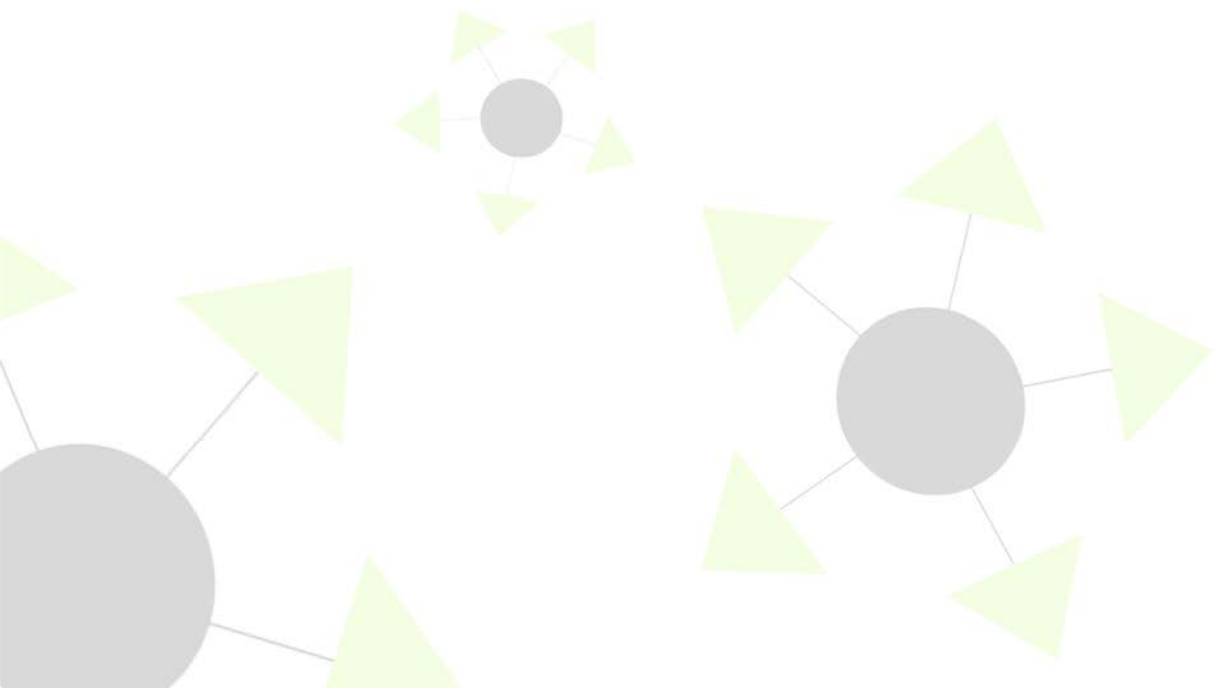
V

Conclusions

1st. Photodynamic treatments with either Na-H$_2$TCPP or its zinc derivative Na-ZnTCPP induced a decrease in the survival of both tumoral SKBR3 and non-tumoral MCF10A breast cells in a concentration-dependent manner. However, at low concentrations of any of the two photosensitizers (0,5 and 1 µM), non-tumoral MCF10A cells showed higher resistance to induced cell death than tumoral SKBR3 cells.

2nd. Photodynamic treatments triggered different cell death pathways depending on the cell line and the photosensitizer used. Whereas Na-ZnTCPP induced mainly necrosis, regardless of the cell line, Na-H$_2$TCPP triggered either necrosis or parthanatos in tumoral SKBR3 cells and either necrosis or apoptosis in non-tumoral MCF10A cells.

3rd. Biofunctionalization of polystyrene µPs with an anti-HER2 antibody resulted in higher percentages of internalization in the isogenic breast epithelial cell lines D492 and D492HER2 than biofunctionalization with a non-specific secondary antibody, regardless of the culture conditions.

4th. Although D492 cells showed a higher µP internalization capacity than their Her-2-overexpressing counterparts, the percentage of increase in internalization rates of µP-antiH versus µP-secAb was higher in D492HER2 cells than in D492 cells, especially in fluidic culture conditions. Therefore, HER2 is a suitable target molecule for directing µPs to tumorigenic cells that overexpress this transmembrane receptor.

5th. Cell culture conditions (mono- *versus* coculture and static *versus* microfluidics) influence cell receptor interactions with biofunctionalized µPs, highlighting the importance of performing *in vitro* targeting studies in an environment more similar to *in vivo* conditions (cocultures in microfluidics).

6th. PCI with AlPc allowed the release of endocytosed Tf-A488 molecules from the endolysosomes into the cytosol, but the extent of endolysosomal membrane disruption was not sufficient for the release of polystyrene μPs.

7th. PCI induces a certain degree of endolysosomal membranes disruption, evidenced by the lack of LAMP1 signal (CLSM), diffuse appearance (TEM) and larger width (STEM-EDX), but it does not cause their complete disintegration.

VI

References

ACHARYA, S., DILNAWAZ, F. AND SAHOO, S. K. 2009. Targeted epidermal growth factor receptor nanoparticle bioconjugates for breast cancer therapy, *Biomaterials. Elsevier Ltd*, 30(29), pp. 5737–5750.

ACHARYA, S. AND SAHOO, S. K. 2011. PLGA nanoparticles containing various anticancer agents and tumour delivery by EPR effect, *Advanced Drug Delivery Reviews. Elsevier B.V.*, 63(3), pp. 170–183.

ADLAKHA-HUTCHEON, G. ET AL. 1999. Controlled destabilization of a liposomal drug delivery system enhances mitoxantrone antitumor activity., *Nature biotechnology*, 17, pp. 775–779.

AGIRRE, M. ET AL. 2014. Low molecular weight chitosan (LMWC)-based polyplexes for pDNA delivery: From bench to bedside, *Polymers*, 6(6), pp. 1727–1755.

AGOSTINIS, P. ET AL. 2011. Photodynamic Terapy of cancer: an update, *CA Cancer J Clin.*, 61(4), pp. 250–281.

AKI, T., FUNAKOSHI, T. AND UEMURA, K. 2015. Regulated necrosis and its implications in toxicology, *Toxicology. Elsevier Ireland Ltd*, 333, pp. 118–126.

ALAM, F. ET AL. 2014. Unique roles of nanotechnology in medicine and cancer, *Indian Journal of Cancer*, 51(4), p. 506.

ALAM, F. ET AL. 2015. Unique roles of nanotechnology in medicine and cancer-II., *Indian journal of cancer*, 52(1), pp. 1–9.

ALARCÓN, E. ET AL. 2009. Photophysics and photochemistry of rose bengal bound to human serum albumin, *Photochemical & Photobiological Sciences*, 8(7), p. 933.

ALBANESE, A., TANG, P. S. AND CHAN, W. C. W. 2012. The Effect of Nanoparticle Size, Shape, and Surface Chemistry on Biological Systems, *Annual Review of Biomedical Engineering*, 14(1), pp. 1–16.

ALBERTS, B. ET AL. 2014. *Molecular Biology of The Cell*. 6th edn. Chapter 13: intracellular membrane traffic. Edited by Garland Sciences. pp.695-752.

ALEA-REYES, M. E. ET AL. 2017. Amphiphilic gemini pyridinium-mediated incorporation of Zn(II)meso-tetrakis(4-carboxyphenyl)porphyrin into water-soluble gold nanoparticles for photodynamic therapy, *Colloids and Surfaces B: Biointerfaces*, 158(October), pp. 602–609.

ALEA-REYES, M. E. ET AL. 2017. Amphiphilic Gemini Pyridinium-mediated incorporation of Zn(II)meso-tetrakis(4-carboxyphenyl)porphyrin into water-soluble gold nanoparticles for

photodynamic therapy, *Colloids and Surfaces B: Biointerfaces*. *Elsevier B.V.*, 158(October), pp. 602–609.

ALLEN, T. M. AND CULLIS, P. R. 2013. Liposomal drug delivery systems: From concept to clinical applications, *Advanced Drug Delivery Reviews*. *Elsevier B.V.*, 65(1), pp. 36–48.

ALLISON, R. R. AND MOGHISSI, K. 2013. Photodynamic therapy (PDT): PDT mechanisms, *Clinical Endoscopy*, 46(1), pp. 24–29.

ALLISON, R. R. AND SIBATA, C. H. 2010. Oncologic photodynamic therapy photosensitizers: A clinical review, *Photodiagnosis and Photodynamic Therapy*. *Elsevier B.V.*, 7(2), pp. 61–75.

ANGLIN, E. J. ET AL. 2008. Porous silicon in drug delivery devices and materials, *Advanced Drug Delivery Reviews*, 60(11), pp. 1266–1277.

ARSIANTI, M. ET AL. 2010. Polyethylenimine based magnetic iron-oxide vector: The effect of vector component assembly on cellular entry mechanism, intracellular localization, and cellular viability, *Biomacromolecules*, 11(9), pp. 2521–2531.

ARVIZO, R. R. ET AL. 2011. Modulating pharmacokinetics, tumor uptake and biodistribution by engineered nanoparticles, *PLoS ONE*, 6(9), pp. 3–8.

AWADA, G. ET AL. 2016. Emerging Drugs Targeting Human Epidermal Growth Factor Receptor 2 (Her2) In The Treatment Of Breast Cancer, *Expert Opinion on Emerging Drugs*. *Taylor & Francis*, 8214(February), p. 14728214.2016.1146680.

VI   B

BAREFORD, L. M. AND SWAAN, P. W. 2007. Endocytic mechanisms for targeted drug delivery, *Advanced Drug Delivery Reviews*, 59(8), pp. 748–758.

BARGHEER, D. ET AL. 2015. The fate of a designed protein corona on nanoparticles in vitro and in vivo, *Beilstein Journal of Nanotechnology*, 6(1), pp. 36–46.

BARITAUD, M. ET AL. 2010. Histone H2AX: The missing link in AIF-mediated caspase-independent programmed necrosis, *Cell Cycle*, 9(16), pp. 3166–3173.

BERG, K. ET AL. 1999. Photochemical internalization: A novel technology for delivery of macromolecules into cytosol, *Cancer Research*, 59(6), pp. 1180–1183.

BERG, K. 2005. Site-Specific Drug Delivery by Photochemical Internalization Enhances the Antitumor Effect of Bleomycin, *Clinical Cancer Research*, 11(23), pp. 8476–8485.

BHUVANESWARI, R. ET AL. 2009. The effect of photodynamic therapy on tumor angiogenesis, *Cellular and Molecular Life Sciences*, 66(14), pp. 2275–2283.

BOE, S. L. AND HOVIG, E. 2013. Enhancing nucleic acid delivery by photochemical

internalization, *Therapeutic Delivery*, 4(9), pp. 1125–1140.

BONSTED, A. ET AL. 2008. Photochemical Enhancement of DNA Delivery by EGF Receptor Targeted Polyplexes, in *Gene Therapy Protocols. Totowa, NJ: Humana Press*, pp. 171–181.

BOSMAN, A. W., JANSSEN, H. M. AND MEIJER, E. W. 1999. About Dendrimers: Structure, Physical Properties, and Applications, *Chemical Reviews*, 99(7), pp. 1665–1688.

BOUSSIF, O. ET AL. 1995. A versatile vector for gene and oligonucleotide transfer into cells in culture and in vivo: Polyethylenimine, *Proceedings of the National Academy of Sciences of the United States of America*, 92(August), pp. 7297–7301.

BRACKETT, C. M. AND GOLLNICK, S. O. 2011. Photodynamic therapy enhancement of anti-tumor immunity, *Photochemical & Photobiological Sciences*, 10(5), p. 649.

BROCK, R. 2014. The uptake of arginine-rich cell-penetrating peptides: Putting the puzzle together, *Bioconjugate Chemistry*, 25(5), pp. 863–868.

BROWN, S. D. ET AL. 2010. Gold Nanoparticles for the Improved Anticancer Drug Delivery of the Active Component of Oxaliplatin, *Journal of the American Chemical Society*, 132(13), pp. 4678–4684.

BURKE, A. ET AL. 2009. Long-term survival following a single treatment of kidney tumors with multiwalled carbon nanotubes and near-infrared radiation, *Proceedings of the National Academy of Sciences of the United States of America*, 106(31), pp. 12897–12902.

BUYTAERT, E., DEWAELE, M. AND AGOSTINIS, P. 2007. Molecular effectors of multiple cell death pathways initiated by photodynamic therapy, *Biochimica et Biophysica Acta - Reviews on Cancer*, 1776(1), pp. 86–107.

VI   C

CALIXTO, G. M. ET AL. 2016. Nanotechnology-Based Drug Delivery Systems for Photodynamic Therapy of Cancer: A Review., *Molecules (Basel, Switzerland)*, 21(3), p. 342.

CALVO, P., VILA-JATO, J. L. AND ALONSO, M. J. 1997. Evaluation of cationic polymer-coated nanocapsules as ocular drug carriers, *International Journal of Pharmaceutics*, 153(1), pp. 41–50.

CAÑETE, M. ET AL. 2004. Necrotic cell death induced by photodynamic treatment of human lung adenocarcinoma A-549 cells with palladium(II)-tetraphenylporphycene., *Int J Oncol*, 24, pp. 1221–1228.

CAÑETE, M., STOCKERT, J. C. AND VILLANUEVA, A. 2009. Preclinical photodynamic therapy research in Spain. 3. Localization of photosensitizers and mechanisms of cell death in vitro, *J. Porphyrins Phthalocyanines*, 13, pp. 544–551.

Cassidy, C. M. et al. 2009. Drug delivery strategies for photodynamic antimicrobial chemotherapy: From benchtop to clinical practice, *Journal of Photochemistry and Photobiology B: Biology*. Elsevier B.V., 95(2), pp. 71–80.

Chatterjee, D. K., Fong, L. S. and Zhang, Y. 2008. Nanoparticles in photodynamic therapy: An emerging paradigm, *Advanced Drug Delivery Reviews*. Elsevier B.V., 60(15), pp. 1627–1637.

Chen, J. et al. 2009. Cationic nanoparticles induce nanoscale disruption in living cell plasma membranes, *Journal of Physical Chemistry B*, 113(32), pp. 11179–11185.

Cheng, Y. et al. 2011. Design of biocompatible dendrimers for cancer diagnosis and therapy: current status and future perspectives, *Chemical Society Reviews*, 40(5), p. 2673.

Chin, W. W. L. et al. 2008. Improved formulation of photosensitizer chlorin e6 polyvinylpyrrolidone for fluorescence diagnostic imaging and photodynamic therapy of human cancer, *European Journal of Pharmaceutics and Biopharmaceutics*, 69(3), pp. 1083–1093.

Chithrani, B. D., Ghazani, A. A. and Chan, W. C. W. 2006. Determing the Size and Shape Dependence of Gold Nanoparticles Uptake Into Mammalian Cells, *Nano letters*, 6(4), pp. 662–668.

Chu, Z. et al. 2014. Unambiguous observation of shape effects on cellular fate of nanoparticles, *Scientific Reports*, 4(1), p. 4495.

Chung, C.-W. et al. 2013. 5-Aminolevulinic Acid-Incorporated Nanoparticles of Methoxy Poly(Ethylene Glycol)-Chitosan Copolymer for Photodynamic Therapy., *International journal of nanomedicine*, 8, pp. 809–19.

Conner, S. D. and Schmid, S. L. 2003. Regulated portals of entry into the cell, *Nature*, 422(6927), pp. 37–44.

Cooper, G. M. 2008. The Cell, *Cell*, 77(011600), pp. 67–109.

Copolovici, D. M. et al. 2014. Cell-penetrating peptides: Design, synthesis, and applications, *ACS Nano*, 8(3), pp. 1972–1994.

VI	D

Davis, M. E., Chen, Z. G. and Shin, D. M. 2008. Nanoparticle therapeutics: an emerging treatment modality for cancer, *Nature Reviews Drug Discovery*, 7(9), pp. 771–782.

Dawidczyk, C. M., Russell, L. M. and Searson, P. C. 2014. Nanomedicines for cancer therapy: state-of-the-art and limitations to pre-clinical studies that hinder future developments, *Frontiers in Chemistry*, 2(September 2015).

DECUZZI, P. ET AL. 2009. Intravascular delivery of particulate systems: Does geometry really matter?, *Pharmaceutical Research*, 26(1), pp. 235–243.

DELLINGER, M. 1996. Apoptosis or Necrosis Following Photofrin® Photosensitization: Influence of the Incubation Protocol, *Photochemistry and Photobiology*, 64(1), pp. 182–187.

ST. DENIS, T. G. ET AL. 2011. All you need is light, *Virulence*, 2(6), pp. 509–520.

DIETZE, A. ET AL. 2005. Enhanced photodynamic destruction of a transplantable fibrosarcoma using photochemical internalisation of gelonin., *British journal of cancer*, 92(11), pp. 2004–2009.

DING, X. ET AL. 2011. Development of iron-containing multiwalled carbon nanotubes for MR-guided laser-induced thermotherapy, *Nanomedicine*, 6(8), pp. 1341–1352.

DOLMANS, D. E. J. G. J., FUKUMURA, D. AND JAIN, R. K. 2003. Photodynamic therapy for cancer, *Nature Reviews Cancer*, 3(5), pp. 380–387.

VAN DONGEN, G. A. M. S., VISSER, G. W. M. AND VROUENRAETS, M. B. 2004. Photosensitizer-antibody conjugates for detection and therapy of cancer, *Advanced Drug Delivery Reviews*, 56(1), pp. 31–52.

DOUGHERTY, T. J. ET AL. 1975. Photoradiation therapy. II. Cure of animal tumors with hematoporphyrin and light., *J Natl Cancer Inst.*, 55(1), pp. 115–121.

DOUGHERTY, T. J. 1983. Hematoporphyrin As a Photosensitizer of Tumors, *Photochemistry and Photobiology*, 38(3), pp. 377–379.

DOUGHERTY, T., POTTER, W. AND WEISHAUPT, K. 1984. The structure of the active component of hematoporphyrin derivative, *Prog Clin Biol Res*, (170), pp. 301–314.

VI E

EL-SAYED, A. AND HARASHIMA, H. 2013. Endocytosis of gene delivery vectors: From clathrin-dependent to lipid raft-mediated endocytosis, *Molecular Therapy*, 21(6), pp. 1118–1130.

VI F

FABRIS, C. ET AL. 2007. Tumour-localizing and -photosensitising properties of meso-tetra(4-nido-carboranylphenyl)porphyrin (H2TCP), *Journal of Photochemistry and Photobiology B: Biology*, 89(2–3), pp. 131–138.

FATOKUN, A. A., DAWSON, V. L. AND DAWSON, T. M. 2014. Parthanatos: Mitochondrial-linked mechanisms and therapeutic opportunities, *British Journal of Pharmacology*, 171(8), pp. 2000–2016.

Fayter, D. et al. 2010. A systematic review of photodynamic therapy in the treatment of pre-cancerous skin conditions, Barrett's oesophagus and cancers of the biliary tract, brain, head and neck, lung, oesophagus and skin., *Health technology assessment (Winchester, England)*, 14(37), pp. 1–288.

Fernandez-Fernandez, A., Manchanda, R. and McGoron, A. J. 2011. Theranostic applications of nanomaterials in cancer: Drug delivery, image-guided therapy, and multifunctional platforms, *Applied Biochemistry and Biotechnology*, 165(7–8), pp. 1628–1651.

Fonda-Pascual, P. et al. 2016. In situ production of ROS in the skin by photodynamic therapy as a powerful tool in clinical dermatology, *Methods. Elsevier Inc.*, 109, pp. 190–202.

Fuchs, H., Weng, A. and Gilabert-Oriol, R. 2016. Augmenting the Efficacy of Immunotoxins and Other Targeted Protein Toxins by Endosomal Escape Enhancers, *Toxins*, 8(7), p. 200.

VI G

Galluzzi, L. et al. 2007. Cell death modalities: classification and pathophysiological implications, *Cell Death and Differentiation*, 14(7), pp. 1237–1243.

Galluzzi, L. et al. 2008. No death without life: vital functions of apoptotic effectors, *Cell Death and Differentiation*, 15(7), pp. 1113–1123.

Galluzzi, L., Kepp, O., et al. 2012. Mitochondrial control of cellular life, stress, and death, *Circulation Research*, 111(9), pp. 1198–1207.

Galluzzi, L., Vitale, I., et al. 2012. Molecular definitions of cell death subroutines: recommendations of the Nomenclature Committee on Cell Death 2012, *Cell Death and Differentiation*, 19(1), pp. 107–120.

Galluzzi, L. et al. 2015. Essential versus accessory aspects of cell death : recommendations of the NCCD 2015, pp. 58–73.

Galluzzi, L. et al. 2018. Molecular mechanisms of cell death: recommendations of the Nomenclature Committee on Cell Death 2018, *Cell Death & Differentiation*.

Garg, A. D. et al. 2010. Immunogenic cell death, DAMPs and anticancer therapeutics: An emerging amalgamation, *Biochimica et Biophysica Acta - Reviews on Cancer. Elsevier B.V.*, 1805(1), pp. 53–71.

Garg, A. D. et al. 2012. In vitro studies on erythrosine-based photodynamic therapy of malignant and pre-malignant oral epithelial cells, *PLoS ONE*, 7(4), pp. 1–12.

Geyer, C. E. et al. 2006. Lapatinib plus capecitabine for HER2-positive advanced breast cancer., *The New England journal of medicine*, 355(26), pp. 2733–2743.

GRATTON, S. E. A., NAPIER, M. E., ET AL. 2008. Microfabricated particles for engineered drug therapies: Elucidation into the mechanisms of cellular internalization of PRINT particles, *Pharmaceutical Research*, 25(12), pp. 2845–2852.

GRATTON, S. E. A., ROPP, P. A., ET AL. 2008. The effect of particle design on cellular internalization pathways., *Proceedings of the National Academy of Sciences of the United States of America*, 105(33), pp. 11613–11618.

GRECO, F. 2008. Polymer-drug conjugates: current status and future trends, *Frontiers in Bioscience*, 13(13), p. 2744.

GREEN, D. R. ET AL. 2009. Immunogenic and tolerogenic cell death, *Nature Reviews Immunology*, 9(5), pp. 353–363.

GUDJONSSON, T. ET AL. 2002. Isolation, immortalization and Characterization of a Human Breast Epithelial Cell Line With Stem Cell Properties, *Genes & Development*, pp. 693–706.

VI | H

HÄFELI, U. O. 2004. Magnetically modulated therapeutic systems, *International Journal of Pharmaceutics*, 277(1–2), pp. 19–24.

HAMPTON, M. B. AND ORRENIUS, S. 1997. Dual regulation of caspase activity by hydrogen peroxide: implications for apoptosis, *FEBS Letters. Federation of European Biochemical Societies*, 414(3), pp. 552–556.

HARUSH-FRENKEL, O. ET AL. 2007. Targeting of nanoparticles to the clathrin-mediated endocytic pathway, *Biochemical and Biophysical Research Communications*, 353(1), pp. 26–32.

HAUCK, T. S., GHAZANI, A. A. AND CHAN, W. C. W. 2008. Assessing the Effect of Surface Chemistry on Gold Nanorod Uptake, Toxicity, and Gene Expression in Mammalian Cells, *Small*, 4(1), pp. 153–159.

HEWLETT, L. J., PRESCOTT, A. R. AND WATTS, C. 1994. The coated pit and macropinocytic pathways serve distinct endosome populations, *Journal of Cell Biology*, 124(5), pp. 689–703.

HIGUCHI, M. ET AL. 1998. Regulation of reactive oxygen species-induced apoptosis and necrosis by caspase 3-like proteases, *Oncogene*, 17(21), pp. 2753–2760.

HÖGEMANN-SAVELLANO, D. ET AL. 2003. The transferrin receptor: a potential molecular imaging marker for human cancer., *Neoplasia (New York, N.Y.)*, 5(6), pp. 495–506.

HSIEH, Y. J. ET AL. 2003. Subcellular localization of photofrin® determines the death phenotype of human epidermoid carcinoma A431 cells triggered by photodynamic therapy: When plasma membranes are the main targets, *Journal of Cellular Physiology*,

194(3), pp. 363–375.

HUANG, C. ET AL. 2011. Surface modified superparamagnetic iron oxide nanoparticles (SPIONs) for high efficiency folate-receptor targeting with low uptake by macrophages, *Journal of Materials Chemistry*, 21(40), p. 16094.

HUANG, X. AND EL-SAYED, M. A. 2011. Plasmonic photo-thermal therapy (PPTT), *Alexandria Journal of Medicine. Alexandria University Faculty of Medicine*, 47(1), pp. 1–9.

VI   I

ICHIM, G. AND TAIT, S. W. G. 2016. A fate worse than death: Apoptosis as an oncogenic process, *Nature Reviews Cancer. Nature Publishing Group*, 16(8), pp. 539–548.

INGTHORSSON, S. ET AL. 2016. HER2 induced EMT and tumorigenicity in breast epithelial progenitor cells is inhibited by coexpression of EGFR, *Oncogene. Nature Publishing Group*, 35(32), pp. 4244–4255.

VI   J

JAIN, S., HIRST, D. G. AND O'SULLIVAN, J. M. 2012. Gold nanoparticles as novel agents for cancer therapy, *The British Journal of Radiology*, 85(1010), pp. 101–113.

JEONG, H. ET AL. 2011. Photosensitizer-conjugated human serum albumin nanoparticles for effective photodynamic therapy., *Theranostics*, 1, pp. 230–239.

JIN, C. S. AND ZHENG, G. 2011. Liposomal nanostructures for photosensitizer delivery, *Lasers in Surgery and Medicine*, 43(7), pp. 734–748.

JORDAN, A. ET AL. 1999. Magnetic fluid hyperthermia (MFH): Cancer treatment with AC magnetic field induced excitation of biocompatible superparamagnetic nanoparticles, *Journal of Magnetism and Magnetic Materials*, 201(1–3), pp. 413–419.

JUARRANZ, Á. ET AL. 2008. Photodynamic therapy of cancer. Basic principles and applications, *Clinical and Translational Oncology*, 10(3), pp. 148–154.

VI   K

KARIMI, M. ET AL. 2016. Smart micro/nanoparticles in stimulus-responsive drug/gene delivery systems, *Chem. Soc. Rev.*, 45(5), pp. 1457–1501.

KENNEDY, L. C. ET AL. 2011. A new era for cancer treatment: Gold-nanoparticle-mediated thermal therapies, *Small*, 7(2), pp. 169–183.

KIM, H. R. ET AL. 2007. Low-density lipoprotein receptor-mediated endocytosis of PEGylated nanoparticles in rat brain endothelial cells, *Cellular and Molecular Life*

Sciences, 64(3), pp. 356–364.

KOLHATKAR, R., LOTE, A. AND KHAMBHATI, H. 2011. Active Tumor Targeting of Nanomaterials Using Folic Acid, Transferrin and Integrin Receptors, *Current Drug Discovery Technologies*, 8(3), pp. 197–206.

KOOPAEI, M. N. ET AL. 2011. Docetaxel immunonanocarriers as targeted delivery systems for HER 2-positive tumor cells: preparation, characterization, and cytotoxicity studies., *International journal of nanomedicine*, 6, pp. 1903–1912.

KORBELIK, M. 1996. Induction of tumor immunity by photodynamic therapy, *Journal of Clinical Laser Medicine and Surgery*, 14(5), pp. 329–334.

KOSSODO, S. AND LAMURAGLIA, G. M. 2001. Clinical Potential of Photodynamic Therapy in Cardiovascular Disorders, *American Journal of Cardiovascular Drugs*, 1(1), pp. 15–21.

KRAMMER, B. AND VERWANGER, T. 2012. Molecular Response to Hypericin-Induced Photodamage, *Current Medical Chemistry*, 19(6), pp. 793–798.

KROEMER, G. ET AL. 2009. Classification of cell death: recommendations of the Nomenclature Committee on Cell Death 2009, *Cell Death and Differentiation*, 16(1), pp. 3–11.

KROEMER, G., GALLUZZI, L. AND BRENNER, C. 2007. Mitochondrial Membrane Permeabilization in Cell Death, *Physiology Reveiw*, pp. 99–163.

KROEMER, G. AND LEVINE, B. 2008. Autophagic cell death: the story of a misnomer, *Nature Reviews Molecular Cell Biology*, 9(12), pp. 1004–1010.

VI   L

LABALA, S. ET AL. 2015. Layer-by-layer polymer coated gold nanoparticles for topical delivery of imatinib mesylate to treat melanoma, *Molecular Pharmaceutics*.

LEE, C.-S. ET AL. 2013. Endolysosomal environment-responsive photodynamic nanocarrier to enhance cytosolic drug delivery via photosensitizer-mediated membrane disruption., *Biomaterials. Elsevier Ltd*, 34(36), pp. 9227–36.

LEWIS PHILLIPS, G. D. ET AL. 2008. Targeting HER2-positive breast cancer with trastuzumab-DM1, an antibody-cytotoxic drug conjugate, *Cancer Research*, 68(22), pp. 9280–9290.

LIANG, W. AND LAM, J. K. W. 2012. Molecular Regulation of Endocytosis, *Energy Procedia*. Edited by B. Ceresa. *InTech*.

LIONG, M. ET AL. 2008. Multifunctional inorganic nanoparticles for imaging, targeting, and drug delivery, *ACS Nano*, 2(5), pp. 889–896.

LIPSON, R., BALDES, E. AND OLSEN, A. 1961. The use of a derivative of hematoporhyrin in tumor

detection., *Journal of the National Cancer Institute*, 26, pp. 1–11.

LIPSON, R. L. AND BALDES, E. J. 1960. The Photodynamic Properties of a Hematoporphyrin Derivative, *Test*, 82, pp. 508–516.

LOOS, C. ET AL. 2014. Functionalized polystyrene nanoparticles as a platform for studying bio-nano interactions, *Beilstein Journal of Nanotechnology*, 5(1), pp. 2403–2412.

LU, X. ET AL. 2005. High level expression of apoptosis inhibitor in hepatoma cell line expressing hepatitis B virus, *International Journal of Medical Sciences*, 2(1), pp. 30–35.

LUKIANOVA-HLEB, E. Y. ET AL. 2012. Biomaterials Plasmonic nanobubble-enhanced endosomal escape processes for selective and guided intracellular delivery of chemotherapy to drug-resistant cancer cells, *Biomaterials*. *Elsevier Ltd*, 33(6), pp. 1821–1826.

LUO, Y. AND KESSEL, D. 1997. Initiation of Apoptosis versus Necrosis by Photodynamic Therapy with Chloroaluminum Phthalocyanine, *Photochemistry and Photobiology*, 66(4), pp. 479–483.

LUO, Z. ET AL. 2012. Redox-Responsive Molecular Nanoreservoirs for Controlled Intracellular Anticancer Drug Delivery Based on Magnetic Nanoparticles, *Advanced Materials*, 24(3), pp. 431–435.

VI	M

MA, X. ET AL. 2013. Integrated hollow mesoporous silica nanoparticles for target drug/siRNA co-delivery, *Chemistry - A European Journal*, 19(46), pp. 15593–15603.

MADURAY, K. ET AL. 2011. In vitro toxicity testing of zinc tetrasulfophthalocyanines in fibroblast and keratinocyte cells for the treatment of melanoma cancer by photodynamic therapy, *Journal of Photochemistry and Photobiology B: Biology*. *Elsevier B.V.*, 103(2), pp. 98–104.

MADURAY, K., ODHAV, B. AND NYOKONG, T. 2012. In vitro photodynamic effect of aluminum tetrasulfophthalocyanines on melanoma skin cancer and healthy normal skin cells, *Photodiagnosis and Photodynamic Therapy*. *Elsevier B.V.*, 9(1), pp. 32–39.

MAEDA, H. 2010. Tumor-selective delivery of macromolecular drugs via the EPR effect: Background and future prospects, *Bioconjugate Chemistry*, 21(5), pp. 797–802.

MAJOROS, I. J. ET AL. 2006. PAMAM Dendrimer-Based Multifunctional Conjugate for Cancer Therapy: Synthesis, Characterization, and Functionality, *Biomacromolecules*, 7(2), pp. 572–579.

MAO, S. ET AL. 2005. Uptake and transport of PEG-graft-trimethyl-chitosan copolymer-insulin nanocomplexes by epithelial cells, *Pharmaceutical Research*, 22(12), pp. 2058–2068.

Marchal, S. et al. 2005. Necrotic and apoptotic features of cell death in response to Foscan® photosensitization of HT29 monolayer and multicell spheroids, *Biochemical Pharmacology*, 69(8), pp. 1167–1176.

Martinez de Pinillos Bayona, A. et al. 2016. Enhancing the efficacy of cytotoxic agents for cancer therapy using photochemical internalisation, *International Journal of Cancer*, 138(5), pp. 1049–1057.

Mayor, S. and Pagano, R. E. 2007. Pathways of clathrin-independent endocytosis, *Nature Reviews Molecular Cell Biology*, 8(8), pp. 603–612.

McCarthy, J. R. and Weissleder, R. 2008. Multifunctional magnetic nanoparticles for targeted imaging and therapy, *Advanced Drug Delivery Reviews*, 60(11), pp. 1241–1251.

McMahon, H. T. and Boucrot, E. 2011. Molecular mechanism and physiological functions of clathrin-mediated endocytosis, *Nature Reviews Molecular Cell Biology*. *Nature Publishing Group*, 12(8), pp. 517–533.

Meng, H. et al. 2013. Codelivery of an Optimal Drug/siRNA Combination Using Mesoporous Silica Nanoparticles To Overcome Drug Resistance in Breast Cancer in Vitro and in Vivo, *ACS Nano*, 7(2), pp. 994–1005.

Mercer, J. and Helenius, A. 2012. Gulping rather than sipping: Macropinocytosis as a way of virus entry, *Current Opinion in Microbiology. Elsevier Ltd*, 15(4), pp. 490–499.

van Midwoud, P. M. et al. 2012. Comparison of biocompatibility and adsorption properties of different plastics for advanced microfluidic cell and tissue culture models, *Anal Chem*, 84(9), pp. 3938–3944.

Milla Sanabria, L. et al. 2013. Direct and indirect photodynamic therapy effects on the cellular and molecular components of the tumor microenvironment, *Biochimica et Biophysica Acta (BBA) - Reviews on Cancer. Elsevier B.V.*, 1835(1), pp. 36–45.

Misra, R. and Sahoo, S. K. 2010. Intracellular trafficking of nuclear localization signal conjugated nanoparticles for cancer therapy, *European Journal of Pharmaceutical Sciences*, 39(1–3), pp. 152–163.

Monopoli, M. P. et al. 2011. Physical-Chemical aspects of protein corona: Relevance to in vitro and in vivo biological impacts of nanoparticles, *Journal of the American Chemical Society*, 133(8), pp. 2525–2534.

Moubarak, R. S. et al. 2007. Sequential Activation of Poly(ADP-Ribose) Polymerase 1, Calpains, and Bax Is Essential in Apoptosis-Inducing Factor-Mediated Programmed Necrosis, *Molecular and Cellular Biology,* 27(13), pp. 4844–4862.

Muehlmann, L. A. et al. 2011. Liposomal photosensitizers: Potential platforms for anticancer photodynamic therapy, *Brazilian Journal of Medical and Biological Research*, 44(8), pp. 729–737.

Mura, S., Nicolas, J. and Couvreur, P. 2013. Stimuli-responsive nanocarriers for drug delivery, *Nature Publishing Group*. *Nature Publishing Group*, 12(11), pp. 991–1003.

Muro, S. et al. 2008. Control of Endothelial Targeting and Intracellular Delivery of Therapeutic Enzymes by Modulating the Size and Shape of ICAM-1-targeted Carriers, *Molecular Therapy*, 16(8), pp. 1450–1458.

VI	N	

Nagasaki, Y. et al. 2004. Novel molecular recognition via fluorescent resonance energy transfer using a biotin-PEG/polyamine stabilized CdS quantum dot., *Langmuir : the ACS journal of surfaces and colloids*, 20(15), pp. 6396–6400.

Nel, A. E. et al. 2009. Understanding biophysicochemical interactions at the nano–bio interface, *Nature Materials*. *Nature Publishing Group*, 8(7), pp. 543–557.

Nguyen, J. and Szoka, F. C. 2012. Nucleic Acid Delivery : The Missing Pieces of the Puzzle?, *Acc Chem Res*, 45, pp. 1153–62.

Nishiyama, N. et al. 2005. Light-induced gene transfer from packaged DNA enveloped in a dendrimeric photosensitizer, *Nature Materials*, 4(12), pp. 934–941.

Noodt, B. B. et al. 1998. Apoptosis induction by different pathways with methylene blue derivative and light from mitochondrial sites in V79 cells, *International Journal of Cancer*, 75(6), pp. 941–948.

Nowis, D. et al. 2005. Direct tumor damage mechanisms of photodynamic therapy, *Acta Biochimica Polonica*, 52(2), pp. 339–352.

VI	O	

Ohtsuki, T. et al. 2015. The molecular mechanism of photochemical internalization of cell penetrating peptide-cargo-photosensitizer conjugates., *Scientific reports*. *Nature Publishing Group*, 5(December), p. 18577.

Omata, D. et al. 2011. Bubble Liposomes and Ultrasound Promoted Endosomal Escape of TAT-PEG Liposomes as Gene Delivery Carriers, *Molecular Pharmaceutics*, 8(6), pp. 2416–2423.

Oniszczuk, A. et al. 2016. The potential of photodynamic therapy (PDT)-Experimental investigations and clinical use, *Biomedicine and Pharmacotherapy*. *Elsevier Masson SAS*, 83, pp. 912–929.

Otto, W. et al. 2011. The enlightenment of bladder cancer treatment: origin and progress

of photodynamic diagnosis., *Future oncology (London, England)*, 7(9), pp. 1057–1066.

VI	P	

PARTON, R. G. AND SIMONS, K. 2007. The multiple faces of caveolae, *Nature Reviews Molecular Cell Biology*, 8(3), pp. 185–194.

PATIÑO, T. ET AL. 2015. Surface modification of microparticles causes differential uptake responses in normal and tumoral human breast epithelial cells., *Scientific reports*. *Nature Publishing Group*, 5(May), p. 11371.

PATIÑO, T. ET AL. 2016. Polysilicon-chromium-gold intracellular chips for multi-functional biomedical applications, *Nanoscale*. *Royal Society of Chemistry*, 8(16), pp. 8773–8783.

PENG, Q., MOAN, J. AND NESLAND, J. M. 1996. Correlation of subcellular and intratumoral photosensitizer localization with ultrastructural features after photodynamic therapy., *Ultrastructural pathology*, 20(2), pp. 109–129.

PENON, O. ET AL. 2016. Iron oxide nanoparticles functionalized with novel hydrophobic and hydrophilic porphyrins as potential agents for photodynamic therapy, *Journal of Colloid and Interface Science*. *Elsevier Inc.*, 462, pp. 154–165.

PETROS, R. A. AND DESIMONE, J. M. 2010. Strategies in the design of nanoparticles for therapeutic applications, *Nature Reviews Drug Discovery*. *Nature Publishing Group*, 9(8), pp. 615–627.

POLO, L. ET AL. 2002. Low-density lipoprotein receptors in the uptake of tumour photosensitizers by human and rat transformed fibroblasts, *International Journal of Biochemistry and Cell Biology*, 34(1), pp. 10–23.

POON, I. K. H., HULETT, M. D. AND PARISH, C. R. 2010. Molecular mechanisms of late apoptotic/necrotic cell clearance, *Cell Death and Differentiation*. *Nature Publishing Group*, 17(3), pp. 381–397.

PRASMICKAITE, L. ET AL. 2002. Photochemical disruption of endocytic vesicles before delivery of drugs: a new strategy for cancer therapy, *British Journal of Cancer*, 86(4), pp. 652–657.

VI	Q	

QIAO, X.-F. ET AL. 2012. Triple-functional core–shell structured upconversion luminescent nanoparticles covalently grafted with photosensitizer for luminescent, magnetic resonance imaging and photodynamic therapy in vitro, *Nanoscale*, 4(15), p. 4611.

VI	R	

RAFF, M. C. 1992. Social controls on cell survival and cell death, *Nature*, 356, pp. 397–399.

RAMP, U. ET AL. 2005. XIAP Expression is an Independent Prognostic Marker in Clear-Cell Renal Carcinomas, *The Journal of Urology*, 174, pp. 112–114.

RANA, S. ET AL. 2007. On the suitability of nanocrystalline ferrites as a magnetic carrier for drug delivery: Functionalization, conjugation and drug release kinetics, *Acta Biomaterialia*, 3(2), pp. 233–242.

RAY, S. ET AL. 2012. Virtual Labs in proteomics: New E-learning tools, *Journal of Proteomics. Elsevier B.V.*, 75(9), pp. 2515–2525.

REJMAN, J. ET AL. 2004. Size-dependent internalization of particles via the pathways of clathrin- and caveolae-mediated endocytosis, *Biochemical Journal*, 377(1), pp. 159–169.

RHYNER, M. N. ET AL. 2006. Quantum dots and multifunctional nanoparticles: new contrast agents for tumor imaging, *Nanomedicine*, 1(2), pp. 209–217.

RITZ, S. ET AL. 2015. Protein Corona of Nanoparticles: Distinct Proteins Regulate the Cellular Uptake, *Biomacromolecules*, 16(4), pp. 1311–1321.

ROGER, E. ET AL. 2010. Biopharmaceutical parameters to consider in order to alter the fate of nanocarriers after oral delivery, *Nanomedicine*, 5(2), pp. 287–306.

ROSADO, C. J. ET AL. 2014. A Common Fold Mediates Vertebrate Defense and Bacterial Attack, *Science*, 1548(317), pp. 1548–1551.

VI	S

SAKULKHU, U. ET AL. 2014. Protein Corona Composition of Superparamagnetic Iron Oxide Nanoparticles with Various Physico-Chemical Properties and Coatings, *Scientific Reports*, 4(1), p. 5020.

SALONEN, J. ET AL. 2005. Mesoporous silicon microparticles for oral drug delivery: Loading and release of five model drugs, *Journal of Controlled Release*, 108(2–3), pp. 362–374.

SALVATI, A. ET AL. 2013. Transferrin-functionalized nanoparticles lose their targeting capabilities when a biomolecule corona adsorbs on the surface, *Nature Nanotechnology. Nature Publishing Group*, 8(2), pp. 137–143.

SANDVIG, K. ET AL. 2008. Clathrin-independent endocytosis: From nonexisting to an extreme degree of complexity, *Histochemistry and Cell Biology*, 129(3), pp. 267–276.

SANVICENS, N. AND MARCO, M. P. 2008. Multifunctional nanoparticles - properties and prospects for their use in human medicine, *Trends in Biotechnology*, 26(8), pp. 425–433.

SARGENT JR., J. F. 2014. The National Nanotechnology Initiative: Overview, Reauthorization, and Appropriations Issues, *Congressional research service reports*, p. 71.

SEITZ, G. ET AL. 2012. Molecular imaging and photodynamic therapy in hepatoblastoma, *Frontiers in Bioscience*, E4(1), pp. 487–492.

SELBO, P. K. ET AL. 2001. In vivo documentation of photochemical internalization, a novel approach to site specific cancer therapy, *International Journal of Cancer*, 92(5), pp. 761–766.

SELBO, P. K. ET AL. 2010. Photochemical internalization provides time- and space-controlled endolysosomal escape of therapeutic molecules., *Journal of controlled release*. *Elsevier B.V.*, 148(1), pp. 2–12.

SELIGER, B. AND KIESSLING, R. 2013. The two sides of HER2/neu: Immune escape versus surveillance, *Trends in Molecular Medicine*. *Elsevier Ltd*, 19(11), pp. 677–684.

SHADIDI, M. AND SIOUD, M. 2003. Selective targeting of cancer cells using synthetic peptides, *Drug Resistance Updates*, 6(6), pp. 363–371.

SHETE, H. K., PRABHU, R. H. AND PATRAVALE, V. B. 2014. Endosomal Escape: A Bottleneck in Intracellular Delivery, *Journal of Nanoscience and Nanotechnology*, 14(1), pp. 460–474.

SHRESTHA, R. ET AL. 2012. Endosomal escape and siRNA delivery with cationic shell crosslinked knedel-like nanoparticles with tunable buffering capacities, *Biomaterials*, 33(33), pp. 8557–8568.

SIGURDSSON, V. ET AL. 2011. Endothelial induced EMT in breast epithelial cells with stem cell properties, *PLoS ONE*, 6(9), pp. 1–11.

SINGH, M. ET AL. 2000. Cationic microparticles: A potent delivery system for DNA vaccines., *Proceedings of the National Academy of Sciences of the United States of America*, 97(2), pp. 811–816.

SLAMON, D. J. ET AL. 2001. Use of Chemotherapy plus a Monoclonal Antibody against HER2 for Metastatic Breast Cancer That Overexpresses HER2, *New England Journal of Medicine*, 344(11), pp. 783–792.

SORIANO, J. ET AL. 2013. Liposomal temocene (m-THPPo) photodynamic treatment induces cell death by mitochondria-independent apoptosis, *Biochimica et Biophysica Acta - General Subjects*. *Elsevier B.V.*, 1830(10), pp. 4611–4620.

STELLER, H. 1995. Mechanisms and genes of cellular suicide, *Science*, 267(5203), pp. 1445–1449.

STUCHINSKAYA, T. ET AL. 2011. Targeted photodynamic therapy of breast cancer cells using antibody-phthalocyanine-gold nanoparticle conjugates., *Photochemical & photobiological sciences : Official journal of the European Photochemistry Association and the European Society for Photobiology*, 10(5), pp. 822–831.

SUNG, J. C., PULLIAM, B. L. AND EDWARDS, D. A. 2007. Nanoparticles for drug delivery to the

lungs, *Trends in Biotechnology*, 25(12), pp. 563–570.

VI	T	

Tallury, P., Payton, K. and Santra, S. 2008. Silica-based multimodal/multifunctional nanoparticles for bioimaging and biosensing applications, *Nanomedicine*, 3(4), pp. 579–592.

Tan, J. et al. 2013. The influence of size, shape and vessel geometry on nanoparticle distribution, *Microfluidics and Nanofluidics*, 14(1–2), pp. 77–87.

Tanaka, T. et al. 2010. Sustained small interfering RNA delivery by mesoporous silicon particles, *Cancer Research*, 70(9), pp. 3687–3696.

Tekle, C. et al. 2008. Cellular trafficking of quantum dot-ligand bioconjugates and their induction of changes in normal routing of unconjugated ligands, *Nano Letters*, 8(7), pp. 1858–1865.

Thorek, D. L. J. and Tsourkas, A. 2008. Size, charge and concentration dependent uptake of iron oxide particles by non-phagocytic cells, *Biomaterials*, 29(26), pp. 3583–3590.

Torchilin, V. P. et al. 2003. Immunomicelles: Targeted pharmaceutical carriers for poorly soluble drugs., *Proceedings of the National Academy of Sciences of the United States of America*, 100(10), pp. 6039–6044.

Tros de Ilarduya, C. and Düzgüneş, N. 2013. Delivery of therapeutic nucleic acids via transferrin and transferrin receptors: lipoplexes and other carriers., *Expert opinion on drug delivery*, 10(November), pp. 1583–91.

VI	U	

Uehara, N. 2010. Polymer-functionalized Gold Nanoparticles as Versatile Sensing Materials, *Analytical Sciences*, 26(12), pp. 1219–1228.

Ulukaya, E. et al. 2011. Apoptosis: why and how does it occur in biology?, *Cell Biochemistry and Function*, 29(6), pp. 468–480.

VI	V	

Vargas, A. et al. 2004. Improved photodynamic activity of porphyrin loaded into nanoparticles: An in vivo evaluation using chick embryos, *International Journal of Pharmaceutics*, 286(1–2), pp. 131–145.

Villanueva, A. 1993. The cationic meso-substituted porphyrins: an interesting group of photosensitizers, *Journal of Photochemistry and Photobilogy B: Biology*, 18, pp. 295–296.

Vrouenraets, M. B. et al. 2000. Targeting of a hydrophilic photosensitizer by use of

internalizing monoclonal antibodies: A new possibility for use in photodynamic therapy, *International Journal of Cancer*, 88(1), pp. 108–114.

VI	W

WANG, J. ET AL. 2010. The complex role of multivalency in nanoparticles targeting the transferrin receptor for cancer therapies, *Journal of the American Chemical Society*, 132(32), pp. 11306–11313.

WANG, T. ET AL. 2014. Enhanced tumor delivery and antitumor activity in vivo of liposomal doxorubicin modified with MCF-7-specific phage fusion protein, *Nanomedicine: Nanotechnology, Biology, and Medicine. Elsevier B.V.*, 10(2), pp. 421–430.

WANG, Y., DAWSON, V. L. AND DAWSON, T. M. 2009. Poly(ADP-ribose) signals to mitochondrial AIF: A key event in parthanatos, *Experimental Neurology. Elsevier Inc.*, 218(2), pp. 193–202.

WEYERGANG, A. ET AL. 2011. Photochemical internalization of tumor-targeted protein toxins, *Lasers in Surgery and Medicine*, 43(7), pp. 721–733.

WEYERGANG, A. ET AL. 2015. Photochemical activation of drugs for the treatment of therapy-resistant cancers., *Photochemical & photobiological sciences : Official journal of the European Photochemistry Association and the European Society for Photobiology. Royal Society of Chemistry*, 14(8), pp. 1465–75.

WEYERGANG, A., SELBO, P. K. AND BERG, K. 2006. Photochemically stimulated drug delivery increases the cytotoxicity and specificity of EGF-saporin, *Journal of Controlled Release*, 111(1–2), pp. 165–173.

WHITE, E. 1996. Life, death, and the pursuit of apoptosis, *Genes & Development*, 10(1), pp. 1–15.

WONG, P. T. AND CHOI, S. K. 2015. Mechanisms and implications of dual-acting methotrexate in folate-targeted nanotherapeutic delivery, *International Journal of Molecular Sciences*, 16(1), pp. 1772–1790.

WYLD, L., REED, M. W. AND BROWN, N. J. 2001. Differential cell death response to photodynamic therapy is dependent on dose and cell type., *British journal of cancer*, 84(10), pp. 1384–1386.

VI	Y

YAN, Y. ET AL. 2013. Differential roles of the protein corona in the cellular uptake of nanoporous polymer particles by monocyte and macrophage cell lines, *ACS Nano*, 7(12), pp. 10960–10970.

YANG, F. ET AL. 2011. Magnetic functionalised carbon nanotubes as drug vehicles for cancer

lymph node metastasis treatment, *European Journal of Cancer*, 47(12), pp. 1873–1882.

YANG, F. ET AL. 2012. Emerging inorganic nanomaterials for pancreatic cancer diagnosis and treatment, *Cancer Treatment Reviews*, 38(6), pp. 566–579.

YANG, P., GAI, S. AND LIN, J. 2012. Functionalized mesoporous silica materials for controlled drug delivery, *Chemical Society Reviews*, 41(9), p. 3679.

YOFFE, S. ET AL. 2012. Superparamagnetic Iron Oxide Nanoparticles (SPIONs): Synthesis and Surface Modification Techniques for use with MRI and Other Biomedical Applications, *Current Pharmaceutical Design*, 19(3), pp. 493–509.

YOON, I., LI, J. Z. AND SHIM, Y. K. 2013. Advance in photosensitizers and light delivery for photodynamic therapy, *Clinical Endoscopy*, 46(1), pp. 7–23.

YU, Q. ET AL. 2015. Synthesis and photodynamic activities of a new metronidazole-appended porphyrin and its Zn(II) complex, *Journal of Porphyrins and Phthalocyanines*, 19(10), pp. 1107–1113.

YUHONG XU AND FRANCIS C. SZOKA, J. ET AL. 1996. Mechanism of DNA Release from Cationic Liposome / DNA Complexes Used in, *Biochemistry*, 2960(96), pp. 5616–5623.

VI	Z	

ZAUNER, W., FARROW, N. A. AND HAINES, A. M. . 2001. In vitro uptake of polystyrene microspheres: effect of particle size, cell line and cell density, *Journal of Controlled Release*, 71(1), pp. 39–51.

ZHANG, D., WANG, J. AND XU, D. 2016. Cell-penetrating peptides as noninvasive transmembrane vectors for the development of novel multifunctional drug-delivery systems ☆, *Journal of Controlled Release. The Authors*, 229, pp. 130–139.

ZHANG, L. ET AL. 2013. Hydrolytic cationic ester microparticles for highly efficient DNA vaccine delivery, *Small*, 9(20), pp. 3439–3444.

ZHENG, X. AND PANDEY, R. K. 2008. Porphyrin-Carbohydrate Conjugates : Photodynamic Therapy (PDT) Impact of Carbohydrate Moieties in, *Anti-Cancer Agents in Medicinal Chemistry*, 8, pp. 241–268.

ZONG, W. X. ET AL. 2004. Alkylating DNA damage stimulates a regulated form of necrotic cell death, *Genes and Development*, 18(11), pp. 1272–1282.